University of Massachusetts Medical School

eScholarship@UMMS

GSBS Dissertations and Theses   Graduate School of Biomedical Sciences

2017-12-07

Molecular Players in Preserving Excitatory-Inhibitory Balance in the Brain

Wenjie Mao
University of Massachusetts Medical School

Let us know how access to this document benefits you.

MOLECULAR PLAYERS IN PRESERVING EXCITATORY-INHIBITORY BALANCE IN THE BRAIN

A Dissertation Presented

By

Wenjie Mao

Submitted to the Faculty of the
University of Massachusetts Graduate School of Biomedical Sciences, Worcester
in partial fulfillment of the requirements for the degree of

DOCTOR OF PHILOSOPHY

December 7th, 2017

Neuroscience

MOLECULAR PLAYERS IN PRESERVING EXCITATORY-INHIBITORY BALANCE IN THE BRAIN

A Dissertation Presented by

Wenjie Mao

This work was undertaken in the Graduate School of Biomedical Sciences
Program in Neuroscience

Under the mentorship of

Kensuke Futai, Ph.D., Thesis Advisor

Anthony Imbalzano, Ph.D., Member of Committee

Joel Richter, Ph.D., Member of Committee

Paul Gardner, Ph.D., Member of Committee

Gina Turrigiano, Ph.D., External Member of Committee

Ann Rittenhouse, Ph.D., Chair of Committee

Anthony Carruthers, Ph.D.,
Dean of the Graduate School of Biomedical Sciences

December 7th, 2017

To Mum and Dad,
who listened, believed, and taught me to be happy

And to my love, my best friend, Xi,
without whom none of this would matter

ACKNOWLEDGEMENTS

First and foremost, I would like to thank my mentor Dr. Kensuke Futai. Pursuing a PhD has been a long journey. Here standing at the end of the road, I cannot say there are no regrets, but I certainly could not wish for a better mentor than Kenny. Kenny has always guided and supported me without reservation, through the good times and the bad. When I bulldozed my way through learning electrophysiology, when I spent years failing to make an antibody, when I got no positive hit from a genomic screen, Kenny has always been there, unwavering, encouraging, daring me to take the risk and make the breakthrough. He taught me to be observant, determined and always think critically. Most importantly, he has allowed me to be a partner in this scientific endeavor we took on. I thank him for that.

I would also like to thank my TRAC and QE committee members, our BNRI faculty and our collaborators, who have constantly provided valuable insights and stimulating scientific conversations - Schahram Akbarian, Tony Imbalzano, Andrew Tapper, Ann Rittenhouse, Joel Richter, Haley Melikian, Gilles Martin, Paul Gardner, Carlos Lois, Maria Morabito, Mike Francis, Tom Fazzio, Dorothy Schafer, Hanno Hock, Masahiko Watanabe, Anna Salzberg and Yuka Imamura.

I am also grateful to all my wonderful labmates, everyone in Futai lab both past and present, Motokazu, Amy, Naoe, Yuto, Tamami, Takuya, Mai. They make me smile when I come to the lab every morning. My special thanks to Motokazu for helping me with my project and being an awesome scientist that I greatly admire.

I wouldn't be here if not for my dear parents, who worked hard and gave me the best life. I thank them for letting me pursue what is meaningful to me. I would also like to thank my grandparents and my extended family in China, for always believing in me. Lastly, to the one person who I owe my thanks the most, thank you for being in my life, for your understanding and your patience, and for the whispered words when I need them the most.

ABSTRACT

Information processing in the brain relies on a functional balance between excitation and inhibition, the disruption of which leads to network destabilization and many neurodevelopmental disorders, such as autism spectrum disorders. One of the homeostatic mechanisms that maintains the excitatory and inhibitory balance is called synaptic scaling: Neurons dynamically modulate postsynaptic receptor abundance through activity-dependent gene transcription and protein synthesis. In the first part of my thesis work, I discuss our findings that a chromatin reader protein L3mbtl1 is involved in synaptic scaling. We observed that knockout and knockdown of L3mbtl1 cause a lack of synaptic downscaling of glutamate receptors in hippocampal primary neurons and organotypic slice cultures. Genome-wide mapping of L3mbtl1 protein occupancies on chromatin identified Ctnnb1 and Gabra2 as downstream target genes of L3mbtl1-mediated transcriptional regulation. Importantly, partial knockdown of Ctnnb1 by itself prevents synaptic downscaling. Another aspect of maintaining E/I balance centers on GABAergic inhibitory neurons. In the next part of my thesis work, we address the role of the scaffold protein Shank1 in excitatory synapses onto inhibitory interneurons. We showed that parvalbumin-expressing interneurons lacking Shank1 display reduced excitatory synaptic inputs and decreased levels of inhibitory outputs to pyramidal neurons. As a consequence, pyramidal neurons in Shank1 mutant mice exhibit increased E/I ratio. This is accompanied by a reduced

expression of an inhibitory synapse scaffolding protein gephyrin. These results provide novel insights into the roles of chromatin reader molecules and synaptic scaffold molecules in synaptic functions and neuronal homeostasis.

Table of Contents

List of Figures

List of Tables

List of Electronic Files

Tables that are too large to be incorporated are listed below and provided as Excel files. Tables are numbered according to the chapter number.

Table 2.2 Datasets of RNA-seq

Table 2.3 Datasets for ChIP-seq

List of Copyright Materials Produced by the Author

Chapter III of this dissertation has appeared in a separate publication:

*Mao, W., *Watanabe, T., Cho, S., Frost, J.L., Truong, T., Zhao, X., and Futai, K. (2015). Shank1 regulates excitatory synaptic transmission in mouse hippocampal parvalbumin-expressing inhibitory interneurons. European Journal of Neuroscience *41*, 1025–1035. (* Equal contribution)

List of Abbreviations

AMPA	α-amino-3-hydroxy-5-methyl-4-isoxazolepropionic acid
AMPAR	AMPA receptor
aCSF	artificial cerebrospinal fluid
AMPAR-EPSC	AMPA receptor-mediated excitatory postsynaptic current
ANOVA	analysis of variance
APV or DAPV	D(-)-2-Amino-5-phosphonopentanoic acid
ASD	autism spectrum disorder
ATAC-seq	assay for transposase-accessible chromatin sequencing
BDNF	brain-derived neurotrophic factor
CA1	cornu ammonis region 1
CA3	cornu ammonis region 3
CB	calbindin
CB1R	cannabinoid type 1 receptor
CCK	cholecystokinin
ChIP	chromatin immunoprecipitation
ChIP-qPCR	chromatin immunoprecipitation followed by quantitative PCR
ChIP-seq	chromatin immunoprecipitation sequencing
CNS	central nervous system
CR	calretinin
DAVID	database for annotation, visualization and integrated discovery
DIG	digoxigenin
DIV	days in vitro
DMEM	Dulbecco's Modified Eagle's Medium
DMSO	dimethyl sulfoxide
DSB	double strand break
DSG	disuccinimidyl glutarate
E/I balance	excitatory and inhibitory balance
EPSC	excitatory postsynaptic current
ES cell	embryonic stem cell
FACS	fluorescence-activated cell sorting
FMRP	fragile X mental retardation protein
GABA	gamma-aminobutyric acid
$GABA_AR$	GABA(A) receptor
$GABA_AR$-IPSC	GABA(A) receptor-mediated inhibitory postynaptic current

GFP	green fluorescent protein
GLP	G9a-like protein
GO	gene ontology
GST	glutathione S-transferase
H3K27ac (etc.)	histone H3 lysine 27 acetylation
H4K20me (etc.)	histone H4 lysine 20 mono-methylation
HDAC	histone deacetylase
HP1γ	heterochromatin protein 1γ
HRP	horseradish peroxidase
I/V curve	current/voltage curve
IDR	irreproducible discovery rate
Ig	immunoglobin
INTACT	isolation of nuclei tagged in specific cell types
IPSC	inhibitory postsynaptic current
KD	knockdown
KO	knockout
KS test	kolmogorov smirnov test
LCM	laser capture microdissection
LTD	long term depression
LTP	long term potentiation
MBT	malignant brain tumor
mEPSC	miniature excitatory postsynaptic current
mGluR	metabotropic glutamate receptor
mIPSC	miniature inhibitory postsynaptic current
NBQX	2,3-dihydroxy-6-nitro-7-sulfamoyl-benzo[f]quinoxaline-2,3-dione
NMDA	N-Methyl-D-Aspartate
NMDAR	NMDA receptor
NPY	neuropeptide Y
P7	postnatal day 7
PcG	polycomb group
PCR	polymerase chain reaction
PFA	paraformaldehyde
PPD	paired-pulse depression
PPF	paired-pulse facilitation
PRC	polycomb repressive complex
PSD	postsynaptic density
PTM	post-translational modifications
PTX	picrotoxin

PTZ	pentylenetetrazole
PV	parvalbumin
PV+	parvalbumin expressing
qPCR	quantitative polymerase chain reaction
RA	retinoic acid
Rb	retinoblastoma protein
RFP	red fluorescent protein
RNA-seq	RNA sequencing
RT-qPCR	reverse transcription quantitative PCR
shRNA	short hairpin RNA
shScr	scrambled short hairpin RNA
SOM	somatostatin
SP	stratum pyramidale
SR	stratum radiatum
STDP	spike timing-dependent plasticity
TNFα	tumor necrosis factor α
TSS	transcriptional start site
TTX	tetrodotoxin
uIPSC	unitary inhibitory postsynaptic current
VIP	vasoactive intestinal peptide
WNT	wingless type
WT	wild type

CHAPTER I

Introduction

CHAPTER I

INTRODUCTION

Neural plasticity

The brain is not a static structure consists of billions of neurons ready to activate predefined orderly events upon stimuli, but rather an ecosystem of interconnections in an ongoing state of change. This ability of the brain to change and adapt, referred to as "plasticity" by neuroscientists, was first described by Santiago Ramon y Cajal, who discovered that new nerve paths can form in the brain after injury, and proposed mechanisms and theories for the potential of the brain to adapt to the environment (Cajal, 1913). In 1949, the concept of synaptic plasticity was more clearly defined by Donald Hebb as the Hebb's rule (Hebb, 1949), commonly summarized as "Neurons that fire together wire together". This theory described a process that repetitive stimulation between presynaptic neuron and postsynaptic neuron reinforces and strengthens the synaptic connections between them, which later shaped the cellular basis for experience-dependent learning. We now know that neural plasticity can manifest at various scales temporally and spatially. For temporal scales, neural plasticity can occur within milliseconds, or involve changes that last throughout lifetime; for spatial scales, plasticity can be observed at individual synapses, or it can affect the neural circuits, or involve large scale remapping of activity patterns in different brain regions.

At the center of all types of neural plasticity, activity is the main driving force.

Changes in activity level may trigger two major aspects of plasticity: positive feedback plasticity that sets the synapses and circuits to a new functional state, and negative feedback plasticity that constrains the activity levels of synapses and circuits to their homeostatic set point. These two sides of neural plasticity work coherently with each other to provide both flexibility and stability needed for the development and maintenance of proper neuronal functions.

One most important form of a positive feedback type of plasticity mechanism is Hebbian-type homosynaptic plasticity such as long term potentiation (LTP) and long term depression (LTD). In 1973, Bliss and Lomo reported that high-frequency stimulation to presynaptic fibers induced potentiation of a postsynaptic response that persisted for hours (LTP), while low-frequency stimulation resulted in depression of postsynaptic efficacy (LTD) (Bliss and Lomo, 1973). Both LTP and LTD are triggered by Ca^{2+} influx resulting from correlated firing of pre- and postsynaptic neurons. For NMDA (N-Methyl-D-Aspartate) receptor-dependent LTP and LTD, depolarization leads to release of the Mg^{2+} block on postsynaptic NMDA receptors, which allows Ca^{2+} influx through channel opening. High and moderate levels of intracellular Ca^{2+} influx trigger LTP and LTD, respectively, by modulating AMPA (α-amino-3-hydroxy-5-methyl-4-isoxazolepropionic acid) receptors at postsynaptic sites through a cascade of Ca^{2+}-dependent signaling pathways (Lisman, 1989; Yang et al., 1999). For metabotropic glutamate receptor (mGluR)-dependent and/or cannabinoid type 1 receptor (CB1R)-dependent LTD, the induction instead requires Ca^{2+} release mediated by postsynaptic mGluRs,

and/or presynaptic CB1Rs (Bender et al., 2006; Sjöström et al., 2003). It was later found that the sign and magnitude of LTP and LTD are determined by the precise temporal order of presynaptic and postsynaptic action potentials (spiking), characterized as spike timing-dependent plasticity (STDP) (Bi and Poo, 1998; Debanne et al., 1998; Magee and Johnston, 1997; Markram et al., 1997). LTP and LTD are also found to be associated with structural and morphological changes of synapses. For example, LTP induces new spine formation (Engert and Bonhoeffer, 1999); LTP and LTD can bring about the enlargement and retraction of dendritic spines (Matsuzaki et al., 2004; Nägerl et al., 2004; Zhou et al., 2004).

The Hebbian type of plasticity, while contributing to the experience-dependent learning process (Pastalkova et al., 2006; Whitlock et al., 2006), also may generate unconstrained instability in neuronal network activity that potentially leads to detrimental effects. Runaway potentiation may lead to overexcitation and cell death, while runaway depression may result in synapse elimination and silencing of neurons (Abbott and Nelson, 2000; Davis, 2006; Turrigiano and Nelson, 2004), thus disrupting the excitatory and inhibitory balance in the brain. In the mammalian central nervous system (CNS), a variety of homeostatic plasticity mechanisms exist to provide compensatory negative feedback and to stabilize neuronal networks. Examples include homeostatic regulation of intrinsic excitability (Desai et al., 1999; Zhang and Linden, 2003), homeostatic synaptic scaling (O'Brien et al., 1998; Turrigiano et al., 1998), heterosynaptic plasticity (Abraham and Goddard, 1983; Lynch et al., 1977), metaplasticity that adjusts the

ability to further induce plasticity based on a history of recent activity (Abraham and Bear, 1996; Colino et al., 1992; Deisseroth et al., 1995).

Synaptic scaling and activity-dependent gene expression

In this part, I focus on a crucial form of homeostatic plasticity that regulates synaptic strength - synaptic scaling. Synaptic scaling always scales synaptic strength in the direction that compensates for the activity perturbation, and this applies for both excitatory synapses and inhibitory synapses. For example, in dissociated cultures, excitatory synapses onto excitatory neurons can be scaled up by activity blockade, whereas excitatory synapses onto inhibitory neurons are scaled up by activity elevation (Rutherford et al., 1998). As for inhibitory synapses onto excitatory neurons, the inhibitory synaptic strength is reduced by activity blockade and increased by activity elevation (Hartman et al., 2006; Kilman et al., 2002; Swanwick et al., 2006). In principle, synaptic strength can be regulated at the level of presynaptic vesicle release and reuptake, functional synapse numbers, and postsynaptic receptor accumulation. For scaling of inhibitory synapses, both pre- and postsynaptic mechanisms are involved, including regulation of release probability of GABA from presynaptic terminals and change of postsynaptic $GABA_A$ receptor accumulation (Hartman et al., 2006; Kilman et al., 2002; Peng et al., 2010; Swanwick et al., 2006). For scaling of excitatory synapses, although presynaptic changes were found in some cases to accompany synaptic scaling (Burrone et al., 2002; Murthy et al., 2001; Thiagarajan et al., 2002), the central mechanism is

attributed to changes of postsynaptic glutamate receptor abundance (O'Brien et al., 1998; Turrigiano et al., 1998). In the mammalian CNS, AMPA and NMDA receptors are the major ionotropic glutamate receptors that mediate excitatory synaptic transmission, and both can be regulated by synaptic scaling (Lissin et al., 1998; O'Brien et al., 1998; Rao and Craig, 1997; Turrigiano et al., 1998; Watt et al., 2000).

A synaptic scaling phenomenon was first discovered in dissociated primary neuronal cultures (Turrigiano et al., 1998), a model system where activity can be easily manipulated; for instance, bath application of the $GABA_A$ receptor blocker bicuculline/picrotoxin (PTX) elevates neuronal activity, whereas the sodium channel blocker tetrodotoxin (TTX) induces activity blockade. In the original study, chronic network activity elevation or blockade (24~48 hours) triggers a bidirectional scaling of AMPA receptor-mediated miniature excitatory postsynaptic current (mEPSC) amplitude (quantal amplitude) (**Fig 1.1**). This scaling is multiplicative, meaning that AMPA receptors are inserted or removed from all synapses in proportion to the existing number of receptors at the synapse, which allows the relative differences between synaptic strengths to be preserved (Turrigiano et al., 1998).

In the mammalian CNS, AMPA receptors are hetero-tetramers assembled from dimers of dimers of differing combinations of GluA1-A4 subunits. In cortical and hippocampal pyramidal neurons, the majority of synaptic and extrasynaptic AMPA receptors are the GluA1/2 subtype, and most of the remaining receptors

Figure 1.1
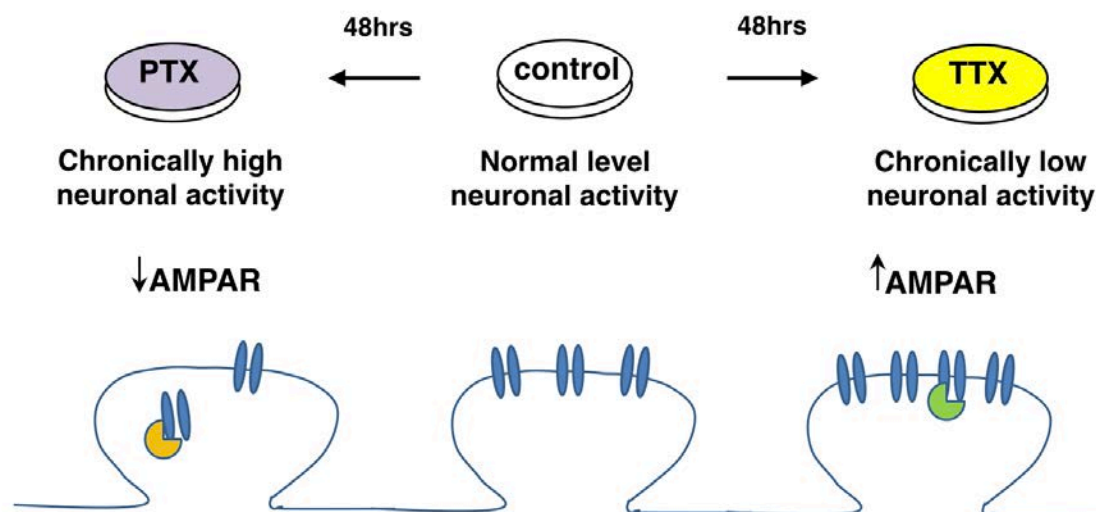
Figure 1.1 Schematics for synaptic scaling of AMPARs in dissociated culture.

Bath application of the GABA$_A$ receptor blocker picrotoxin (PTX) elevates neuronal activity, and induces a decrease of number of postsynaptic AMPA receptors through scaling factors (orange). The sodium channel blocker tetrodotoxin (TTX) induces activity blockade, and triggers an increase in the number of postsynaptic AMPA receptors through scaling factors (green).

are GluA2/3 subtype (Lu et al., 2009b). GluA2-containing AMPA receptors are Ca^{2+}-impermeable, and have a slightly outwardly rectifying current/voltage (I/V) curve, while GluA2-lacking AMPA receptors are Ca^{2+}-permeable and show inward rectification (Boulter et al., 1990). This is functionally important because GluA2-lacking AMPA receptors exist in intracellular receptor pools, and can be incorporated transiently to the synapses in an activity-dependent manner (Ju et al., 2004; Plant et al., 2006; Sutton et al., 2006). Which AMPA receptor subtypes are regulated during synaptic scaling remains controversial. Many studies have found that activity blockade induces a coordinated increase of GluA1 and GluA2 (Anggono et al., 2011; Cingolani et al., 2008; O'Brien et al., 1998; Qiu et al., 2012; Shin et al., 2012; Wierenga et al., 2005), but others reported selective enhancement of GluA1-containing/GluA2-lacking receptors, thus changing AMPA receptor composition (Ju et al., 2004; Sutton et al., 2006; Thiagarajan et al., 2005). Interestingly, local activity inhibition at individual synapses, induced by genetically silencing presynaptic input, selectively enhances GluA1-containing/GluA2-lacking receptors (Hou et al., 2008). Chen et al. recently proposed that the discrepancy can be explained by two distinct mechanisms induced by activity blockade. When action potential blockade is accompanied by reduction of dendritic calcium levels (application of TTX together with NMDA receptor blocker APV), a rapid retinoic acid-dependent form of synaptic scaling is induced that requires local synthesis and insertion of GluA1-containing/GluA2-lacking receptors (Aoto et al., 2008; Chen et al., 2014). On the other hand, activity elevation is shown to preferably target

GluA2-containing AMPA receptors (Goold and Nicoll, 2010), thus both GluA1 and GluA2 are scaled down (Fu et al., 2011; Qiu et al., 2012; Shin et al., 2012; Tan et al., 2015).

How is the change of activity sensed by the neuron and signaled to the synapses? Is it a cell autonomous process or does it require additional signaling from the network? Like the Hebbian forms of plasticity, intracellular calcium, an indicator for activity, is essential for induction of synaptic scaling. Neurons sense their own action potential firing through a change of calcium influx, which in turn activates a cascade of Ca^{2+}-dependent signaling pathways that eventually leads to regulation of postsynaptic receptors (Goold and Nicoll, 2010; Ibata et al., 2008) (**Fig 1.2**). A number of molecules have been identified that bridge the induction and expression steps of synaptic scaling (reviewed in Chen et al., 2014; Pozo and Goda, 2010; Rich and Wenner, 2007; Turrigiano, 2012). It is not surprising that a lot of these molecules directly contribute to receptor stabilization and trafficking machineries, including receptor endo- and exocytosis, receptor turnover rate, and scaffolding proteins that tether receptors at synapses (Ehlers, 2000; Ehlers, 2003; O'Brien et al., 1998; Turrigiano and Nelson, 2004). For example, the immediate-early gene Arc/Arg3.1 has been shown to modulate synaptic scaling through an AMPA receptor endocytic pathway (Shepherd et al., 2006). Kinases such as CaMKIV and CaMKK act as calcium sensors and mediate transcriptional events essential for synaptic scaling (Goold and Nicoll, 2010; Ibata et al., 2008). Polo-like kinase2 (Plk2) and cyclin-dependent kinases 5 (Cdk5) induce synaptic

downscaling by phosphorylation of a scaffold protein SPAR (Seeburg and Sheng, 2008; Seeburg et al., 2008). Many scaffold molecules such as PSD93, PSD95, SynGap, GRIP1, GKAP/SAPAP are also involved (Gainey et al., 2015; Kim et al., 2007; Shin et al., 2012; Sun and Turrigiano, 2011; Tan et al., 2015; Wang et al., 2013). Cell adhesion molecules have been shown to stabilize receptors at synapses and modulate synaptic efficacy during scaling; examples include β3 integrins (Cingolani et al., 2008) and the N-cadherin/β-catenin complex (Okuda et al., 2007).

So far, cell-autonomous mechanisms have been discussed. However, synaptic scaling has also been found to involve inter-cellular interactions, such as soluble factors released from neurons or glia in an activity-dependent manner. Cytokine tumor-necrosis factor α (TNFα) released from glia is crucial for AMPA receptor upscaling in response to activity blockade (Stellwagen and Malenka, 2006). Brain-derived neurotrophic factor (BDNF) can differentially influence synaptic strength depending on the postsynaptic neuron type through TrkB activation (Rutherford et al., 1998). Another soluble factor is retinoic acid (RA). As discussed above, a RA-dependent form of synaptic scaling was discovered when neural activity was blocked with TTX and APV (Aoto et al., 2008). This is suggested to be a distinct mechanism from global cell-autonomous synaptic scaling, because it is a rapid process independent of transcription and requires local synthesis of GluA1 (Chen et al., 2014; Sutton et al., 2006).

Synaptic scaling also occurs *in vivo*. The most-studied synaptic scaling *in*

Figure 1.2
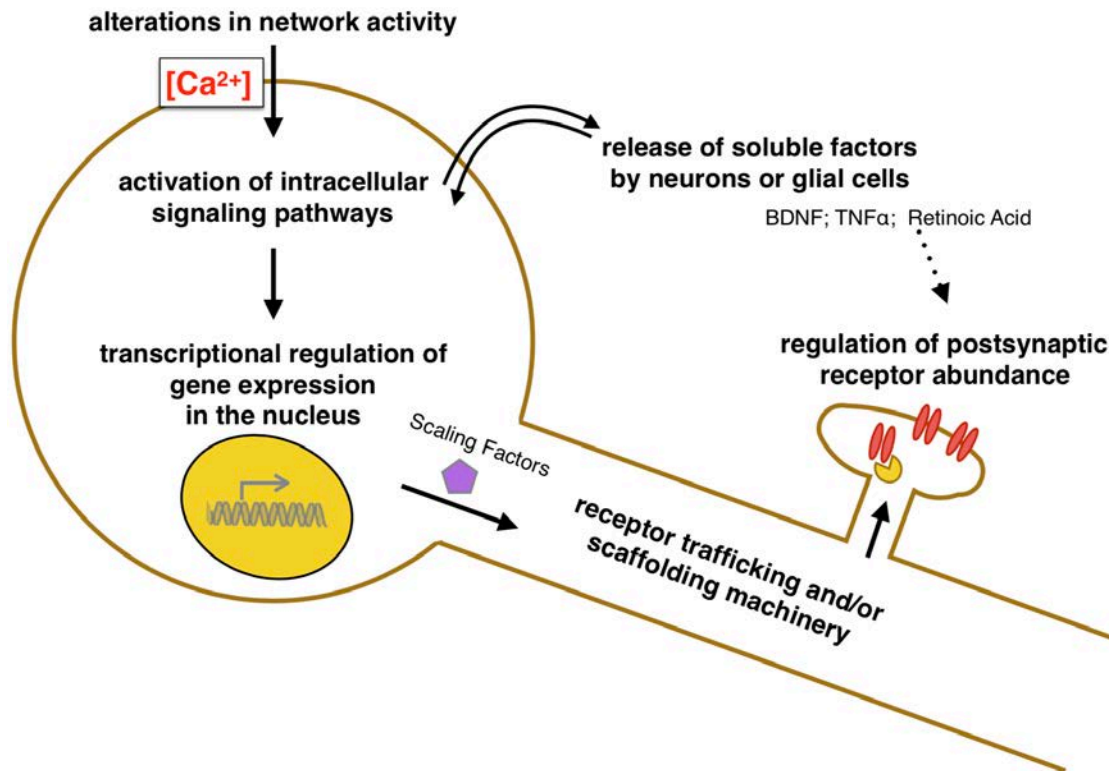
Figure 1.2 Schematics for cellular mechanisms of synaptic scaling.

Activity alterations induce transcriptional regulation of gene expression via Ca^{2+}-dependent pathways, eventually leading to changes in the abundance of neurotransmitter receptors at postsynaptic sites.

vivo is driven by sensory input during visual cortex development. It has been shown that increased synaptogenesis associated with eye opening is accompanied by a homeostatic downscaling of synaptic strength (Desai et al., 2002). In addition, monocular visual deprivation (activity blockade on one eye) induces synaptic upscaling of GluA2-containing AMPA receptors (Desai et al., 2002; Gainey et al., 2009; Maffei and Turrigiano, 2008). In contrast, binocular visual deprivation (dark rearing of animals) triggers synaptic upscaling of GluA2-lacking AMPA receptors via GluA1 phosphorylation, and this form of experience-dependent synaptic scaling has been shown to persist through adulthood (Goel and Lee, 2007; Goel et al., 2011). Recently, Keck et al. showed similar synaptic upscaling in visual cortex induced by bilateral retinal lesions in awake animals (Keck et al., 2013). A form of homer1a-driven synaptic scaling-down has also been found *in vivo* during sleep (Diering et al., 2017). Interestingly, the scaling-up in visual cortex is inhibited by sleep and enhanced by wake (Hengen et al., 2016). Additionally, synaptic scaling has also been observed in auditory cortex following auditory deprivation (Teichert et al., 2017).

Overall, synaptic scaling, with exceptions (discussed above), is generally considered a slow, cumulative, cell-autonomous process that requires gene transcription and protein synthesis (Goold and Nicoll, 2010; Ibata et al., 2008; Schanzenbächer et al., 2016; Sutton et al., 2004). Importantly, many of these synaptic scaling factors are themselves regulated by activity, and activity-dependent transcription has been shown to be critical for the expression of

synaptic scaling. For example, activity-dependent upregulation of Arc protein induces downscaling of synaptic AMPA receptors; overexpression of Arc reduces excitatory synaptic strength and disrupts synaptic upscaling (Shepherd et al., 2006). Another example is the activity-dependent shift of CaMKII α/β ratio observed in synaptic scaling; overexpression of αCaMKII or βCaMKII results in opposite effects on synaptic strength (Thiagarajan et al., 2002). Activity also triggers bidirectional regulation of Homer1a expression that is required for synaptic upscaling and downscaling (Diering et al., 2017; Hu et al., 2010). Moreover, a recent study found that neuronal pentraxin-1 (Nptx1) expression increased within 6 hours of activity blockade; knockdown of Nptx1 abolishes synaptic upscaling (Schaukowitch et al., 2017). These results clearly illustrate the critical role of activity-dependent gene expression in synaptic scaling, and point to the importance of identifying epigenetic mechanisms involved. So far, several epigenetic modifications have been identified in homeostatic synaptic scaling. Methyl-CpG-binding protein 2 (MeCP2), a DNA methylation binding protein, can cell-autonomously mediate synaptic scaling by binding to the GluA2 promoter and regulating its expression (Blackman et al., 2012; Qiu et al., 2012). In addition, the level of DNA methylation has been found to be associated with synaptic upscaling (Meadows et al., 2015).

Histone post-translational modifications and chromatin reader proteins

Epigenetic mechanisms provide a crucial regulatory layer for activity-dependent

gene expression. One of the key mechanisms is post-translational modifications (PTM) on the N-terminal tails of histones, known as the "histone code". These covalent modifications, including acetylation, phosphorylation and methylation, alter chromatin structures and affect the accessibility of the underlying genes to regulatory components (Kouzarides, 2007). Methylation of histone lysine residues is a relatively complex "code", which can exist in three different states: mono-, di- and tri-methylation. Depending on which amino acid residue is modified and how many methyl groups are added, the effects on transcriptional regulation could be positive or negative. The proteins that recognize these histone codes, known as "chromatin readers", often evolve structural domains that bind to specific modification sites with remarkable accuracy (Taverna et al., 2007) and translate these codes to the transcriptional status of genes.

One chromatin reader protein family of great interest is the Malignant Brain Tumor (MBT) family, characterized by a tandem repeat called the MBT domain. The MBT domain was first described in Drosophila l(3)mbt, a tumor-suppressor gene in Drosophila larval brain (Wismar et al., 1995). It consists of ~100 amino acids and is structurally related to the Royal family of chromatin binding domains Tudor, Chromo and PWWP (Maurer-Stroh et al., 2003). In mammals, nine MBT proteins have been found to date: L3mbtl1, L3mbtl2, L3mbtl3, L3mbtl4, Mbtd1, Scmh1, Scml2, Sfmbt1, and Sfmbt2, each containing two to four MBT domains. Structural evidence supports that MBT domains bind to methylated histone lysines (Sathyamurthy et al., 2003; Wang et al., 2003). The human L3mbtl1 gene is

located on chromosome 20q12, a region commonly deleted in patients with hematological disorders including polycythemia vera, myelodysplastic syndrome, and acute myeloid leukemia (Perna et al., 2010). L3mbtl1 contains three MBT domains, a C2HC zinc finger and an SPM oligomerization domain (**Fig 1.3**). *In vitro* assays showed that L3mbtl1 preferably binds to mono- and di-methylated histone lysines, as opposed to tri- and unmethylated lysine residues of H4K20 and H1bK26, via the second MBT domain (Kalakonda et al., 2008; Li et al., 2007; Min et al., 2007; Trojer et al., 2007). What is the functional importance of this high specificity for lower methylation status? Studies have found that several mono-methylated histone lysines correlate with gene activation (H3K27me, H3K9me, H4K20me, H3K79me, H2BK5me) (Barski et al., 2007; Vakoc et al., 2006). However, our knowledge about its biological relevance remains limited.

In heterologous cell lines, several lines of evidence suggest that L3mbtl1 acts as a transcriptional repressor upon binding to chromatin. For example, L3mbtl1 was reported to interact with TEL (ETS transcription factor subfamily), a key regulator in hematopoiesis, through SAM-SPM domain interactions, and mediate transcriptional repression of TEL target genes (Boccuni et al., 2003). Furthermore, L3mbtl1 has been shown to repress a subset of E2F target genes including c-myc, at least partly by direct compaction of chromatin via recognition of mono- and di-methylated H4K20 and H1bK26 (Trojer et al., 2007). L3mbtl1 also physically interacts with other non-histone proteins such as heterochromatin protein 1γ (HP1γ) and retinoblastoma protein (Rb) (Trojer et al., 2007), p53 tumor suppressor protein

Figure 1.3

Figure 1.3 Schematics of L3mbtl1 domain structure.

Blue box indicates MBT (Malignant Brain Tumor) domain; purple box indicates C2HC zinc finger domain; red box indicates SPM (SCM, PH, MBT) domain.

(West et al., 2010), and H4K20 mono-methyltransferase PR-SET7 (Kalakonda et al., 2008). Interaction of L3mbtl1 with TEL and E2F transcription factors suggests its possible role in hematopoiesis and cell cycle regulation. Indeed, knockdown of L3mbtl1 in human pluripotent stem cells results in enhanced hematopoiesis (Aziz et al., 2013; Perna et al., 2010), but impaired development of neural progenitors (Perna et al., 2015). However, it was reported that L3mbtl1 knockout mice have normal hematopoiesis, and that mouse embryonic stem (ES) cells lacking L3mbtl1 showed normal cell cycle progression (Qin et al., 2010).

A link between L3mbtl1 and DNA damage has also been reported by *in vitro* studies. The first evidence is that DNA damage decreases the mono-methylation level of p53 at lysine 382, and thus depletes L3mbtl1 from binding to p53 and its target promoters (West et al., 2010). Secondly, L3mbtl1 has also been shown to facilitate 53BP1 (p53 binding protein)-dependent repair of DNA double-strand breaks (DSBs) by dissociating from H4K20me2 sites (Acs et al., 2011). This is interesting because DNA DSBs can be triggered in neurons *in vivo* during seizure-induced overexcitation as well as physiologic neuronal activity involved in learning and memory (Crowe et al., 2006, 2011; Suberbielle et al., 2013). Of note, L3mbtl1 is expressed at high levels in mouse brain (Lein et al., 2007; Qin et al., 2010) and L3mbtl1 knockout mice display an abnormal anxiety and depression phenotype (Shen et al., 2015). This suggests that L3mbtl1 may serve yet unknown functions in post-mitotic neurons, particularly related to activity-induced plasticity.

To date, more than 20 histone methyl-codes and their modifiers have been

described in the context of neuroplasticity and psychiatric diseases. For example, studies suggest that levels of tri-methylation of Histone 3 Lysine 4 residues (H3K4me3), a mark for actively transcribing genes, and di-methylation of Histone 3 Lysine 9 residues (H3K9me2), a mark for transcription repression, are both associated with memory formation in contextual fear conditioning (Gupta et al., 2010). Interestingly, inhibition of histone deacetylase HDAC2 activity enhances memory formation and synaptic plasticity (Guan et al., 2009), elevates H3K4me3 and decreases H3K9me2 (Gupta et al., 2010). Another study identified an essential role for H3K9me2 and its di-methyltransferase G9a/G9a-like protein (GLP) in cocaine-induced plasticity; it was shown that repeated cocaine treatment induced genome-wide heightened gene expression through repression of GLP and H3K9me2 levels on promoter regions (Maze et al., 2010). Chronic social defeat stress induces downregulation of Bdnf expression through enhanced levels of repressive mark H3K27 methylation (Tsankova et al., 2006). In addition, histone methyltransferase mixed-lineage leukemia 1 (Mll1) has been shown to mediate H3K4 methylation at GABAergic gene promoters, a chromatin mark whose alterations are associated with schizophrenia (Huang et al., 2007). Moreover, mutations in many histone lysine methyltransferases and demethylases have been associated with patients with autism spectrum disorder (ASD), including EHMT1 (Kleefstra et al., 2012), JARID1C (Adegbola et al., 2008; Jensen et al., 2005; Santos et al., 2006), and PHF8 (Abidi et al., 2007; Koivisto et al., 2007; Laumonnier et al., 2005). With growing evidence pointing to the role for histone codes in

neuropsychiatric disorders, research on the signal receivers of these codes has only just begun.

Synaptic scaling, E/I balance and neurodevelopmental disorders

Over the past decade, a body of pathophysiological evidence in various neuropsychiatric disorders supports an emerging theme: disruption of E/I balance. Especially during critical developmental stages, a deficit in synapse formation and neural circuit refinement, or failure of maintaining plasticity into maturity could lead to an imbalance of excitatory and inhibitory neurotransmission and impairment of information processing and cognition (Hensch, 2004).

It has been proposed that autism spectrum disorders (ASD) may arise from an increase in the excitatory and inhibitory ratio, leading to hyper-excitability in the network (Rubenstein and Merzenich, 2003). Evidence supporting this theory include reduced GABA level measured in the frontal cortex of autistic children (Harada et al., 2011); decreased levels of GAD65 and GAD67, enzymes that synthesize GABA, in postmortem autistic brain (Fatemi et al., 2002; Yip et al., 2007); and disruption of $GABA_A$ and $GABA_B$ receptor expression (Collins et al., 2006; Fatemi et al., 2009, 2013). Indeed, approximately 30% of patients with autism develop early life epilepsy (Tuchman and Rapin, 2002). This all points to an altered inhibition and possibly a lack of homeostatic mechanisms to restore the E/I balance. To date, mutations in several genes involved in homeostatic synaptic scaling have been found to contribute to at least three forms of ASD described

below.

Rett syndrome, an autism-related disorder and leading cause of mental retardation in females, is caused by mutations in the X-linked gene MeCP2 (Amir et al., 1999). Recent studies have illustrated a critical role for MeCP2 in both synaptic upscaling and downscaling (Blackman et al., 2012; Qiu et al., 2012). The expression level of MeCP2 is shown to be regulated by activity, and knockdown of MeCP2 leads to failure of synaptic scaling during activity elevation and blockade, suggesting a mechanistic link between Rett syndrome and loss of synaptic scaling.

Another example is fragile X syndrome, a common known genetic cause of ASD. It has been reported that disruption of fragile X mental retardation protein (FMRP) caused by Fmr1 gene repeat expansion is responsible for disease development (Verkerk et al., 1991). FMRP binds to mRNA and regulates translation at synapses. Soden and Chen reported that FMRP is required for the retinoic acid (RA)-dependent form of synaptic scaling (discussed above) (Soden and Chen 2010).

Angelman syndrome (AS), characterized by motor dysfunction, mental retardation, seizures and autistic-like behaviors, is caused by deletion of the E3 ubiquitin ligase gene Ube3a (Williams et al., 2006). Contradicting results were reported about whether Ube3a can interact with Arc physically *in vivo* to mediate AMPA receptor internalization (Greer et al., 2010; but see Kühnle et al., 2013; Mabb et al., 2014; Pastuzyn and Shepherd, 2017). Despite a lack of consensus, Pastuzyn and Shepherd showed in a mouse model for AS (with deletion of the

maternal allele of the Ube3a gene) that Arc protein is more stable in dendrites, and synaptic scaling of AMPA receptors is disrupted, suggesting that Ube3a may regulate Arc expression through indirect pathways, but nevertheless is essential for homeostatic synaptic scaling (Pastuzyn and Shepherd, 2017).

In summary, disruption of important scaling factors may lead to unchecked disturbances in neuronal homeostasis and E/I imbalance, a common trait for ASD and other neuropsychiatric disorders (Ramocki and Zoghbi, 2008). Understanding the molecular underpinnings of synaptic scaling will impact discoveries for potential treatment to restore homeostasis in diseased brain.

Excitatory synapses in inhibitory interneurons

GABAergic inhibitory interneuron is another important aspect that contributes to maintenance of the E/I balance. While excitatory neurons often form long range projections and also cluster together with other excitatory neurons (Amaral and Witter, 1989; Song et al., 2005), inhibitory neuron connectivity is mostly local (Fino and Yuste, 2011). GABAergic interneurons form microcircuits with excitatory pyramidal cells and control their synchronized firing, giving rise to gamma oscillations, which is critical for cognitive functions in the brain (Cobb et al., 1995; Tamás et al., 2000; Whittington et al., 1995). Unlike excitatory neurons, which are mostly pyramidal cells, GABAergic interneurons comprise a diverse group of cell types distinguished by their morphologies, synaptic connections, and physiologic characteristics. They can be subcategorized by their expression of calcium-binding

proteins and neuropeptides, such as calbindin (CB), parvalbumin (PV), calretinin (CR), neuropeptide Y (NPY), vasoactive intestinal peptide (VIP), somatostatin (SOM) and cholecystokinin (CCK) (reviewed in Markram et al., 2004). An important factor that influences the strength of inhibition is the excitatory synaptic input onto inhibitory interneurons. Indeed, it has been shown that genetically disrupting AMPA or NMDA receptors at excitatory synapses onto parvalbumin-expressing (PV+) interneurons greatly decreases their inhibitory control over pyramidal neuron activity, causing major disruptions in network synchronization and impaired spatial working memory related behavior (Korotkova et al., 2010; Rácz et al., 2009).

The molecular architecture of excitatory synapses onto interneurons differs from those formed onto excitatory neurons. First, it has been shown that the major AMPA receptor subtypes are different in the two types of synapses (Angulo et al., 1997; Catania et al., 1995; Geiger et al., 1995; Kondo et al., 1997). The levels of NMDA receptors are also lower in interneurons (Goldberg et al., 2003). Postsynaptic molecules that interact with receptors are shown to be distinctly distributed. For example, receptor tyrosine-protein kinase ErbB4 is generally considered a selective marker for excitatory synapses onto interneurons (Fazzari et al., 2010; Vullhorst et al., 2009). ErbB4 directly interacts with the postsynaptic scaffold protein PSD-95 (Garcia et al., 2000; Huang et al., 2000) and plays a major role in the NRG(neuregulin)/ErbB signaling pathway in regulating both excitatory input and inhibitory output of interneurons (Buonanno, 2010). CaMKII and SynGAP are expressed more abundantly at excitatory synapses onto pyramidal neurons,

while Synapse-associated protein 97 (SAP97) and a PSD-95 binding protein Citron are more abundantly expressed in interneurons (Akgul and Wollmuth, 2013; (Zhang et al., 1999) .

Synaptic transmission and plasticity can behave differently depending on the postsynaptic target cells. EPSC kinetics exhibit faster rise times and decay times in interneurons than those in pyramidal neurons (Aaron and Dichter, 2001). Differences were also observed in some but not all forms of short-term plasticity, for example pyramidal-interneuron connections exhibited less paired-pulse facilitation than pyramidal-pyramidal connections (Sun et al., 2005). Long-term plasticity is also different. Whether NMDAR-dependent LTP exists at excitatory synapses onto inhibitory neurons remains controversial (Lamsa et al., 2005; Maccaferri and McBain, 1995; McMahon and Kauer, 1997; Ouardouz and Lacaille, 1995). Lamsa *et al.* showed that a specific form of non-Ca^{2+}/calmodulin-dependent NMDAR-dependent LTP is observed in interneurons, as opposed to the Ca^{2+}/calmodulin-dependent NMDAR-dependent LTP in pyramidal neurons (Lamsa et al., 2007a). Additionally, the same stimulation in mossy fibers that elicits NMDAR-independent LTP in CA3 pyramidal cells induced LTD or no change in interneurons (Maccaferri et al., 1998).

As for homeostatic synaptic scaling, activity triggers opposite effects in excitatory synapses onto excitatory neurons versus excitatory synapses onto inhibitory interneurons. For example, Arc has been shown to promote GluA1-containing AMPA receptor endocytosis in excitatory pyramidal neurons during

activity elevation (Shepherd et al., 2006). In PV+ interneurons, however, a different molecule Narp (neuronal activity-regulated pentraxin) is triggered by activity to insert GluA4-containing AMPA receptors at excitatory synapses, thus complementarily enhancing inhibition in the network (Chang et al., 2010). Understanding the distinct compositions of these synapses and how molecular mechanisms specifying each type of synaptic connection differ are therefore valuable.

Standing questions and the scope of this dissertation

My thesis research focuses on two important components in preserving excitatory and inhibitory balance in the brain: homeostatic control of synaptic strength, and excitatory synaptic scaffold in inhibitory interneurons. Many synaptic scaling factors have been identified that regulate synaptic strength from various aspects. Endocytosis and exocytosis of postsynaptic receptors, scaffold proteins at the postsynaptic densities, kinases associated with Ca^{2+} signaling, cell adhesion molecules, ubiquitin-proteasome system, etc., can all be regulated in an activity-dependent manner and influence the homeostasis of synaptic efficacy. Although much progress has been made in understanding how activity-dependent transcription mediates homeostatic synaptic scaling, the role of epigenetic mechanisms, particularly chromatin regulators, in this process remains to be explored. The work presented in Chapter II describes my discovery of a novel role for the chromatin reader protein L3mbtl1 in synaptic scaling and synaptic

transmission. Using a genome-wide approach, I determined the downstream target genes involved in L3mbtl1-mediated regulation of synaptic scaling. For the last decade, many studies have focused on excitatory synapses and inhibitory synapses onto pyramidal neurons. The research on the molecular architecture of excitatory synapses onto inhibitory interneurons, which serves an important role in controlling circuit excitability and maintaining E/I balance, has just begun. In Chapter III, I will present the work I did in collaboration with Takuya Watanabe et al. to understand the role of the excitatory synaptic scaffold protein Shank1 in parvalbumin-expressing inhibitory interneurons. Finally, in Chapter IV, I will present the conclusions, significance, and limitations of both studies, and discuss the implications for future research.

CHAPTER II

Activity-induced epigenetic regulation of synaptic strength through the chromatin reader, L3mbtl1

CHAPTER II

Activity-induced Epigenetic Regulation of Synaptic Strength through the

Chromatin Reader, L3mbtl1

Preface

This chapter is currently under review as:

Mao, W., Salzberg, A.C., Uchigashima, M., Hasegawa, Y., Hock, H., Watanabe, M., Akbarian, S., Imamura, Y. and Futai, K. Activity-induced epigenetic regulation of synaptic strength through the chromatin reader, L3mbtl1

Author contributions:

K.F. and W.M designed research;

W.M., A.C. S., M.U., K.N. M., Y.H., A.S., Y.I.K., M.W. and K.F. performed experiments;

W.M., Figure 2.1, 2.2A-D, 2.3, 2.4, 2.5, 2.6, 2.7, 2.8, 2.9, 2.10A-D, 2.11, 2.12, 2.13, 2.14, 2.15;

A.C. S., Figure 2.1, 2.2A-B, 2.10E-G, 2.11C;

M.U., Figure 2.2E-G;

Y.H., Figure 2.10A;

W.M., A.C. S., M.U., Y.H., H.H., Y.I.K., S.A. and K.F analyzed data;

W.M., M.U., H.H., Y.I.K., M.W., S.A. and K.F. wrote the paper.

Abstract

Excitatory and inhibitory synaptic strength are finely tuned by homeostatic mechanisms, such as synaptic scaling, which detect and respond to changes in neural network activity. Homeostatic synaptic down-scaling reduces neuronal excitability by modulating the number of postsynaptic receptors via activity-dependent transcription and protein synthesis. The mechanisms underlying neuronal excitation-dependent gene expression have broad implications for neuronal homeostasis and disorders including epilepsy, autism spectrum disorders and Alzheimer's disease. Gene expression, in turn, is affected by chromatin remodeling and histone modification. Histone modification codes are recognized by regulatory proteins, such as chromatin readers, which affect gene expression by altering chromatin structure and recruiting chromatin effector proteins.

We show that L3mbtl1 (Lethal 3 malignant brain tumor like 1), a polycomb chromatin reader, is down-regulated by neuronal activity through the ubiquitin proteasomal pathway and is essential for excitatory synaptic response and homeostatic synaptic plasticity. Genome-scale mapping of L3mbtl1 protein occupancies on chromatin identified Ctnnb1 (ß-Catenin), an essential regulator of synaptic transmission and plasticity, as a key gene downstream of L3mbtl1. Importantly, the occupancy of L3mbtl1 on the Ctnnb1 gene is regulated by neuronal activity. L3mbtl1 knockout neurons exhibited reduced Ctnnb1 expression, while a partial knockdown of Ctnnb1 in wild type neurons, which mimicked the level

of Ctnnb1 in KO neurons, caused reduced excitatory synaptic transmission and a lack of homeostatic down-scaling. These results highlight a unique role for L3mbtl1 in regulating homeostasis of synaptic efficacy through one of its downstream targets, ß-Catenin.

Introduction

Runaway excitation of neuronal circuits induces epileptic seizures, leading to other detrimental consequences, including neuronal cell death. Neurons possess homeostatic mechanisms that compensate for activity perturbations and maintain the excitatory and inhibitory balance (E/I balance). For example, excitatory and inhibitory synaptic strength are regulated by changing the abundance (scale) of ionotropic receptors, including glutamate and GABA$_A$ receptors, at postsynaptic sites through cell autonomous mechanisms, referred to as homeostatic synaptic scaling. Elevated neuronal activity induces Ca^{2+} influx followed by subsequent activation of the Ca^{2+}/calmodulin-dependent signaling cascade and down-regulation of the postsynaptic AMPA-type glutamate receptor (AMPAR)-mediated response at excitatory synapses (Goold and Nicoll, 2010). Furthermore, elevated neuronal activity induces compensatory activation of inhibitory synaptic transmission through the recruitment of GABA$_A$Rs to inhibitory postsynaptic sites (Saliba et al., 2007) and the increased release of GABA from inhibitory terminals (Peng et al., 2010).

A number of molecules that bridge the induction and expression steps of

homeostatic synaptic down-scaling, have been identified. The majority of these molecules are synaptic scaffolds, kinases and phosphatases that directly regulate synaptic function (**Table 2.1**). More than 10 genes, including Arc (Shepherd et al., 2006), Homer1a (Hu et al., 2010), and polo-like kinase 2 (Plk2) (Seeburg et al., 2008), display altered expression levels upon an increase in neuronal activity, and are critical for the expression of homeostatic synaptic down-scaling (**Table 2.1**). Importantly, actinomycin D and anisomycin, inhibitors of transcription and translation, respectively, dysregulate homeostatic synaptic plasticity (Ibata et al., 2008; Schanzenbächer et al., 2016). These results clearly illustrate the critical role of activity-dependent transcriptional and translational machineries in homeostatic synaptic scaling. However, the roles of epigenetic factors, particularly chromatin regulators, in this plasticity is relatively unknown.

Epigenetic modifications, including DNA and histone modifications, provide a crucial regulatory layer for gene expression. Methyl-CpG-binding protein 2 (Mecp2) acts as a DNA reader by binding to methylated DNA (CpG dinucleotides) and represses transcription of target genes, such as Bdnf (Chahrour and Zoghbi, 2007). Knockout, knockdown or functional mutation of Mecp2 causes deficits in long-term synaptic plasticity, motor skills, spatial learning, and homeostatic synaptic plasticity (Asaka et al., 2006; Blackman et al., 2012; Guy et al., 2007; Moretti, 2006; Pelka et al., 2006; Qiu et al., 2012; Shahbazian et al., 2002; Zhong et al., 2012). In addition, DNA methylation status and histone methyltransferase regulate homeostatic synaptic scaling (Benevento et al., 2016; Meadows et al.,

2015). However, knowledge of the functions of chromatin regulators in homeostatic synaptic plasticity is still very limited. Over two hundred chromatin regulators have been identified in mammals and these regulators are sub-classified by function (e.g., readers, erasers or writers of histone modifications, etc.). However, to the best of our knowledge, there are no reports describing a systematic analysis of chromatin regulators for potential roles in homeostatic synaptic plasticity.

Chromatin readers influence chromatin conformation by binding to specific histone modifications, thereby regulating gene expression. One of the chromatin reader genes, L3mbtl1, is a member of the MBT (Malignant Brain Tumor) protein family. The L3mbtl1 protein is classified as a Polycomb group (PcG) protein. PcG proteins exert gene silencing functions in Polycomb Repressive Complexes (PRC), which bind to specific methylated histone tails (Di Croce and Helin, 2013). L3mbtl1 binds to chromatin through three tandem MBT repeats (3xmbt), which facilitates higher order chromatin organization via binding to methylated lysine residues in histone tails (Li et al., 2007; Min et al., 2007; Sims and Rice, 2008; Trojer et al., 2007). Specifically, L3mbtl1 binds to mono- and dimethylated histone tails, but not trimethylated and unmethylated histone tails. Thus, L3mbtl1 protein contributes to the complex organization of chromatin as a chromatin reader (Adams-Cioaba and Min, 2009), and acts as an effector for post-translational histone modifications (Bonasio et al., 2010). The L3mbtl1-containing PRC functions as a repressor in heterologous cell lines (Boccuni et al., 2003; Kalakonda et al., 2008; Trojer et al., 2007) and human pluripotent stem cells (Perna et al., 2015). *Drosophila* l(3)mbt

[dl(3)mbt], the closest homolog of mammalian L3mbtl1, is an embryonic lethal gene associated with malignant transformation in larval brain (Wismar et al., 1995). In mammals, the expression of L3mbtl1 is highest in the brain and testis, and low in bone marrow, thymus and spleen (Qin et al., 2010). The deletion of Chromosome 20q12, the locus of human L3mbtl1, is associated with polycythemia vera, myelodysplastic syndrome, and acute myeloid leukemia (Gurvich et al., 2010; Perna et al., 2010). Of note, L3mbtl1 is expressed at high levels in mouse brain (Lein et al., 2007; Qin et al., 2010) and L3mbtl1 KO mice display abnormal anxiety and depression phenotypes (Shen et al., 2015). These results suggest that L3mbtl1 may serve yet unknown functions in post-mitotic neurons.

β-catenin protein, encoded by Ctnnb1, is known as a core molecule of the WNT signaling pathway and has pivotal roles in neuronal development and synaptic function by acting as a transcriptional factor in neuronal nuclei and as a component of synaptic scaffolding at excitatory synapses (Mosimann et al., 2009; Uchida et al., 1996). β-catenin regulates the expression of bidirectional homeostatic synaptic plasticity via interactions with cadherin, a homophilic trans-synaptic adhesion molecule regulating synaptic structure and function (Okuda et al., 2007). However, the epigenetic regulatory mechanisms underlying β-catenin expression are still largely unknown.

In this study, we demonstrate that L3mbtl1 mRNA is primarily expressed in neurons, and is decreased when neuronal activity is elevated. Knockout of L3mbtl1 causes a reduced excitatory synaptic transmission in primary neurons and

a lack of homeostatic down-scaling at excitatory synapses both in hippocampal primary neurons and organotypic slice cultures. Importantly, L3mbtl1 protein binds to the transcription start sites of Ctnnb1 and Gabra2, whose products mediate homeostatic synaptic scaling and inhibitory synaptic transmission, respectively. These results provide novel insight as to the roles of a chromatin reader molecule in synaptic function and neuronal homeostasis.

Results

L3mbtl1 expression is down-regulated by neuronal activity

To date, 46 genes have been reported as regulators of homeostatic up- and down-scaling in hippocampal and cortical neurons (**Table 2.1**). Because the expression of many of these genes changes during induction and expression of the scaling (red and green highlights in **Table 2.1**), we hypothesized that chromatin regulator molecules, whose expression is altered by neuronal activity, contribute to homeostatic synaptic scaling. To test this hypothesis, we performed unbiased transcriptome analysis by RNA-sequencing of cultured primary neurons after induced homeostatic down-scaling.

Hippocampal primary cultures were prepared from C57BL6 mice and homeostatic synaptic scaling was induced by applying picrotoxin (PTX), a non-competitive $GABA_A R$ blocker, for 15 hours at days *in vitro* 14 (DIV14). Total RNA isolated from Control (DMSO treated) and PTX challenged samples was subjected

to an unbiased transcriptome (RNA-Seq) screen. RNA-seq was performed in quadruplicate for each treatment and the results were highly clustered into two treatment groups (**Fig 2.1**). Using stringent criteria (control versus PTX treatment, *fold change* >2.0, FDR *adjusted p value* < 0.01), we identified 1150 and 689 of up- and down-regulated genes, respectively (**Fig 2.2, Table 2.2**). Multiple genes previously identified as neuronal activity-dependent, including Arc (Shepherd et al., 2006), Bdnf (Ghosh et al., 1994), Plk2 (Seeburg et al., 2008), and Homer1 (Hu et al., 2010), showed a significant change from baseline in our transcriptome profiling, confirming the validity of our system (blue symbols in **Fig 2.2A**). Importantly, 12 out of 246 chromatin regulatory genes showed changes in mRNA expression (**Fig 2.2B, Table 2.2D**). In particular, L3mbtl1 mRNA expression was decreased to 30% of control value (0.33 fold change, Padj = 1.0E-06, differential expression analysis by DESeq2), as the top ranking down-regulated molecule amongst chromatin regulatory genes, (**Fig 2.2B**, blue symbol). Quantitative PCR (qPCR) further confirmed the activity-dependent down-regulation of L3mbtl1 expression (**Fig 2.2C**). In contrast, expression of L3mbtl1 mRNA was insensitive to tetrodotoxin (TTX), a voltage-gated sodium channel blocker, treatment. These results suggest that the expression of L3mbtl1 is regulated only when neuronal activity is elevated.

L3mbtl1 is a MBT gene highly expressed in neurons during early development

We further addressed the expression profiles of L3mbtl1 transcripts and protein in

the hippocampus. Expression of both L3mbtl1 mRNA and protein reached peak levels during postnatal days 7 to 14 after which expression decreased and remained relatively low thereafter (**Fig 2.2D**). Chromogenic *in situ* hybridization indicated wide expression of L3mbtl1 mRNA in the brain with highest intensity in the hippocampus (**Fig 2.2 E**, upper left). The hippocampus exhibited strong signals in the pyramidal cell layer but less so in granule cells in the dentate gyrus (**Fig 2.2E**, upper right). The hybridizing signals were completely abolished in L3mbtl1 KO mice (**Fig 2.2E**, bottom), validating the specificity of the hybridization probes. Double-label fluorescent *in situ* hybridization in the CA3 region confirmed that L3mbtl1 mRNA is expressed in both excitatory and inhibitory neurons, but the signal intensities of L3mbtl1 in non-neuronal cells (astrocytes, oligodendrocytes and microglia) were equivalent to the background level in L3mbtl1 KO (**Fig 2.2 F, G**). These data demonstrate that L3mbtl1 is predominantly expressed in neurons of postnatal brains.

Characterization of neuronal activity-dependent down-regulation of L3mbtl1

Among differentiated tissues, L3mbtl1 is most abundantly expressed in the brain (Qin et al., 2010), and in the hippocampus, exclusively expressed in neurons based on *in situ* hybridization studies (**Fig 2.2 F, G**). To further characterize the regulation of L3mbtl1 expression by neuronal activity, total RNA was extracted from PTX-treated and control hippocampal neuronal cultures at different time points (4, 15, 24 and 48 hours after application of drugs), followed by qPCR.

Consistent with the results of RNA-Seq (**Fig 2.2B**), L3mbtl1 mRNA levels started to decrease 4 hours after application of PTX, and reached the lowest level (less than 30% of control level) after 15 hours (**Fig 2.3A**). Expression of L3mbtl1 protein exhibited a steady reduction and at 48 hours after PTX treatment reached 30% of the control group levels.

Next, we performed pharmacological experiments (**Fig 2.3B**) and observed that blockage of AMPAR, NMDAR or L-type Ca^{2+}-channels alone did not fully rescue PTX-induced down-regulation of L3mbtl1 mRNA. In contrast, simultaneous inhibition of AMPAR, NMDAR and L-type Ca^{2+}-channels completely abolished the neuronal activity-dependent decrease of L3mbtl1 expression. These results suggest that neuronal L3mbtl1 down-regulation requires elevation of the intracellular Ca^{2+} concentration.

In cell lines, DNA double strand breaks (DSBs) induce rapid dissociation of L3mbtl1 protein from chromatin, followed by degradation via the ubiquitin-mediated proteasomal pathway (Acs et al., 2011). We asked whether induction of homeostatic down-scaling induces the ubiquitination and degradation of L3mbtl1. To address this possibility, we cultured hippocampal neurons in the presence of the proteasomal inhibitor, MG-132 and induced homeostatic down-scaling with PTX. Nuclei were harvested 24 hours after PTX treatment with or without MG-132, followed by measurement of L3mbtl1 expression. As shown in **Fig 2.3A**, 24 hours of PTX treatment significantly reduced the expression of L3mbtl1 (**Fig 2.3C**). However, MG-132 blocked the down-regulation of L3mbtl1 protein by PTX,

suggesting a role for ubiquitin-mediated proteasomal signaling in L3mbtl1 down-regulation. MG-132 itself did not cause a significant reduction of L3mbtl1 protein.

Loss of homeostatic down-scaling, reduced excitatory synaptic strength and surface GluA1 expression in primary L3mbtl1 knockout neurons

If the decreases of L3mbtl1 transcripts and protein are part of an essential switch to induce homeostatic synaptic down-scaling, then loss of L3mbtl1 should prevent homeostatic synaptic scaling upon activity elevation. To test this hypothesis, we prepared hippocampal primary cultures from wild type and L3mbtl1 KO mice and compared amplitudes and frequencies of AMPA receptor-mediated miniature excitatory postsynaptic currents (mEPSCs) from neurons in which down-scaling had been induced by PTX treatment for 48 hours (**Fig 2.4**). We found that L3mbtl1 KO cultured neurons failed to induce homeostatic scaling-down by PTX treatment, whereas wild type neurons were capable of inducing bidirectional up- and down-scaling. Homeostatic scaling-up by TTX was intact in L3mbtl1 KO cultures, suggesting that the effects of L3mbtl1 on homeostatic synaptic scaling are unidirectional. Interestingly, we observed that, under basal conditions, L3mbtl1 KO neurons showed significantly smaller mEPSC amplitudes than that of wild type, suggesting that a lack of L3mbtl1 reduces the number and/or conductance of AMPA receptors per synapse (**Fig 2.4C**). This observation raises the possibility that the lack of homeostatic down-scaling results from the floor effect of reduced basal AMPAR-mediated response. The frequencies of mEPSCs were not changed

by L3mbtl1 genetic deletion or drug treatments, suggesting that the number of active excitatory synapses and/or presynaptic release probability remain unaffected (**Fig 2.4C**). Taken together, we conclude that L3mbtl1 regulates basal synaptic transmission and homeostatic synaptic down-scaling at excitatory synapses in primary neurons.

Removal of AMPARs at postsynaptic sites is an established mechanism for down-scaling (Pozo and Goda, 2010). We therefore examined the level of surface GluA1, one of the major AMPAR subunits in hippocampal primary neurons, prepared from wild type and L3mbtl1 KO mice (**Fig 2.5**). Importantly, L3mbtl1 KO neurons showed a lack of PTX-induced down-regulation of surface GluA1 and reduced surface GluA1 expression under basal conditions compared with wild type neurons. These results suggest that the lack of down-scaling and the reduction of basal mEPSC amplitude are a consequence of the decreased surface expression of AMPARs.

The strength of inhibitory synaptic transmission is also regulated bidirectionally dependent on neuronal activity (Turrigiano, 2011). Activity elevation and blockade cause enhancement and suppression of inhibitory synaptic transmission in primary neurons, respectively. To address whether L3mbtl1 is involved in inhibitory synaptic scaling, we induced homeostatic scaling by applying bicuculline, a competitive $GABA_A R$ antagonist, and TTX in wild type and KO neurons, and compared amplitudes and frequencies of $GABA_A$ receptor-mediated miniature inhibitory postsynaptic currents (mIPSCs) (**Fig 2.6**). We found that

L3mbtl1 KO neurons showed reduced basal mIPSC amplitudes compared with those of wild type, but both exhibited intact homeostatic up- and down-scaling. Therefore, in contrast to its effects on excitatory synapses, the role of L3mbtl1 on inhibitory synaptic function is small.

Loss of homeostatic down-scaling in organotypic L3mbtl1 knockout neurons

The results described above were obtained in dissociated primary cultures, raising the question as to whether the function of L3mbtl1 may be different in a more physiological experimental system. Hippocampal CA3 pyramidal neurons in organotypic slice cultures have been shown to self-restore synaptic connectivity and spontaneous network activity to a level resembling the *in vivo* situation situation (Takahashi et al., 2010). Furthermore, it has been reported that CA3 synapses are capable of inducing homeostatic scaling (Lee et al., 2013; Mitra et al., 2012), Therefore, we recorded mEPSCs from hippocampal CA3 pyramidal neurons in organotypic slice cultures. We found that PTX treatment induced scaling down in wild type but not L3mbtl1 KO neurons (**Fig 2.7**). In contrast to the results from primary cultures, basal synaptic transmission was not significantly different between wild type and L3mbtl1 KO neurons in slice culture (**Fig 2.7**). This discrepancy could be due to the differences in experimental systems; for example, dissociated primary cultures have been shown to exhibit higher network neuronal activity compared to organotypic hippocampal neurons that display *in vivo*-like

activity levels (Cingolani and Goda, 2008; Takahashi et al., 2010). While loss of L3mbtl1 in primary cultures impairs basal excitatory synaptic transmission, our results suggest that L3mbtl1 specifically regulates homeostatic down-scaling but not basal excitatory synaptic strength in hippocampal CA3 neurons.

Acute knockdown of L3mbtl1 causes a lack of homeostatic down-scaling in hippocampal CA3 pyramidal neurons

It is possible that developmental effects underlie the loss of homeostatic down-scaling in L3mbtl1 KO neurons. To address the role of L3mbtl1 in postnatal neurons, we acutely knocked down (KD) L3mbtl1 and measured homeostatic down-scaling in CA3 pyramidal neurons. shRNA directed against L3mbtl1 (**Fig 2.8**) was transfected into organotypic hippocampal slice cultures from wild type mice using a biolistic gene gun that allows us to test cell-autonomous function of genes of interest. Importantly, L3mbtl1 KD blocked homeostatic down-scaling in CA3 pyramidal neurons without affecting basal synaptic strength (**Fig 2.9**), a finding consistent with the results obtained from L3mbtl1 KO slice cultures (**Fig 2.7**). This result suggests that L3mbtl1 plays a critical and cell-autonomous role in homeostatic down-scaling in CA3 pyramidal neurons.

L3mbtl1 occupies gene promoters in hippocampus

To determine the binding loci of L3mbtl1 protein on a genome-wide scale, we performed chromatin immunoprecipitation (ChIP) followed by deep sequencing

(ChIP-seq). ChIP-seq experiments were performed with an antibody against endogenous L3mbtl1 in P7 hippocampus when the expression of L3mbtl1 reaches a maximal level, using KO mouse hippocampus as control (**Fig 2.10**). Reproducible peaks were obtained from three biological replicates using MACS2 with Irreproducible Discovery Rate (IDR) threshold of 0.0025 as a consistency test (**Table 2.3A**). We identified 4677 highly consistent L3mbtl1-bound regions, 93% of which are located within 5kb up- and down-stream of a transcriptional start site (TSS) (**Fig 2.10C**), and 47% of which are located in promoter regions (within -1kb to 100bp of a TSS) (**Fig 2.10B, Table 2.3B**), consistent with the notion that L3mbtl1 is a regulator of gene expression.

For gene ontology analysis, bound regions within 1kb up- and down-stream from a TSS were assigned to the nearest genes. We assigned 3188 genes as targets for L3mbtl1 (**Table 2.3C**) and the 3000 genes with the highest peak scores were tested for functional enrichment by DAVID (Database for Annotation, Visualization and Integrated Discovery) (Huang et al., 2009a, 2009b) (**Fig 2.10D, Table 2.3D**). Of note, L3mbtl1 target genes were significantly enriched for GO terms related to transcriptional regulation, nucleosome assembly and other nuclear signaling, as observed for Sfmbt1 and Scml2, other members of the MBT domain-containing protein family in the cell lines (Bonasio et al., 2014; Zhang et al., 2013). We also found "synapse" among the top 20 enriched terms, which may include genes responsible for the defects in synaptic transmission and homeostatic synaptic plasticity in L3mbtl1 KO mice.

Previous studies showed that human L3mbtl1 binds to mono- and di-methylated histone lysine residues of H1bK26 and H4K20 and generally acts as a nucleosome compactor and transcriptional repressor in cell lines (Boccuni et al., 2003; Kalakonda et al., 2008; Trojer et al., 2007) and pluripotent stem cells (Perna et al., 2015). To analyze L3mbtl1 binding specificity *in vivo,* we investigated whether L3mbtl1 binds to chromatin regions with active or inactive chromatin marks. Using a published ATAC-seq and ChIP-seq dataset (GEO GSE63137) generated from mouse cortical excitatory neurons (Mo et al., 2015), we performed correlation analysis of L3mbtl1 binding sites with those of multiple histone marks (H3K27ac, H3K27me3, H3K4me1 and H3K4me3) and open chromatin sites marked by ATAC-seq signals (**Fig 2.10E**). Interestingly, L3mbtl1 binding correlates with open chromatin sites as well as potential active transcription initiation sites marked by H3K4me3 and H3K27ac. L3mbtl1, H3K4me3 and H3K27ac also showed a similar distribution pattern near TSS (**Fig 2.10 F, G**). Genome-wide analysis of L3mbtl1 ChIP-seq signals near TSS revealed four clusters with distinct patterns for L3mbtl1 binding (**Fig 2.10G**), which highly correlate with signal patterns for ATAC, H3K4me3 and H3K27ac. In contrast, L3mbtl1 binding was not correlated with H3K27me3 or H3K4me1. Therefore, L3mbtl1 primarily localizes to open chromatin sites associated with active chromatin marks H3K4me3 and H3K27ac.

L3mbtl1 regulates genes that control synaptic strength

To understand how L3mbtl1 mediates the homeostatic control of synaptic strength, we focused on a list of putative target genes that have been previously associated with synaptic scaling or synaptic transmission (**Table 2.1, Fig 2.11A**). Total mRNA was isolated from primary cultures prepared from wild type and L3mbtl1 KO mice, and RT-qPCRs were carried out to identify differentially expressed genes. The expression of two genes, Ctnnb1 and Gabra2, were significantly decreased in the absence of L3mbtl1 (**Fig 2.11B**). Importantly, both genes showed L3mbtl1 binding and the presence of H3K4me3 and H3K27ac near their TSS (**Fig 2.11C**). To verify the ChIP-seq results, we confirmed the enrichment for L3mbtl1, H3K4me3 and H3K27ac at Ctnnb1 and Gabra2 promoter regions in both P7 hippocampus and cultured neurons by ChIP-qPCR (**Fig 2.11 D, E**). We also examined the levels of L3mbtl1, H3K4me3 and H3K27ac at Ctnnb1 and Gabra2 promoter regions after 24 hours of PTX treatment in primary cultures (**Fig 2.11 D, E**), and found that while H3K4me3 and H3K27ac were still enriched at promoter regions, L3mbtl1 was no longer enriched. Together, these findings demonstrate that L3mbtl1 occupies Ctnnb1 and Gabra2 gene promoters in an activity-dependent manner, suggesting a possible role for L3mbtl1 in regulating the activity-dependent expression of Ctnnb1 and Gabra2.

To address whether Ctnnb1 contributes to the effects of L3mbtl1 on synaptic scaling, we tested if knockdown of Ctnnb1 expression affects synaptic scaling and synaptic transmission. Using shRNA that induces partial KD of Ctnnb1 in wild type neurons (**Fig 2.12**), we showed that partial KD of Ctnnb1 was sufficient to abolish

homeostatic down-scaling and weaken basal excitatory synaptic transmission (**Fig 2.13**), thus mimicking the phenotype observed in L3mbtl1 KO primary neurons (**Fig 2.4**). These results suggest that Ctnnb1 mediates part of the effect of L3mbtl1 on homeostatic control of synaptic strength, but additional L3mbtl1 targets may also be involved. Another L3mbtl1 target gene Gabra2 encodes the alpha-2 subunit of GABA$_A$ receptors. The reduced expression of the Gabra2 gene in L3mbtl1 KO neurons is likely responsible for our finding that basal inhibitory synaptic transmission is decreased in L3mbtl1 KO neurons compared to that in wild type (**Fig 2.6**).

Discussion

The number of neurotransmitter receptors located postsynaptically is dynamically regulated through many different mechanisms. Homeostatic synaptic scaling is one of the most important regulatory mechanisms of synaptic strength that prevent the detrimental consequences of runaway neuronal over excitation. However, in contrast to long-term synaptic plasticity (e.g., long-term potentiation) for which a growing body of evidence indicates the importance of epigenetic mechanisms (Vogel-Ciernia and Wood, 2014), our understanding of chromatin regulatory mechanisms underlying homeostatic scaling remains relatively limited. In the present study, we found that the chromatin reader molecule, L3mbtl1, is down-regulated when neuronal activity is increased. Hippocampal primary neurons prepared from L3mbtl1 KO mice show reduced quantal amplitude of AMPAR

current and a lack of homeostatic down-scaling in excitatory synapses. Furthermore, L3mbtl1 KO and KD neurons in organotypic hippocampal neurons specifically abolished down-scaling without changing basal transmission, supporting the importance of L3mbtl1 in homeostatic down-scaling. Our ChIP-seq and ChIP-qPCR studies identified Ctnnb1 and Gabra2 genes as activity-dependent targets of L3mbtl1 protein. Ctnnb1 expression is reduced in L3mbtl1 KO and partial KD of Ctnnb1 causes a lack of homeostatic down-scaling, suggesting that Ctnnb1 contributes to the role of L3mbtl1 in controlling synaptic strength. Our results highlight a critical role for the activity-regulated chromatin reader molecule, L3mbtl1, in homeostatic control of synaptic strength and adds to our understanding of epigenetic mechanisms of activity-dependent gene regulation.

Roles of L3mbtl1 in synaptic transmission and synaptic scaling

Neuronal activity perturbation induces a series of transcriptional regulatory events that alter chromatin structure, leading to a long-lasting effect on gene expression (Guan et al., 2002). These activity-dependent transcriptional regulations are involved in homeostatic scaling of synaptic strength, which is of critical importance for maintenance of the proper level of neuronal activity and connectivity. The present study identified an activity-regulated chromatin reader, L3mbtl1, whose expression is exclusive to neurons in hippocampus, as a key regulator for homeostatic synaptic scaling.

We observed differential effects of L3mbtl1 KO in dissociated primary cultures and organotypic slice cultures. Although both L3mbtl1 KO primary and organotypic neurons displayed disruption of synaptic down-scaling, L3mbtl1 KO primary neurons also showed reduced basal excitatory synaptic transmission. L3mbtl1 may be a regulator for basal AMPAR-mediated synaptic strength and the failure of homeostatic down-scaling could be attributed to a floor effect of a reduced number of AMPARs per synapses in primary neurons. However, arguments could be made that the activity-regulated L3mbtl1 transcript and protein levels, and the activity-dependent dissociation of chromatin-bound L3mbtl1 from its target promoters strongly suggest a tightly controlled signaling pathway specifically activated during activity elevation. Indeed, both conventional KO and acute KD of L3mbtl1 in organotypic slice cultures blocked homeostatic down-scaling in excitatory synapses without altering baseline AMPAR abundance, indicating a critical and cell-autonomous role for L3mbtl1 and its downstream genes in synaptic down-scaling. The mechanism underlying the differential effect of L3mbtl1 KO in basal synaptic transmission in primary and organotypic slice cultures may be due to, i) the difference of recoding from heterologous primary neurons and homogenous CA3 pyramidal neurons in slice cultures, and/or ii) differential basal synaptic activity between primary and organotypic slice cultures (Cingolani and Goda, 2008).

Our ChIP study identified L3mbtl1 occupancy on 14 genes associated with homeostatic synaptic scaling and 64 synaptic genes (**Table 2.1 and 2.3D**). Among

them, two genes, Ctnnb1 and Gabra2, were shown to contribute to the effect of L3mbtl1 on homeostatic regulation of excitatory synaptic strength and basal inhibitory synaptic transmission, respectively.

Ctnnb1 (β-catenin) has indispensable roles in many neurodevelopmental processes including migration and synapse formation and maturation, as a transcription factor and a synaptic scaffold molecule (Mosimann et al., 2009; Takeichi, 2007). At excitatory synaptic sites, α- and β-catenin, N-cadherin, and actin assemble to form an adhesion complex necessary for synapse formation and maturation (Uchida et al., 1996). β-catenin KO neurons exhibit reduced basal excitatory synaptic transmission and lack of homeostatic up- and down-scaling (Okuda et al., 2007). Goda and colleagues illustrated the importance of interactions between β- catenin and N-cadherin on basal excitatory synaptic transmission and homeostatic synaptic plasticity. Thus, our results suggest that ß-catenin causes at least part of the effect of L3mbtl1 on excitatory synaptic strength. Further studies will allow us to assess whether additional L3mbtl1 target genes are involved.

The composition of $GABA_AR$ subunits in hippocampus changes during development. The expression of Gabra2 is high at postnatal day 0 and decreases during development (Fritschy et al., 1994). Although homeostatic scaling of mIPSCs was intact in L3mbtl1 KO neurons (**Fig 2.6**), we observed a reduced basal inhibitory synaptic transmission in L3mbtl1 KO neurons compared with that in wild type (**Fig 2.6 E, F**). The amplitude of mIPSC in L3mbtl1 KO neurons is smaller

than that in wild type neurons, which can be attributed to the reduced expression of Gabra2 in L3mbtl1 KO neurons.

L3mbtl1-mediated transcriptional regulation

The three MBT domains in L3mbtl1 protein compact chromatin by binding to mono- and dimethylated histone marks, including H1bK26, H3K9 and H4K20 (Li et al., 2007; Min et al., 2007; Sims and Rice, 2008; Trojer et al., 2007). In heterologous cell lines, L3mbtl1 forms a complex with heterochromatin protein 1γ (HP1γ) and retinoblastoma protein (Rb), and contributes to repression of E2F target genes (Trojer et al., 2007). In this study, we for the first time identified the *in vivo* binding sites of L3mbtl1 in the brain. Our analysis of genomic occupancy suggested that L3mbtl1 primarily localizes to open chromatin sites associated with histone marks for active chromatin. Two genes, Ctnnb1 and Gabra2, bound by L3mbtl1 at their promoter regions, showed reduced transcript levels in the absence of L3mbtl1, suggesting that L3mbtl1 may act as an activator of these genes. Taken together with previous reports, the data suggest that L3mbtl1 acts as a transcriptional activator or repressor depending on the gene targets and cell types. We also observed that the binding of L3mbtl1 to the promoters of these genes was abolished by PTX treatment, indicating that upon neuronal activity elevation, L3mbtl1 protein dissociates from chromatin of target genes. Therefore, we suggest that L3mbtl1 regulates basal expression of the Ctnnb1 and Gabra2 genes, and further, that the activity-dependent dissociation of L3mbtl1 from chromatin may

allow the recruitment of other protein complexes required for gene expression or repression upon activity elevation.

The dissociation between L3mbtl1 protein and chromatin complexes is triggered by DNA DSBs followed by degradation via the ubiquitin-mediated proteasomal pathway in heterologous cell lines (Acs et al., 2011). Importantly, DNA DSBs are triggered by epileptic insults, amyloid β, learning and memory, and naïve visual stimuli in the brain, indicating that DSBs are a part of the activity-dependent events *in vivo* and can be events upstream of L3mbtl1 degradation leading to the expression of synaptic down-scaling (Crowe et al., 2006, 2011; Suberbielle et al., 2013).

Our current knowledge on the recruiting mechanisms of L3mbtl1 to its target sites is still limited. Histone mark H4K20me has been shown to promote L3mbtl1 binding in heterologous cell lines (Kalakonda et al., 2008), however the interaction between histone and L3mbtl1 is too weak to be considered solely responsible for recruitment (Trojer and Reinberg, 2008). More likely, synergistic interactions with other proteins may be required to recruit L3mbtl1 to endogenous loci. In this context, it is interesting to note that several non-histone proteins were co-purified with L3mbtl1, including p53 tumor suppressor protein (West et al., 2010), PR-SET7 (H4K20 mono-methyltransferase) (Kalakonda et al., 2008), ETV6 (Boccuni et al., 2003), Rb and HP1γ (Trojer et al., 2007). To test the possibility that L3mbtl1 interacts with additional transcriptional factors, we searched for DNA motifs enriched in L3mbtl1 binding sites. Among the top DNA consensus motifs, we found

one motif matching the E2F transcription factor consensus sequence (TTTTCGCG) (**Fig 2.14**). It has been shown that L3mbtl1 occupies E2F target sites in heterologous cell lines (Trojer et al., 2007), likely through binding to methylated Rb protein via an MBT domain (Saddic et al., 2010). This suggests a model whereby the recruitment of L3mbtl1 to at least a subset of promoter regions *in vivo* is facilitated by E2F/Rb complexes. Given that our ChIP-seq data highlight distinct neuronal gene targets for L3mbtl1 in neurons, a tissue-specific and cell type-specific recruitment mechanism for L3mbtl1 is highly likely and warrants further investigation.

We have identified 12 neuronal activity-sensitive chromatin regulators, including L3mbtl1, out of 246 chromatin regulator genes, (**Fig 2.2B, Table 2.2D**). It is interesting to address whether the protein levels of the remaining 11 genes parallel transcriptional changes and alter downstream gene expression. Among four chromatin regulator groups (erasers, readers, remodelers and writers), there was no specific group that changed expression upon activity elevation. However, it will be particularly interesting to test the roles of three genes, Hdac11, Jarid2 and Cbx6, in homeostatic down-scaling because of their prominent expression in neurons (Zhang et al., 2014).

Our discovery of L3mbtl1 as an activity-dependent chromatin reader that coordinates the homeostatic control of synaptic strength raises the intriguing possibility that other chromatin regulators and their downstream genes are required for homeostatic synaptic plasticity. Elucidating the roles of these other

chromatin regulators in synaptic plasticity coupled with our results presented here will provide a comprehensive view of epigenetic regulation of gene expression in homeostatic synaptic scaling.

Materials and Methods

Animals

All animal protocols were approved by the Institutional Animal Care and Use Committee (IACUC) of the University of Massachusetts Medical School. L3mbtl1 mutant mice were generated previously (Qin et al., 2010) and backcrossed with C57BL/6 for four generations. C57BL/6 mice were also used for primary cultures and ChIP qPCRs. Both sexes were used.

Expression and shRNA vectors

Full-length L3mbtl1 cDNA was PCR-amplified from mRNA isolated from hippocampal primary neurons and cloned in the pCAG vector. The β-catenin construct, mVenus-β-Catenin-20 (gift from Dr. Michael Davidson, Addgene #56604), was used for the validation of shRNA clones. The shRNA vectors targeting L3mbtl1 and Ctnnb1 were purchased from Dharmacon (shL3mbtl1: #488433, shCtnnb1: #491202). The sequences of two control shRNAs, luciferase and scramble shRNA, are 5´-CGTACGCGGAATACTTCGA-3´ (Zhang and Macara, 2006) and 5´-ATCTCGCTTGGGCGAGAGTAAG-3´ (Dharmacon, #RHS4346), respectively.

Antibodies and Biochemistry

L3mbtl1 antibody #58 was generated and purified by peptide aa 1-20 (Ac-MEGHTDMEILRTVKGSSTGE-amide). The N-terminal region of L3mbtl1 (aa 140-279, NP_001074807.1) was PCR-amplified and subcloned into pGEX-5X or -4T vector (glutathione *S*-transferase (GST) fusion protein, Amersham Pharmacia Biotech) to generate L3mbtl1 antibody. GST fusion proteins were purified using glutathione-Sepharose 4B resin (Amersham Pharmacia Biotech) and used to immunize rabbits. L3mbtl1 antibody #703 was affinity-purified using synthesized peptide (aa 140-169, Ac- RHEGGMARRDAGIQHPDVHQDRQDITSLEP-amide, AminoLink Coupling Gel, Pierce). The following antibodies were used (dilutions used for immunochemistry are indicated in parentheses): mouse anti-tubulin (1:3000, abcam); HRP-conjugated anti-mouse and -rabbit IgG antibodies (GE Healthcare, 1:2000); normal rabbit IgG (CST, #2729); anti-GluA1 (Calbiochem #PC246, 1:200); anti-H3K4me3 (Abcam, ab8580); anti-H3K27ac (Abcam, ab4729); rabbit anti-β-catenin (1:10000, Abcam ab32572); mouse anti-GAPDH (1:2000, Millipore MAB374); HRP-conjugated anti-mouse and -rabbit IgG antibodies (GE Healthcare, 1:2000).

RNA Extraction and qPCR

Total RNA was extracted from hippocampus, hippocampal primary cultures, or ES cells using RNAqueous Micro Kits (Ambion) and reverse-transcribed using High

Capacity RNA-to-cDNA Kits (Applied Biosystems). Reverse-transcription-qPCR was performed on an ABI 7500 Fast sequence detection system (Applied Biosystems). For RNA expression analysis, TaqMan assays (Applied Biosystems) were used with GAPDH or Ywhaz as reference genes (see **Primers and probes**). For ChIP-qPCR, EpiTect ChIP qPCR assays (Qiagen) were used (see **Primers and probes**). All reactions were performed with RT^2 SYBR Green according to manufacturer-recommended cycling conditions, and subjected to melting curve analysis. All changes of gene expression were determined using the $2^{-delta(deltaCT)}$ method (Livak and Schmittgen, 2001).

RNA sequencing and analysis

Sequencing libraries were prepared according to ScriptSeq v2 protocol following rRNA depletion (RiboZero, Illumina), and run on single-end 50-bp modules in Illumina HiSeq 2000. Sequencing reads that passed the default purify filtering of Illumina CASAVA pipeline were quality trimmed/filtered using The FASTX-Toolkit (http://hannonlab.cshl.edu/fastx_toolkit) with a quality score cutoff of 20. Raw reads were first mapped to mouse GRCm38 genome using TopHat (v2.0.9) (Trapnell et al., 2009), then read counts were calculated for each replicate using HTSeq (v0.6.1) (Anders et al., 2015) with UCSC gene annotation. Differential gene expression analysis was carried out using DESeq2 (Love et al., 2014). A corrected p<0.01 and fold change >2.0 were applied to determine significant differences between treatment and control conditions (four biological replicates). Functional

enrichment analysis was performed for all differentially expressed genes by DAVID6.8 (Huang et al., 2009a, 2009b). After clustering using default parameters, a representative category within each of the most significant clusters was selected. A heat map was generated by hierarchical clustering using 'hclust' and 'heatmap.2' function in R.

Chromatin Immunoprecipitation (ChIP)

Chromatin was prepared from P7-8 mouse hippocampal tissue and DIV14-16 hippocampal primary cultures. For each preparation, hippocampi or primary cultures from 18-22 mice were crosslinked by 2 mM DSG for 20 min, followed by the addition of 1.5 and 1.0% formaldehyde to hippocampi and primary cultures, respectively, during the last 10 min of DSG crosslinking. For ChIP against histone modifications, native histones were prepared from hippocampus without crosslinking. Nuclei preparation and chromatin digestion steps were done using a SimpleChIP Plus Enzymatic Chromatin IP Kit (Cell Signaling). Chromatin was digested to 100-500-bp fragments for ChIP-sequencing, or 300-1000-bp fragments for ChIP-qPCR. Immunoprecipitation procedures followed conventional procedures (Bharadwaj et al., 2013). MNase (micrococcal nuclease)-digested chromatin from wild type or L3mbtl1 KO mouse hippocampi and primary cultures was immunoprecipitated with 10μg anti-L3mbtl1 (#703), 2μg anti-H3K4me3 (Abcam, ab8580), 2μg immunoprecipitated with 10μg anti-L3mbtl1 (#703), 2μg anti-H3K4me3 (Abcam, ab8580), 2μg anti-H3K27ac (Abcam, ab4729) or normal

rabbit IgG as control. After washing, chromatin complexes were eluted and the crosslinks were reversed. DNA was purified using MinElute columns (Qiagen). For qPCR reactions, 4% of immunoprecipitated DNA was used. Data are presented as the percentage of the unprecipitated (input) DNA or fold change over control sample.

ChIP sequencing and analysis

Libraries from three wild type samples and three L3mbtl1 KO samples were prepared from 10ng ChIP'd DNA each using a NEBNext Ultra DNA Library Prep Kit (NEB) and subjected to 50bp single-end Illumina sequencing. Reads were aligned to the mm10/GRCm38 reference by Bowtie (v2.2.4) (Langmead et al., 2009). Peaks were called using the Irreproducible Discovery Rate (IDR) protocol (Li et al., 2011). In short, all three L3mbtl1 KO samples were pooled and used as control for peak callings. Peaks were called on individual wild type replicates, pooled wild type replicate, pseudoreplicates of individual wild type replicates, and pseudoreplicates of pooled wild type replicate. At least 100k peaks were called for each sample using MACS (v2.1.0) with a relaxed threshold: -p 0.05 --nomodel --extsize 165. IDR threshold of 0.01 and 0.0025 were used for self-consistency and pooled-consistency test respectively to determine the number of final peaks called. Peaks were annotated using HOMER (Heinz et al., 2010). Nearest genes were assigned to peaks within 1kb up- and down-stream from a TSS. Functional enrichment analysis was performed using DAVID6.8 (Huang et al., 2009a, 2009b).

After clustering, a representative category within each of the most significant clusters was selected. For correlation analysis, peak chromosomal ranges generated from L3mbtl1 peaks above IDR threshold and those provided by GEO GSE63137 were mapped into windows of 10k nucleotides of mm10 genome, and pairwise Pearson correlation scores were plotted using R package corrplot v0.77. Read density distributions of ChIP-seq signals centered on the TSS +/- 3kb of each annotated transcript by the GRCm38.80.gtf were plotted using R package seqplots v1.12.0. Heatmaps were organized into 4 clusters based on K-means clustering of L3mbtl1 ChIP-seq signal patterns ("include" parameter). Average plots were plotted using log2 scaling. Motif analysis was performed using the Homer *de novo* motif discovery method.

Data availability

All RNA-Seq and ChIP-Seq raw and processed data have been deposited in NCBI's Gene Expression Omnibus and are accessible through GEO accession number: GSE104802.

***In situ* hybridization**

Fluorescein- or digoxigenin (DIG)-labeled cRNA probes were used for *in situ* hybridization: mouse L3mbtl1 (nucleotides 1289-2577; National Center for Biotechnology Information (NCBI) reference sequence NM_001081338.1), mouse type 1 vesicular glutamate transporter (VGluT1; nucleotides 301–1680; GenBank

accession number BC054462), mouse 67 kDa glutamic acid decarboxylase (GAD67; nucleotides 1036–2015; NM_008077), mouse glutamate/aspartate transporter (GLAST; nucleotides 1571–2473; AF330257), mouse proteolipid protein (PLP; nucleotides 1-1359; NM_011123), and mouse ionized calcium-binding adapter molecule 1 (Iba1; nucleotides 66-540; D86392). cRNA probes were synthesized as described previously (Yamasaki et al., 2010). Chromogenic or double-label fluorescent *in situ* hybridization was carried out as described (Kudo et al., 2012; Yamasaki et al., 2010). Briefly, tissues were prepared from mice at postnatal day 7 under isoflurane anesthesia. Brains were fixed by transcardial perfusion with 4% paraformaldehyde/0.1 M phosphate buffer (PB, pH7.2) for chromogenic *in situ* hybridization, or frozen on powdered dry ice for double-label fluorescent *in situ* hybridization. Brain slices (thickness 20 μm) were prepared with a cryostat (Leica VT1000S or CM3050S), and subjected successively to acetylation and prehybridization. Hybridization was carried out at 63.5°C with the hybridization buffer supplemented with cRNA probes diluted 1:1000. After stringent washing and blocking, immunohistochemical detection was performed. For chromogenic *in situ* hybridization, DIG-labeled cRNA probes were detected with alkaline phosphatase-conjugated anti-DIG antibody (1:500, Roche Diagnostics) and NBT/BCIP solution (1:50; Roche Diagnostics). Images were taken with a stereo microscope (SZX-7, Olympus) equipped with a CCD digital camera (INFINITY3- 1UC, Lumenera). For double-label fluorescent *in situ* hybridization, fluorescein-labeled cRNA probes were visualized with peroxidase-

conjugated anti-fluorescein antibody (1:500, Roche Diagnostics) and the TSA plus Fluorescein system (PerkinElmer). After inactivation of residual peroxidase activity introduced in the detection of fluorescein-labeled cRNA probes, DIG-labeled cRNA probes were detected with peroxidase-conjugated anti-DIG antibody (1:500, Roche Diagnostics) and the TSA plus Cy3 system (PerkinElmer). Nuclear staining was performed with DAPI (1:5000, Sigma). Images were acquired with a confocal laser scanning microscope (TCS SP5, Leica) equipped with a 20x oil immersion objective lens (HCX PL APO CS 20x/0.7 IMM). The specificity of cRNA probes against L3mbtl1 mRNA was confirmed using L3mbtl1 KO mice. Other cRNA probes were validated by lack of hybridization signals with their sense probes. For quantification, the peak intensity for L3mbtl1 mRNA was measured in the soma of each cell type with ImageJ software. Background levels were determined as the mean peak intensity obtained from 80 excitatory neurons in L3mbtl1 KO mice.

Primary and slice culture preparation

Primary hippocampal cultures were prepared from early postnatal (P0-1) mice as described previously (Brewer et al., 1993) with some modifications (Futai et al., 2013). Briefly, hippocampi were dissected and trypsinized, after which neurons were dissociated and plated onto coverslips (Matsunami, Japan) coated with poly-D-lysine (40 µg/ml, BD) and laminin (4 µg/ml, BD) at a density of 1 x 10^5 cell/cm^2. Neurons were maintained in 2% B27 supplement containing medium for 14-16 days *in vitro* (DIV). Organotypic hippocampal slice cultures were prepared from P6

to 7 mice as previously described (Futai et al., 2007; Futai et al., 2013). Neurons were transfected on DIV1-2 via a biolistic gene gun (BioRad) using gold particles coated with plasmid DNA per the manufacturer's protocol.

Immunocytochemistry and neuronal imaging

To identify spiny pyramidal neurons, cultured neurons were transfected with GFP on DIV 12 using Lipofectamine 2000 (Invitrogen). For immunocytochemistry, neurons were fixed at DIV 14 with 4% paraformaldehyde (PFA)/4% sucrose. Primary and secondary antibodies were applied in triton-free buffer (0.1% bovine serum albumin, 4% normal goat serum, in PBS buffer pH 7.4). Images of 2048 x 2048 pixels were taken from hippocampal primary cultures using a confocal microscope (Leica TCS SP8; University of Massachusetts Medical School Imaging Core Facility) with a 40X objective (NA 1.3) and optical zoom of 2.0, with sequential acquisition settings. Each image was a Z-series projection of 8-12 images taken at 0.35-µm depth intervals and pixel size 71 nm. Primary and secondary dendritic segments were defined by GFP epifluorescence and GluA1-immunopositive signals were imaged to quantify surface expressing AMPARs. Morphometric measurements were made using ImageJ. Briefly, maximum intensity projection images were background subtracted, and GluA1 channel signal was thresholded by gray value at 75% of the dynamic range. All puncta within a selected dendrite segment were analyzed as individual objects using the "analyze particles" function, and the total fluorescence intensity was measured. In addition, each dendrite length was recorded to calculate the total fluorescence intensity per 10 µm of

dendrite length.

Electrophysiology and data analysis

Whole-cell recordings were performed from primary hippocampal cultures (DIV 14-16) and organotypic hippocampal slice cultures (DIV 6-8) as described (Futai et al., 2007; Futai et al., 2013). Thick-walled borosilicate glass pipettes were pulled to a resistance of 3–5 MΩ and filled with internal solution containing (in mM): 115 cesium methanesulfonate, 20 CsCl, 10 HEPES, 2.5 MgCl$_2$, 4 ATP disodium salt, 0.4 guanosine triphosphate trisodium salt, 10 sodium phosphocreatine, and 0.6 EGTA, at pH 7.25, with CsOH. For recordings of AMPAR-mediated miniature EPSCs, the extracellular solution consisted of (in mM) 119 NaCl, 2.5 KCl, 4 CaCl$_2$, 4 MgCl$_2$, 26 NaHCO$_3$, 1 NaH$_2$PO$_4$, and 11 glucose, gassed with 5% CO$_2$ and 95% O$_2$, pH 7.4, in the presence of picrotoxin (0.1 mM, Sigma) and tetrodotoxin (TTX, 0.001 mM, Ascent Scientific).

For recordings of GABA$_A$R-mediated miniature IPSCs, whole-cell voltage-clamp recordings were performed at Vhold = -70 mV. Extracellular solution consisted of (in mM) 119 NaCl, 2.5 KCl, 2.0 CaCl$_2$, 2.0 MgCl$_2$, 26 NaHCO$_3$, 1 NaH$_2$PO$_4$, and 11 glucose, gassed with 5% CO$_2$/95% O$_2$, pH 7.4, in the presence of NBQX (0.003 mM, Ascent Scientific), DL-APV (0.05 mM, Ascent Scientific) and TTX (0.001 mM, Ascent Scientific).

All experiments and analyses of data were performed in a blind manner. Recordings were performed using a MultiClamp 700B amplifier and Digidata 1440,

and digitized at 10 kHz and filtered at 4 kHz by low-pass filter. Data were acquired and analyzed using pClamp (Molecular Devices) and Mini Analysis software (Synaptosoft). For mini analysis, approximately three hundred events were sampled from each experiment and events smaller than 5 pA were excluded. To test for multiplicative scaling of mini amplitude distributions, we followed a previously described method (Kim et al., 2012). To ensure that each group had an equal number of events and each cell contributes equally to the group, we randomly picked an equal number of events per cell to make up a total number of 2000 events for each group. Briefly, we scaled down values from the group with larger amplitude ("treat") to the group with smaller amplitude ("control"), by multiplying an arbitrary scaling factor (between 0 and 1), and then excluded any amplitudes that fell below the threshold. The threshold is determined by the smallest amplitude of the "control" group. The degrees of overlap between scaled "treat" and "control" data were assessed with various scaling factors, and the largest p value obtained from the Kolmogorov Smirnov (KS) test was reported for each experiment.

Cell lines and transient transfection

HEK293T cells (American Type Culture Collection, MD, USA) were grown in Dulbecco's Modified Eagle's Medium (DMEM) supplemented with fetal bovine serum (10% v/v) and penicillin/streptomycin (100 units/ml), at 37°C and in an atmosphere of 5% CO_2. Transfections were performed with Lipofectamine 2000

(Invitrogen). Cells were harvested 3 days after transfection.

Lentiviral vector production and infection

Lentiviral particles were produced by co-transfecting HEK293T cells with a 3-plasmid system, including pGIPZ, psPAX2 packaging and pVSVG envelope vectors, as previously described (Lois et al., 2002; Naldini et al., 1996) with modifications. For knockdown experiments, primary neuron cultures were infected with virus particles for 3 days or 7 days. For L3mbtl1 knockdown experiments, infected cultures were selected using puromycin (3 µg/ml) for 48 hours.

Primers and probes

For RNA expression analysis, the following TaqMan gene expression assays (Applied Biosystems) were used:

Taqman gene expression assay

gene	catalog	gene	catalog
Ap2a2	Mm01279159_m1	Gabra2	Mm00433435_m1
Bdnf	Mm04230607_s1	Gabra5	Mm00621092_m1
Camk2b	Mm00432284_m1	Gapdh	Mm99999915_g1
Camkk1	Mm00517053_m1	Homer1	Mm00516275_m1
Cdh2	Mm01162497_m1	Itgb1	Mm01253230_m1
Cfl1	Mm03057591_g1	L3mbtl1	Mm01239967_m1
Ctnnb1	Mm00483039_m1	Nedd4	Mm00456829_m1

Cxcr4	Mm01996749_s1	Shank3	Mm00498775_m1
Dag1	Mm00802400_m1	Ywhaz	Mm03950126_s1
Fxr1	Mm00484523_m1		

For ChIP-qPCR, the following EpiTect ChIP qPCR assays (Qiagen) were used:

Epitect ChIP qPCR Primers

gene	catalog
Ctnnb1	GPM1041109(-)01A
Gabra2	GPM1051280(-)01A
Igx1a (intergenic)	GPM100001C(-)01A

Statistical analyses

Results are reported as mean ± SEM. For two-group comparisons, statistical significance was evaluated by Student's t-test. For multiple comparisons in single-factor experiments, one-way ANOVA was used followed by Sidak's multiple comparisons test. For multiple comparisons in two-factor experiments where factor one is genotype and factor two is treatment, two-way ANOVA was applied followed by Sidak's multiple comparisons test. Statistical significance was set at $p < 0.05$ for Student's t-test and ANOVA and $p < 10^{-4}$ for KS test because the sample number of the miniature/spontaneous E/IPSC was large (Kim et al., 2012).

Acknowledgements:

Table 2.1   Regulators for synaptic upscaling and downscaling

Gene Symbol of scaling regulators	Protein	synaptic up-scaling involved?	synaptic up-scaling expression change	RNA-seq (PTX vs Control) Fold Change >2	RNA-seq FDR <0.01	ChIP-seq L3MBTL1-bound	synaptic down-scaling involved?	synaptic down-scaling expression change	Gene Description
Ap2a1	AP-2			0.858	-	-	yes	Not addressed	Adaptor protein complex AP-2, alpha 1 subunit
Ap2a2	AP-2	yes		1.328	-	yes			Adaptor protein complex AP-2, alpha 2 subunit
Ap3m1	Mu3A-Adaptin	yes	Increased (protein)	1.037	yes	-			Adaptor Related Protein Complex 3 Mu 1 Subunit
Arc	Arc	yes	Decreased (protein)	12.093	yes	yes	yes	Increased (protein)	Activity regulated cytoskeletal-associated protein
B2m	B2M/TAP1	yes	Not addressed	1.2739	-	yes			Beta-2 microglobulin
Tap1	B2M/TAP1			1.3555	-	-			Transporter 1, ATP-binding cassette, sub-family B (MDR/TAP)
Bdnf	BDNF			11.944	yes	yes	yes	Not addressed	Brain derived neurotrophic factor
Camk2a	CaMKII	yes	Decreased (protein)	0.476	yes	-	yes	Increased (protein)	Calcium/calmodulin-dependent protein kinase II alpha
Camk2b	CaMKII	yes	Increased (protein)	0.507	yes	yes	yes	Decreased (protein)	Calcium/calmodulin-dependent protein kinase II, beta
Camk4	CaMKIV	yes	Not addressed	0.637	yes	-	yes	Not addressed	Calcium/calmodulin-dependent protein kinase kinase 4
Camkk1	CaMKK1	yes	Not addressed	2.280	yes	yes	yes	Not addressed	Calcium/calmodulin-dependent protein kinase kinase 1, alpha
Casp3	Caspase-3	yes		2.087	yes	yes	yes	Not addressed	Caspase 3
Cdh2	N-cadherin	yes	Not addressed	0.842	-	yes	yes	Not addressed	Cadherin 2
Cdk5	CDK5	yes		0.578	yes	-	yes	Not addressed	Cyclin-dependent kinase 5
Ctnnb1	Beta catenin	yes	Not addressed	0.917	-	yes	yes	Not addressed	Catenin (cadherin associated protein), beta 1
Dag1	DAG1	yes	Increased (protein)	0.874	-	yes			Dystroglycan 1
Dlg2	PSD-93	yes	Unchanged	1.028	-	yes			Discs, large homolog 2 (Drosophila)
Dlg4	PSD-95	yes	Increased (synaptic protein)	0.838	-	-	yes	Decreased (synaptic protein)	Discs, large homolog 4 (Drosophila)
Dlgap1	GKAP	yes	Increased (protein)	0.819	-	-	yes	Decreased (protein)	Discs, large (Drosophila) homolog-associated protein 1
Dnmt1	DNMT1	yes	Unchanged	1.847	yes	yes			DNA (cytosine-5)-methyltransferase 1
Dnmt3a	DNMT3a	yes	Unchanged	0.689	yes	yes			DNA (cytosine-5)-methyltransferase 3A
Ehmt1	EHMT1	yes	Unchanged	1.049	-	-			Euchromatic Histone Lysine Methyltransferase 1
Ehmt2	EHMT2	yes	Increased (protein)	0.922	-	yes			Euchromatic Histone Lysine Methyltransferase 2
Epha4	EphA4	yes		0.441	yes	-	yes	Not addressed	Eph receptor A4
Fxr1	Fmr1	yes	Not addressed	1.172	yes	yes	yes	Not addressed	Fragile X mental retardation gene 1, autosomal homolog
Grip1	GRIP1	yes	Increased (protein)	1.765	yes	-	yes	Increased total protein / Decreased synaptic protein	Glutamate receptor interacting protein 1
H2-D1	MHC1	yes	Decreased (protein)	1.226	-	-			MHC class I alpha chain
H2-K1				1.423	yes	-			
Homer1	Homer1a	yes	Decreased (mRNA/protein)	2.637	yes	yes	yes	Increased (mRNA/protein)	Homer homolog 1 (Drosophila)
Itgb3	Beta3 integrin	yes	Increased (surface protein)	4.810	yes	-	yes	Decreased (surface protein)	Integrin beta 3
Mecp2	MeCP2	yes	Not addressed	0.958	-	-	yes	Increased (mRNA)	Methyl CpG binding protein 2
miR-92a		yes	Decreased (miRNA)						MicroRNA 92a
Nedd4	Nedd4-1	yes		0.857	-	yes	yes	Increased (protein)	Neural precursor cell expressed, developmentally down-regulated gene 4
Nptx2	Narp	yes	Decreased (surface protein)	14.643	yes	yes	yes	Increased (surface protein)	Neuronal pentraxin 2
Pick1	Pick1	yes	Decreased (protein)	1.049	-	-			Protein interacting with C kinase 1
Plk2	PLK2			5.806	yes	-	yes	Increased (protein)	Polo-like kinase 2
Ppp1cc	PP1	yes	Not addressed	1.282	-	yes	yes	Not addressed	Protein phosphatase-1
Ppp3ca	Calcineurin	yes	Decreased (protein)	0.445	yes	yes			Protein phosphatase 3, catalytic subunit, alpha isoform
Psen1	PSEN-1	yes	Not addressed	1.287	-	yes			Presenilin-1
Ptpn5	STEP	yes	Decreased (mRNA/protein)	1.454	-	-			Protein tyrosine phosphatase, non-receptor type 5
Rara	RARA	yes	Increased RARA protein and RA	1.659	yes	-			Retinoic acid receptor, alpha
Rps6ka5	RPS6KA5 (MSK1)	yes	Not addressed	0.375	yes	yes			Ribosomal Protein S6 Kinase A5
Senp1	SENP1	yes	Decreased (protein)	1.124	-	-			SUMO1/sentrin specific peptidase 1
Syngap1	SynGAP	yes	Not addressed	0.738	yes	-			Synaptic Ras GTPase activating protein 1
Tnf	TNFa	yes	Increased (protein)	1.099	-	-			Tumor necrosis factor

Figure 2.1
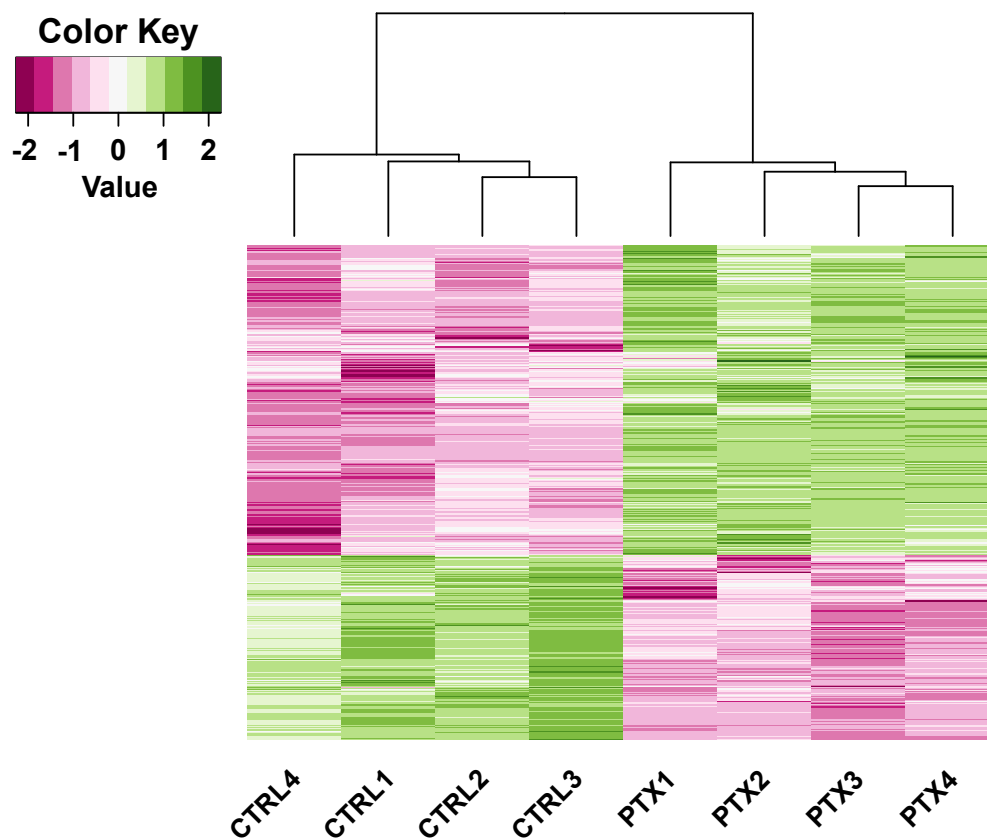
Figure 2.1 Heat map of activity-dependent gene expression.

Heat map of 1839 significant genes by RNA-seq analysis from control and PTX-treated hippocampal primary neurons. p<0.01 and fold change>2.0 were applied to determine significant differences between control (CTRL1 to 4) and PTX-treated (PTX1 to 4) groups. Hierarchical clustering tree of the samples is shown at the top of the figure.
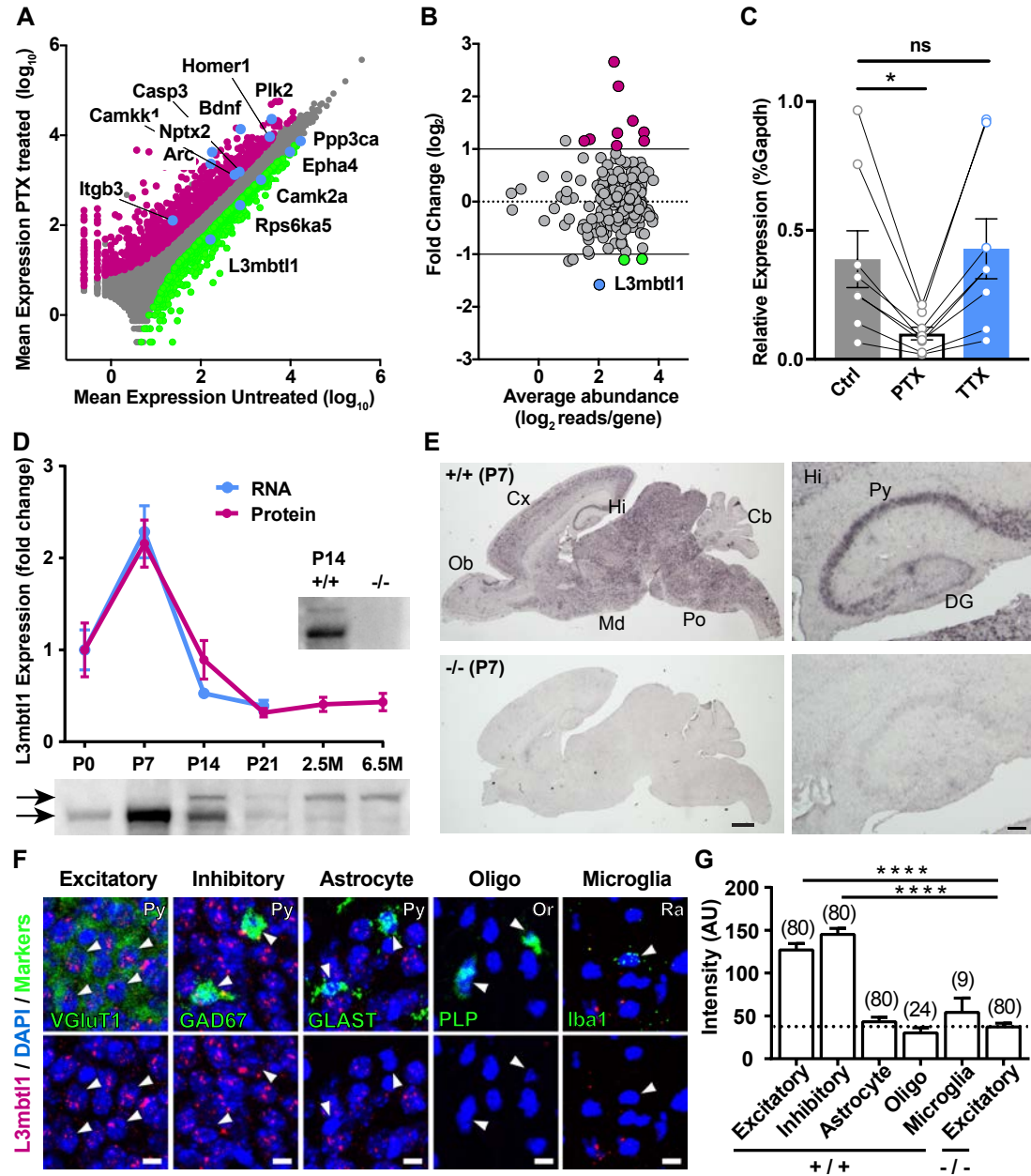
Figure 2.2

Figure 2.2 Neuronal activity elevation reduced L3mbtl1 expression.

(A) Scatter plot of genes that were up-regulated (magenta symbols) and down-regulated (green) after 15 hours of PTX (100 µM) treatment. Grey symbols are genes that were not differentially expressed. (B) MA-plot (log ratio-mean average plot) of chromatin regulators that were up-regulated (magenta symbols) and down-regulated (green) after PTX treatment (fold change > 2, Padj < 0.01). (C) Activity elevation but not suppression changed the expression of L3mbtl1. Activity blockage by TTX (1 µM) did not induce a change in expression in primary cultures. Data shown are means ± SEM. * p=0.026, one-way ANOVA followed by Sidak's multiple comparisons test, N = 8. Connecting lines indicate matched samples from the same batch. (D) Developmental profile of L3mbtl1 mRNA (blue circles) and protein (magenta circles) levels in mouse hippocampus from postnatal 0-21 days (P0-21) to adulthood (2.5 and 6.5 months). mRNA and protein expression were normalized to the control gene, ywhaz, and the immunoblotting signal of L3mbtl1 at P0, respectively.   N = 4 - 7 independent culture batches.   Bottom, Immunoblotting images of L3mbtl1 at different postnatal days. The pattern of L3mbtl1 signal changed during development. The upper bands, presumably due to post-translational modification, were observed from P14 hippocampus. Note that these two bands are not detected in the P14 L3mbtl1 KO sample (-/-, P14). (E) Chromogenic *in situ* hybridization against P7 brain sections prepared from wild type (upper) and L3mbtl1 KO (bottom) mouse brains. Right panels show high power-magnified images of the hippocampus. Cb, cerebellum; Cx, neocortex; Hi, hippocampus; Md, midbrain; Ob, olfactory bulb; Po, pons; DG, dentate gyrus; Py, pyramidal cell layer. (F) FISH images in the CA3 regions against L3mbtl1 and cell-type specific markers, VGluT1 (excitatory neurons (excitatory)), GAD67 (inhibitory neurons (inhibitory)), GLAST (astrocyte), PLP (oligodendrocyte (Oligo)), or Iba1 (microglia). Or, stratum oriens; Py, pyramidal cell layer; Ra, stratum radiatum. (G) Summary bar graph of cell-type-specific expression showing the mean peak intensity of L3mbtl1 signals in distinct cell types in wild type (+/+) and L3mbtl1 KO (-/-) mice. The number in the parentheses above each column indicates the number of cells analyzed. ****p < 0.0001, One-way ANOVA with Sidak's multiple comparisons test. Scale bars: 1 mm (E, left); 100 µm (E, right) 10 µm (F).
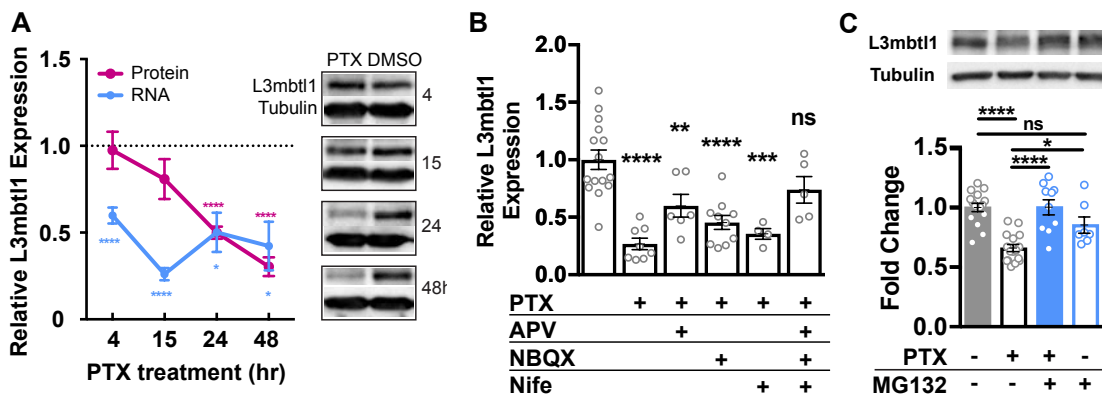
Figure 2.3

Figure 2.3 Calcium influx and the proteasomal pathway are involved in activity-dependent down-regulation of L3mbtl1.

(A) Time course of L3mbtl1 expression (mRNA, blue circles: protein, magenta circles) after application of PTX. mRNA and protein expression, relative to GAPDH and tubulin respectively, were normalized to untreated samples. One sample t-test was performed to compare mean value to 1: ****p < 0.0001, *p<0.05, N = 4 - 6. (B) Pharmacological characterization of activity-dependent down-regulation of L3mbtl1. Primary cultures were incubated with PTX alone, or with D-APV (APV, 50 μM), NBQX (5 μM) and nifedipine (Nife, 10 μM) for 15 hours. Expression of L3mbtl1 was normalized to that of GAPDH. One-way ANOVA with Sidak's multiple comparisons test compares each condition with control: **p<0.01, ***p<0.001, ****p<0.0001, ns: not significant. N = 4-15. (C) The proteasome inhibitor, MG-132, blocked activity-dependent degradation of L3mbtl1. Nuclear lysates were prepared from primary cultures 24 hours after PTX and/or MG-132. Top, immunoblotting images of L3mbtl1 and tubulin. Bottom, quantification of immunoblotting. Expression of L3mbtl1 was normalized to that of tubulin. One-way ANOVA with Sidak's multiple comparisons test: *p<0.05, ****p<0.0001, N = 7-16 independent culture batches. Data shown are means ± SEM.

Figure 2.4
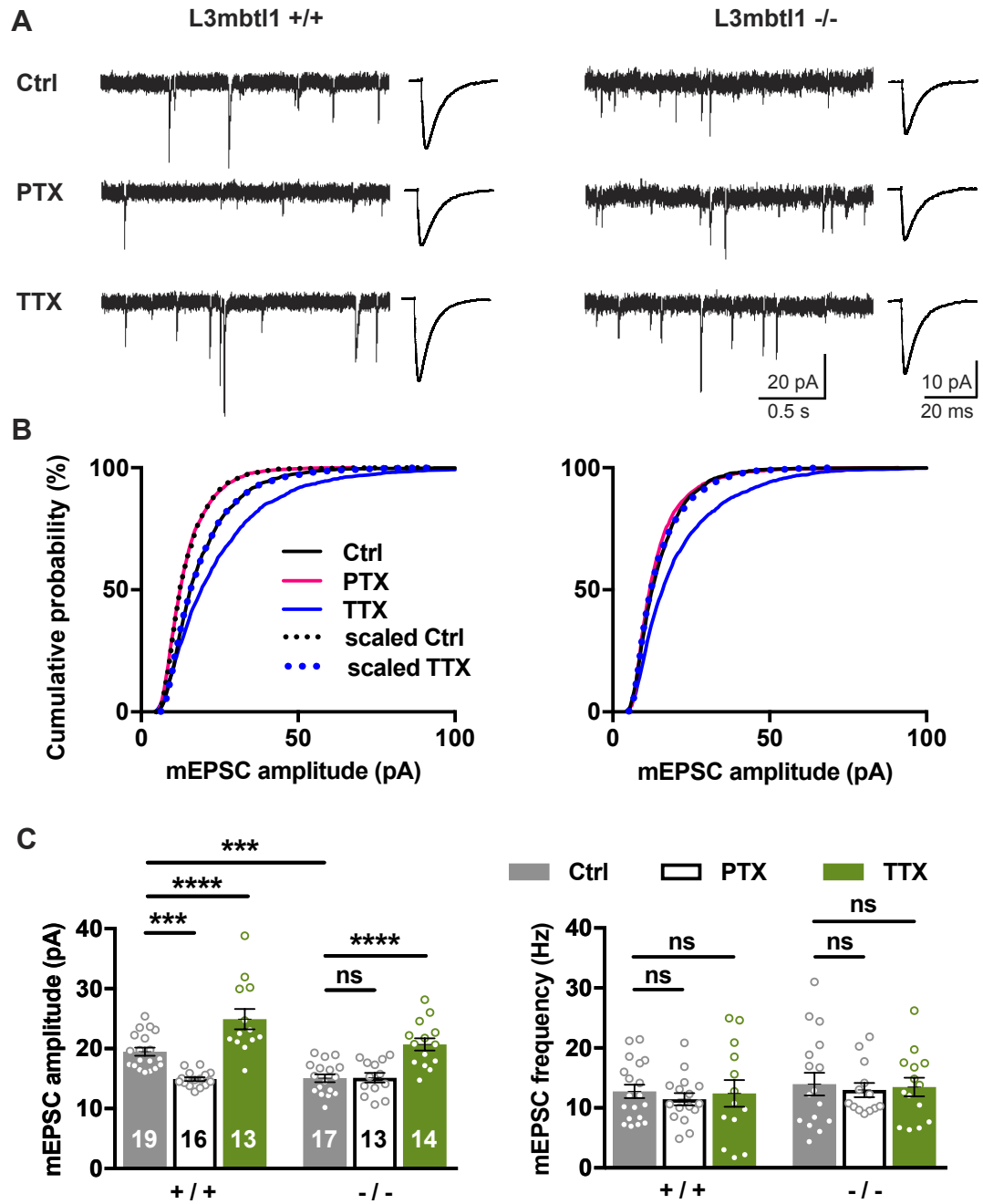
Figure 2.4 L3mbtl1 is required for basal excitatory synaptic transmission and homeostatic down-scaling in hippocampal primary neurons.

Hippocampal primary cultures were prepared from wild type (L3mbtl1 +/+) or L3mbtl1 KO (L3mbtl1 -/-) mice. They were treated with PTX (100µM), TTX (1µM) or DMSO as control for 48 hrs. (A) Representative mEPSC traces (left) and average mEPSC event traces (right). (B) Cumulative distribution of mEPSC amplitudes obtained from L3mbtl1 wild type and KO primary cultures under three different conditions. Scaled distributions were plotted by multiplying the distribution by a scaling factor and removing values that fell below the detection threshold. Kolmogorov Smirnov (KS) tests for wild type distributions: Ctrl vs PTX, $p=1.6 \times 10^{-31}$; Ctrl vs TTX, $p=5.9 \times 10^{-18}$; scaled Ctrl vs PTX, not significant; scaled TTX vs Ctrl, not significant. KS tests for KO distributions: Ctrl vs PTX, not significant; Ctrl vs TTX, $p=1.1 \times 10^{-24}$; scaled TTX vs Ctrl, not significant. (C) Quantification of mean mEPSC amplitudes (left) and frequencies (right). Data shown are means ± SEM. ****p<0.0001, ***p<0.001, ns: not significant, two-way ANOVA with Sidak's multiple comparisons test. Numbers in each bar represents the number of neurons tested (N = 5 - 8 mice were tested).

Figure 2.5

A

B
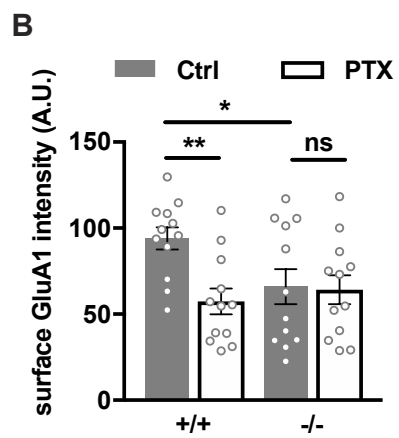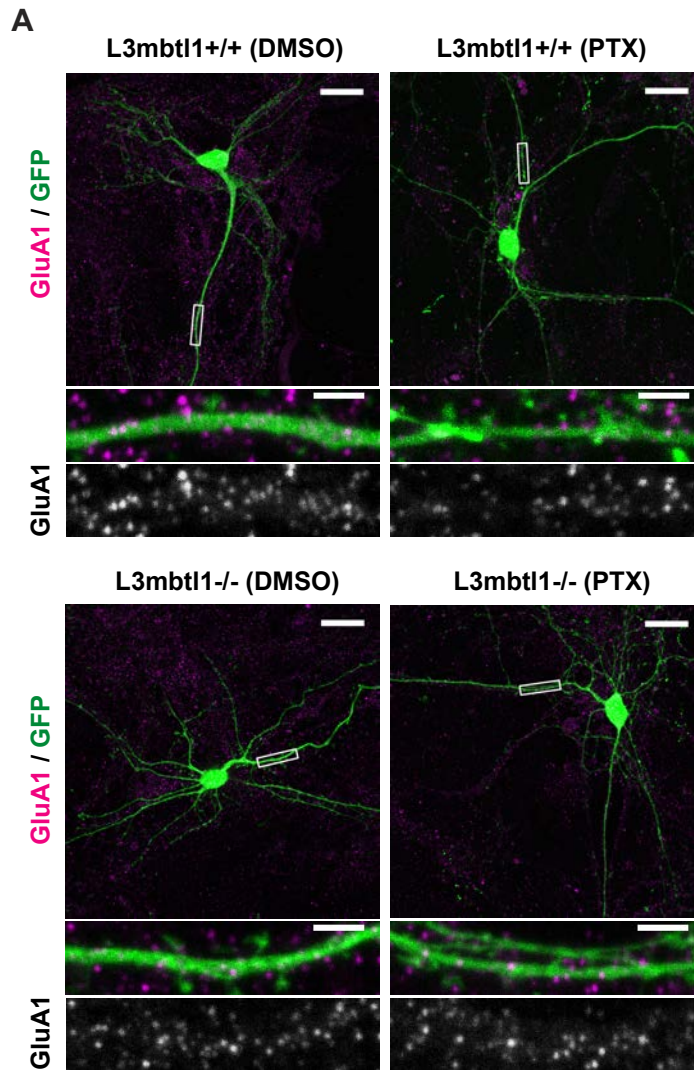
Figure 2.5 L3mbtl1 is required for surface GluA1-containing AMPAR expression and homeostatic down-scaling in hippocampal primary neurons.

Hippocampal primary cultures were prepared from wild type (L3mbtl1 +/+) or L3mbtl1 KO (L3mbtl1 -/-) mice. Spiny neurons were transfected with EGFP and treated with PTX (100μM) or DMSO as control for 48 hrs, fixed and stained for endogenous surface GluA1. (A) Representative images of intrinsic EGFP fluorescence (green) and surface GluA1 immunostaining (magenta) at low magnification (top; scale bar: 20μm) and high magnification (middle and bottom; scale bar: 3μm). (B) Quantification of surface GluA1 intensity per 10μm dendritic length in arbituary units. A total of 4000-5000 puncta from 12 neurons of three mice were analyzed for each condition. Data shown are means ± SEM. **$p<0.01$, *$p<0.05$, ns: not significant, two-way ANOVA with Sidak's multiple comparisons test.

Figure 2.6
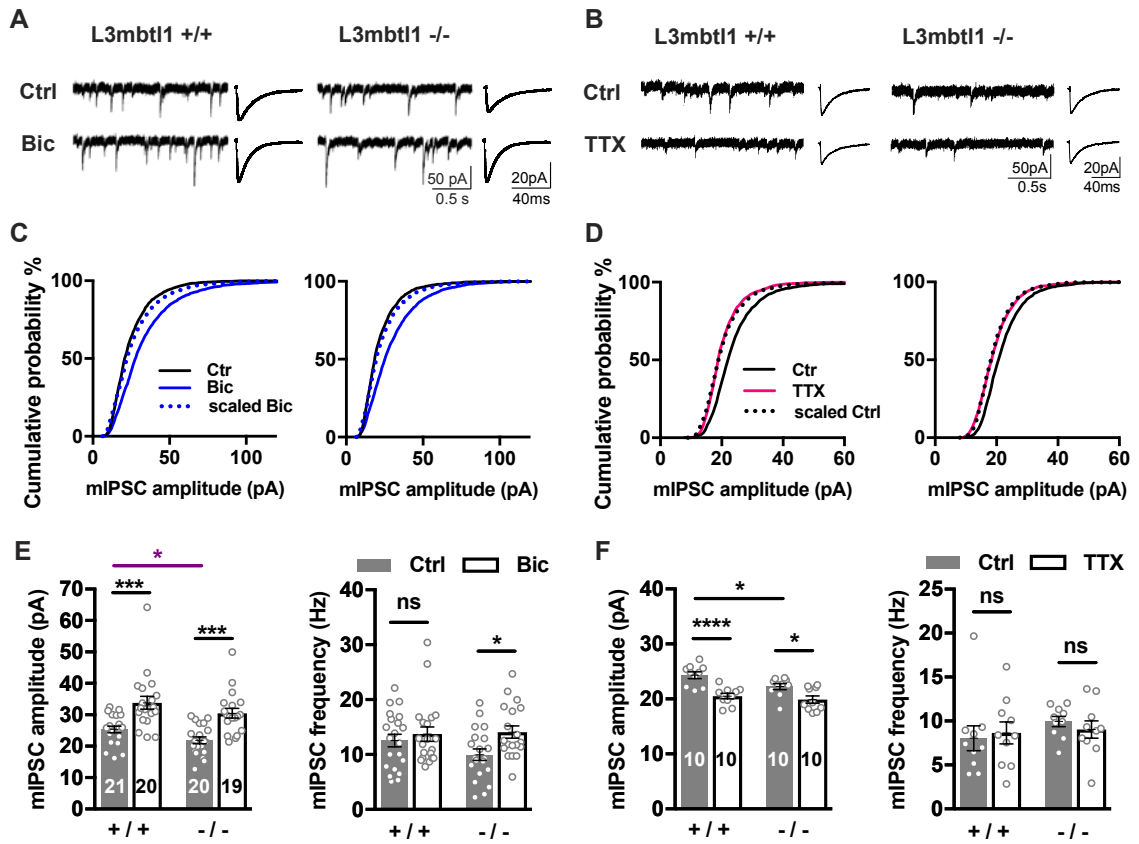
Figure 2.6 L3mbtl1 is not required for homeostatic up-scaling and down-scaling in inhibitory synapses.

Hippocampal primary cultures were treated with Bicuculline (100µM) to induce up-scaling (A, C, E) or TTX (1µM) to induce down-scaling (B, D, F). Amplitudes and frequencies of mIPSCs were measured after 48hrs of treatment from wild type (L3mbtl1 +/+) or L3mbtl1 KO (L3mbtl1 -/-) neurons. DMSO treatment was used as control. (A, B) Representative mIPSC traces (left) and average mIPSC event traces (right). (C, D) Cumulative distribution of mIPSC amplitudes. Scaled distributions were plotted by multiplying the distribution by a scaling factor and removing values that fell below the detection threshold. KS tests for wild type distributions: Ctrl vs Bic, $p=1.6 \times 10^{-46}$; Ctrl vs scaled Bic, not significant; Ctrl vs TTX, $p=9.3 \times 10^{-53}$; scaled Ctrl vs TTX, not significant. KS tests for KO distributions: Ctrl vs Bic, $p=7.6 \times 10^{-51}$; Ctrl vs scaled Bic, not significant; Ctrl vs TTX, $p=2.0 \times 10^{-31}$; scaled Ctrl vs TTX, not significant. (E, F) Quantification of mean mIPSC amplitudes (left) and frequencies (right). Data shown are means ± SEM. ****$p<0.0001$, ***$p<0.001$, *$p<0.05$, ns, not significant. Student's t-test was performed between wild type and knockout control groups in E (purple asterisk); all other comparisons were two-way ANOVA with Sidak's multiple comparisons test. N = 6 - 7 mice were tested for up-scaling; N = 4 mice were tested for down-scaling.

Figure 2.7

A

L3mbtl1 +/+   L3mbtl1 -/-

Ctrl

PTX

25 pA   15pA
2 sec   20ms

B

C
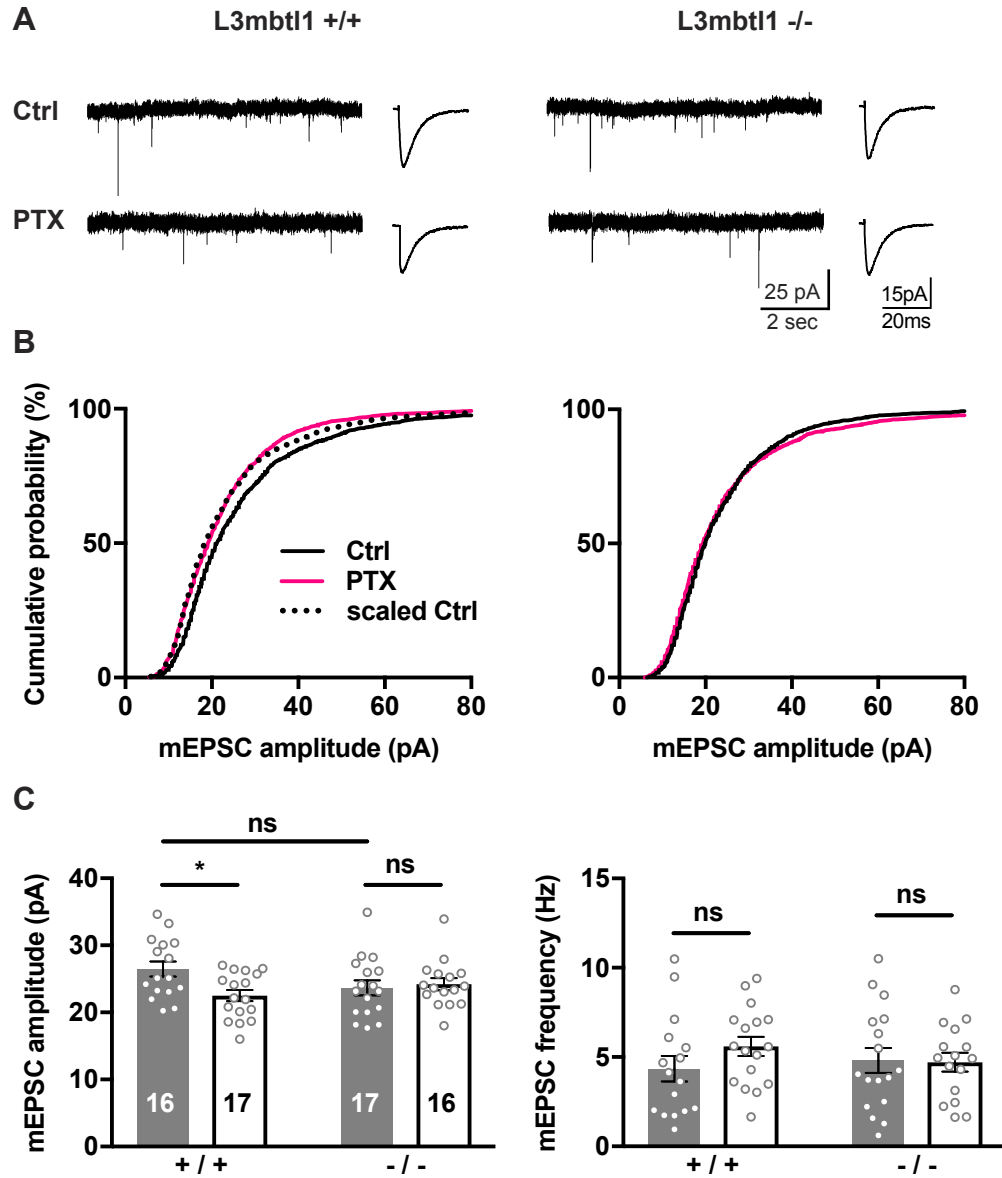
Figure 2.7 L3mbtl1 is required for homeostatic down-scaling in hippocampal CA3 synapses.

Organotypic hippocampal slice cultures of wild type or L3mbtl1-/- mice were treated with PTX or DMSO for 48 hrs. mEPSC were recorded from CA3 pyramidal neurons. (A) Representative mEPSC traces (left) and average mEPSC event traces (right) are shown. (B) Cumulative distribution of mEPSC amplitudes. Scaled distributions were plotted by multiplying the distribution by a scaling factor and removing values that fell below the detection threshold. KS tests for distributions in wild type group: Ctrl vs PTX, $p=2.8 \times 10^{-11}$; scaled Ctrl vs PTX, not significant. (C) Mean mEPSC amplitude (left) and frequency (right). Data shown are means ± SEM. *$p<0.05$, ns: not significant, two-way ANOVA with Sidak's multiple comparisons test, N = 6 mice were tested.

Figure 2.8
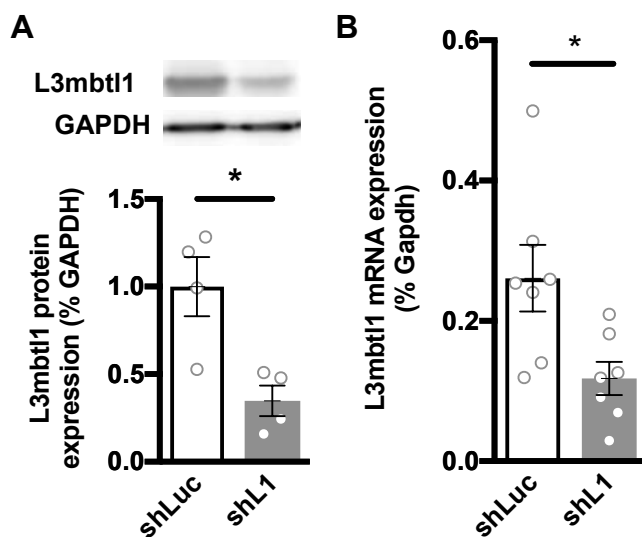
Figure 2.8 Validation of L3mbtl1 shRNA.

(A) Representative blots of L3mbtl1 (antibody #58) and GAPDH (top) and quantification (bottom) of exogenously expressed L3mbtl1 protein in HEK293T cells transfected with L3mbtl1 shRNA (shL1) or luciferase control shRNA (shLuc). *p=0.014, student's t-test, N = 4. (B) Endogenous L3mbtl1 mRNA levels in primary cultures expressing L3mbtl1 shRNA (shL1) or luciferase control shRNA (shLuc). Primary neurons were infected with high-titer lenti virus-packaged shRNAs for seven days. *p=0.019, student's t-test, N = 7. Data shown are means ± SEM.

Figure 2.9

Figure 2.9 Effect of acute knockdown of L3mbtl1 on homeostatic down-scaling in hippocampal CA3 synapses.

(A) Homeostatic down-scaling induced by PTX-treatment for 48 hours in hippocampal CA3 pyramidal neurons. Pyramidal neurons were transfected with expression vectors for shRNA directed against luciferase (middle) and L3mbtl1 (right). Left, representative mEPSC traces; right, averaged mEPSC traces. The shRNAs were biolistically transfected at DIV1. PTX or DMSO was applied two days before recording. mEPSCs were recorded from CA3 pyramidal neurons. (B) Cumulative distribution of mEPSC amplitudes. Scaled distributions were plotted by multiplying the distribution by a scaling factor and removing values that fell below the detection threshold. KS tests for distributions in untransfected group: Ctrl vs PTX, $p=1.8 \times 10^{-31}$; scaled Ctrl vs PTX, not significant. KS tests for distributions in shScrambled group: Ctrl vs PTX, $p=2.1 \times 10^{-26}$; scaled Ctrl vs PTX, not significant. KS tests for distributions in shL3mbtl1 group: Ctrl vs PTX, not significant. (C) Quantification of mean mEPSC amplitudes (left) and frequencies (right). Data shown are means ± SEM. $**p<0.01$, $*p<0.05$, ns: not significant, two-way ANOVA with Sidak's multiple comparisons test, N = 8 mice were tested.

Figure 2.10

A

MW

WT   KO

250
150
100 →
75

50

Lane   1   2   3   4   5   6   7   8

B

13.66% CpG-Island
5.59% 5UTR
46.75% Promoter
0.57% ncRNA
6.31% Exon
0.04% pseudo
1.09% TTS
21.17% Intron
0.41% 3UTR
4.42% Intergenic

C

Distance to TSS (kb)

D

transcription 436
cell cycle 189
nucleotide binding 434
zinc-finger 314
DNA damage stimulus 121
nucleosome core 41
mRNA processing 85
kinase 157
cell-cell adherens junction 82
nucleosome assembly 19
centromere 43
viral nucleoprotein 12
glioma 20
protein phosphatase 39
synapse 64
eIF3 complex 9
GTP-binding 65
translational initiation 18
histone H3K4 methylation 8
methyltransferase 38

enrichment score

E

	ATAC	H3K27ac	H3K27me3	H3K4me1	H3K4me3	L3mbtl1
ATAC	1					
H3K27ac	0.5	1				
H3K27me3	−0.29	−0.26	1			
H3K4me1	0.47	0.83	−0.3	1		
H3K4me3	0.39	0.33	−0.11	0.23	1	
L3mbtl1	0.23	0.12	−0.05	0.08	0.38	1

F

L3mbtl1
ATAC
H3K4me1
H3K4me3
H3K27ac
H3K27me3

log2 (read count)

-3kb   TSS   +3kb

G

L3mbtl1   ATAC   H3K4me1   H3K4me3   H3K27ac   H3K27me3

C1
C2
C3
C4

-3kb TSS 3kb   -3kb TSS 3kb   -3kb TSS 3kb   -3kb TSS 3kb   -3kb TSS 3kb   -3kb TSS 3kb
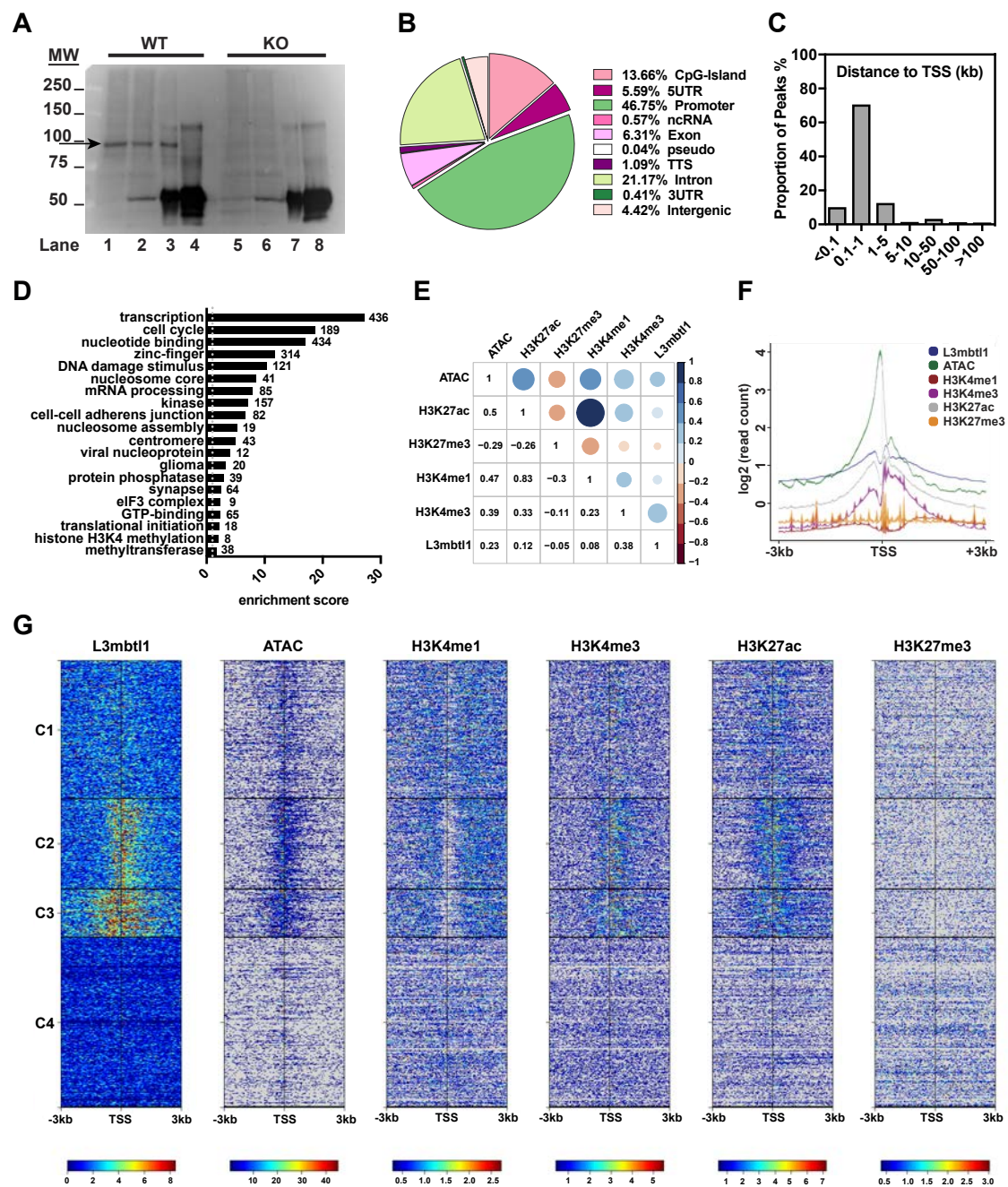
Figure 2.10 Genome-wide mapping of L3mbtl1 chromatin binding sites.

(A) Validation of antibody specificity in ChIP assays. Crosslinked chromatin prepared from wild type or KO P7 mouse hippocampus was pulled down by Ig-L3mbtl1 or normal rabbit IgG, and immunoblotted against L3mbtl1. Lanes 1 and 5, input lysate; lanes 2 and 6, unbound fraction; lanes 3 and 7, immunoprecipitated (IP) with Ig-L3mbtl1; lanes 4 and 8, IP with IgG. (B) Distribution of 4677 L3mbtl1 bound regions at various genomic locations. Promoters are defined as -1kb to 100bp of a transcription start site (TSS). TTS, transcription termination site; pseudo, pseudogenes. (C) Distribution of L3mbtl1 binding sites around TSS. Proportion of L3mbtl1 bound regions is plotted at increasing distance from the nearest TSS. Distance is absolute, regardless of direction (up- or downstream) from TSS. (D) Functional enrichment analysis of the genes obtained by ChIP-seq. Genes assigned to bound regions were tested by DAVID enrichment analysis. Clusters are sorted by enrichment score with the number of genes within each cluster labeled at the side of the bars. (E) Correlation analysis of L3mbtl1 peaks with peaks of multiple histone PTMs and ATAC-seq data from neocortical excitatory neurons (provided by GEO GSE63137). Peak chromosomal ranges were mapped into windows of 10k nucleotides of the mouse genome and pairwise Pearson correlation scores were plotted. Blue represents positive correlation, and red represents negative correlation. (F-G) Read density distributions of L3mbtl1 and multiple histone PTMs and ATAC-seq (GEO GSE63137) centered on the TSS ±3kb of each transcript in mouse genome. (F) Averaged profiles of read densities were plotted with log2 scale for all factors. (G) Heatmaps of read densities. All heatmaps were organized into 4 clusters (C1, C2, C3, C4) based on K-means clustering of L3mbtl1 ChIP-seq signal profiles.
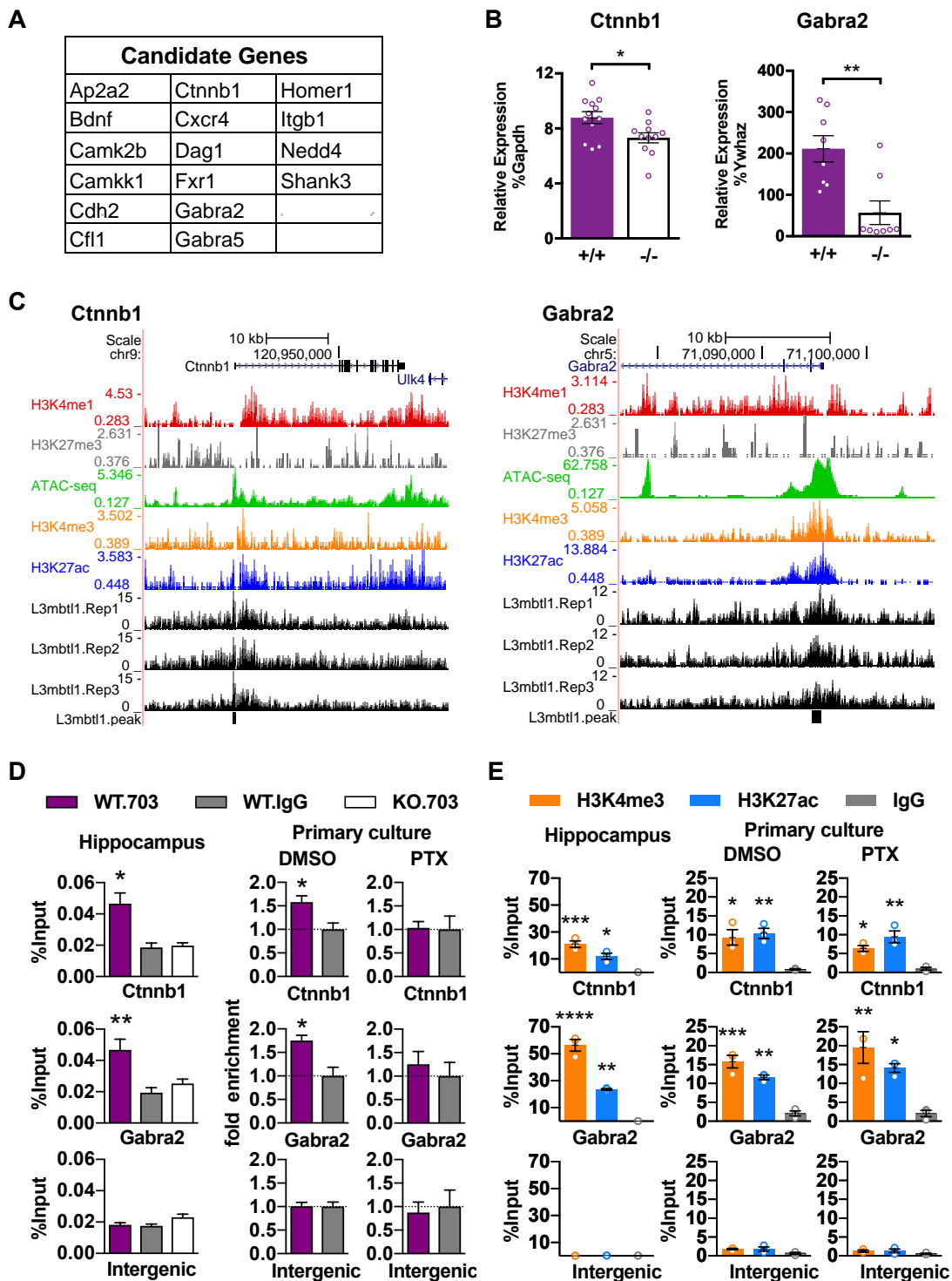
Figure 2.11

Figure 2.11 Identification of L3mbtl1 target genes.

(A) List of selected putative L3mbtl1 target genes that have known functions in synaptic transmission and/or homeostatic synaptic plasticity. (B) Quantification of Ctnnb1 and Gabra2 RNA expression by qPCR. Hippocampal primary cultures prepared from wild type (+/+) and L3mbtl1 KO (-/-) mice were treated with PTX for 15 hr and expression of Ctnnb1 and Gabra2 was determined. $**p < 0.01$, $*p < 0.5$, student's t-test. N = 8-12 independent cultures. (C) L3mbtl1-binding events at the promoter regions of the Ctnnb1 (left) and Gabra2 (right) genes, obtained from ChIP-seq of P7 mouse hippocampus. ChIP-seq tracks for L3mbtl1 from wild type samples (L3mbtl1.Rep1-3), various histone markers and ATAC-seq tracks (provided by GEO GSE63137) are shown. Black blocks indicate signal peaks for L3mbtl1 bound regions. (D) L3mbtl1 binding validated by direct ChIP-qPCR assays at Ctnnb1 and Gabra2 promoter regions. ChIP was performed from P7 hippocampus (left), or primary cultures treated with DMSO (middle) or PTX (right) for 24 hours. Note that PTX treatment abolished L3mbtl1-binding in primary cultures. $**p < 0.01$, $*p < 0.5$, one-way ANOVA with Sidak's multiple comparisons test for hippocampus, and student's t-test for primary culture. N = 3 biological replicates. (E) Enrichment for H3K4me3 and H3K27ac validated by direct ChIP-qPCR assays at Ctnnb1 and Gabra2 promoter regions. ChIP was performed from P7 hippocampus (left), or primary cultures treated with DMSO (middle) or PTX (right). Note that PTX treatment did not change H3K4me3 or H3K27ac profiles at promoter regions. $****p < 0.0001$, $***p < 0.001$, $**p < 0.01$, $*p < 0.5$, one-way ANOVA with Sidak's multiple comparisons test. N = 3 biological replicates.

Figure 2.12
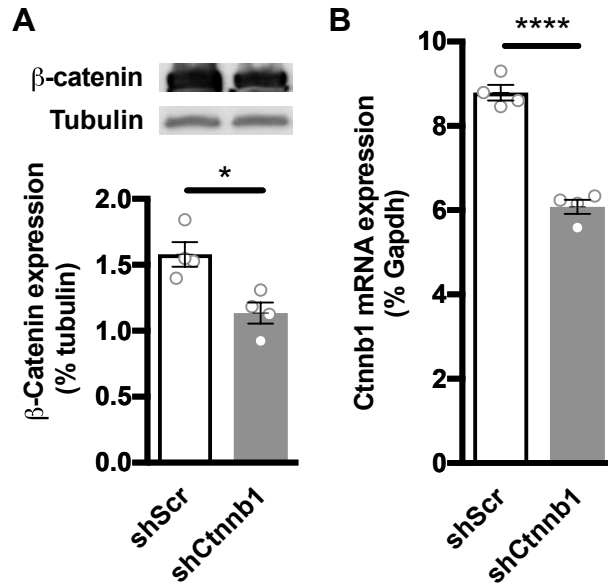
Figure 2.12 Validation of Ctnnb1 shRNA.

(A) Representative blots of Ctnnb1 and tubulin (top) and quantification (bottom) of exogenously expressed Ctnnb1 protein in HEK cells transfected with Ctnnb1 shRNA (shCtnnb1) or scramble control shRNA (shScr). *p=0.012, student's t-test, N = 4. (B) Endogenous Ctnnb1 mRNA levels in primary cultures expressing Ctnnb1 shRNA (shCtnnb1) or scramble control shRNA (shScr). Primary neurons were infected with high-titer lenti virus-packaged shRNAs for three days. ****p<0.0001, student's t-test. N = 4. Data shown are means ± SEM.

Figure 2.13
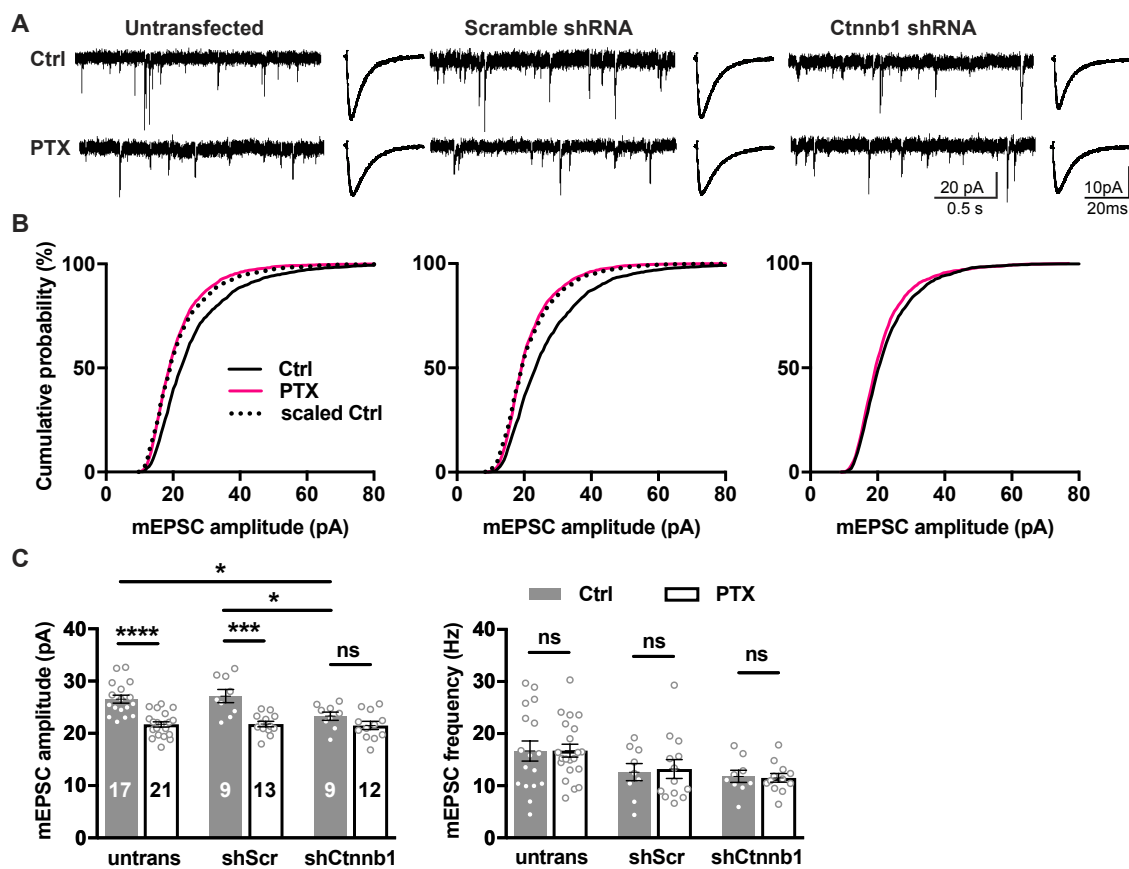
Figure 2.13 Reduced basal synaptic transmission and a lack of homeostatic down-scaling in hippocampal primary neurons by partial knockdown of Ctnnb1.

Hippocampal primary cultures were prepared from wild type (L3mbtl1 +/+) mice. Primary neurons were transfected with shRNA against Ctnnb1 (shCtnnb1) for three days and treated with PTX (100µM) or DMSO as control for two days. Untransfected and those transfected with scrambled shRNA (shScr) are shown as controls. (A) Representative mEPSC traces (left) and average mEPSC event traces (right). (B) Cumulative distribution of mEPSC amplitudes. Scaled distributions were plotted by multiplying the distribution by a scaling factor and removing values that fell below the detection threshold. KS tests for distributions in untransfected group: Ctrl vs PTX, $p=4.9 \times 10^{-31}$; scaled Ctrl vs PTX, not significant. KS tests for distributions in shScr group: Ctrl vs PTX, $p=1.1 \times 10^{-40}$; scaled Ctrl vs PTX, not significant. KS tests for distributions in shCtnnb1 group: Ctrl vs PTX, not significant. (C) Quantification of mean mEPSC amplitudes (left) and frequencies (right). Data shown are means ± SEM. ****$p<0.0001$, ***$p<0.001$, *$p<0.05$, ns: not significant, two-way ANOVA with Sidak's multiple comparisons test. N = 4 - 5 mice were tested.

Figure 2.14

Best matched transcription factor	*de novo* sequence motif	% peaks with motif (% backgroud)	p-value
ETV5		76.97% (58.85%)	1E-147
E2F		68.10% (54.90%)	1E-74
BARHL2		44.61% (31.93%)	1E-71
NFkB-p65-Rel		44.37% (32.37%)	1E-64
Arnt:Ahr(bHLH)		66.02% (56.84%)	1E-36

Figure 2.14 Motif analysis for L3mbtl1-binding sites.

List of top enriched DNA-binding motifs identified by motif analysis performed on L3mbtl1 ChIP-seq peaks using HOMER *de novo* motif discovery.

CHAPTER III

Shank1 regulates excitatory synaptic transmission in mouse hippocampal parvalbumin-expressing inhibitory interneurons

CHAPTER III

Shank1 regulates excitatory synaptic transmission in mouse hippocampal parvalbumin-expressing inhibitory interneurons

Preface

This chapter has been published separately in:

*Mao, W., *Watanabe, T., Cho, S., Frost, J.L., Truong, T., Zhao, X., and Futai, K. (2015). Shank1 regulates excitatory synaptic transmission in mouse hippocampal parvalbumin-expressing inhibitory interneurons. European Journal of Neuroscience *41*, 1025–1035. (* Equal contribution)

Author contributions:

K.F. designed research;

W.M., T.W., S.C., J.L.F., T.T., X.Z. and K.F. performed research;

W.M. Figure 3.1;

W.M., T.W., T.T., and K.F analyzed data;

T.W., W.M. and K.F. wrote the paper.

Abstract

The Shank genes (SHANK1, 2, 3) encode scaffold proteins highly enriched in postsynaptic densities where they regulate synaptic structure in spiny neurons. Mutations in human Shank genes are linked to autism spectrum disorder (ASD) and schizophrenia. Shank1 mutant mice exhibit intriguing cognitive phenotypes reminiscent of ASD individuals. However, the molecular mechanisms leading to the human pathophysiological phenotypes and mouse behaviors have not been elucidated.

We show in this study that Shank1 protein is highly localized in Parvalbumin-expressing (PV+) fast-spiking inhibitory interneurons in hippocampus. Importantly, lack of Shank1 in hippocampal CA1 PV+ neurons reduced excitatory synaptic inputs and inhibitory synaptic outputs to pyramidal neurons. Furthermore, we demonstrate that hippocampal CA1 pyramidal neurons in Shank1 mutant mice exhibit a shift in the *excitatory and inhibitory balance (E-I balance)*, a pathophysiological hallmark of ASD. The mutant mice also exhibit lower expression of gephyrin (a scaffold component of inhibitory synapses), supporting the dysregulation of *E-I balance* in hippocampus. These results suggest that Shank1 scaffold in PV+ interneurons regulates excitatory synaptic strength and participates in the maintenance of *E-I balance* in excitatory neurons.

Introduction

The Shank family proteins (Shank1, 2, 3, also known as ProSAP, Synamon, CortBP, Spank and SSTRIP) are enriched in postsynaptic densities (PSDs) and serve as scaffolds for a variety of postsynaptic molecules in excitatory neurons (Jiang and Ehlers, 2013). All Shank isoforms regulate the structure of dendritic spines, particularly spine heads, and are critical for the maturation of their structure in excitatory and medium spiny neurons (Durand et al., 2012; Haeckel et al., 2008; Peça et al., 2011; Roussignol et al., 2005; Sala et al., 2001). Consistent with these findings, knockdown of any of the Shank isoforms leads to reduced spine size and/or density in neurons thereby perturbing excitatory synaptic transmission (Berkel et al., 2012; Grabrucker et al., 2011; Verpelli et al., 2011). Furthermore, Shank knockout mouse lines exhibit abnormal synaptic structure and/or function in various brain regions (Hung et al., 2008; Peça et al., 2011; Schmeisser et al., 2012; Wang et al., 2011; Won et al., 2012; Yang et al., 2012). However, the pattern of expression of the SHANK genes and their functions in non-spiny neurons, such as inhibitory interneurons, are largely unknown.

Multiple lines of evidence indicate that the molecular organization of excitatory synapses in interneurons is different from that in excitatory neurons. In this regard, the subunit composition of AMPA receptors in interneurons is distinct from that in excitatory neurons (Jonas et al., 1994).The receptor tyrosine-protein kinase ErbB4, the PSD-95 binding protein CITRON (a putative Rho effecter), and Synapse-Associated Protein 97 are expressed more abundantly in interneurons

than in pyramidal neurons (Akgul and Wollmuth, 2013; Fazzari et al., 2010; Jaaro-Peled et al., 2009; Mei and Xiong, 2008; Zhang et al., 1999). Furthermore, there are fundamental differences in short- and long-term synaptic plasticity between inhibitory and excitatory neurons (Lamsa et al., 2007b; McMahon and Kauer, 1997; Sun et al., 2005). Taken together, the excitatory postsynaptic molecular architecture of interneurons is different from that of excitatory neurons, and the types of postsynaptic neurons (projection versus inhibitory neurons) likely determine the physiological characteristics of excitatory synapses.

Parvalbumin-expressing (PV+) fast-spiking inhibitory interneurons send inhibitory axons to perisomatic areas of excitatory neurons and regulate neuronal synchronization (Freund and Katona, 2007). The dysregulation of PV+ neurons can cause a shift of the excitatory and inhibitory balance (*E-I balance*), which is considered one of the endophenotypes of several psychiatric disorders (Rossignol, 2011; Rubenstein and Merzenich, 2003). However, the molecular architecture of excitatory synapses in PV+ neurons, which serves an important role in regulating excitability of cortical and hippocampal circuits, is largely unknown.

In this study, we found that Shank1 is highly expressed in PV+ neurons, and its deficiency in PV+ neurons causes a reduction of excitatory synaptic inputs and inhibitory outputs to CA1 pyramidal neurons. Furthermore, we observed that loss of Shank1 causes increased *E-I balance* by reducing inhibitory synaptic function and lowers expression of gephyrin in the hippocampal CA1 area. These results

indicate that the Shank1 scaffold plays an important role in PV+ neuron-mediated synaptic circuits in hippocampus.

Results

Shank1 is highly expressed in PV+ inhibitory interneurons

Shank family scaffolds are densely localized in spines of excitatory and medium-spiny neurons (Jiang and Ehlers, 2013). To investigate the expression of Shank in hippocampal non-spiny inhibitory interneurons, we performed double immunostaining against Shank1 and inhibitory neuronal markers. Importantly, we identified that Shank1 is highly expressed in adult hippocampal PV+ interneurons in wild-type but, as expected, not in Shank1$^{-/-}$ mice (**Fig 3.1A**). PV+ neurons in hippocampal CA1 area were highly reactive against Shank1 antibody (**Fig 3.1B**). We compared the signal of Shank1 staining in the dendritic segment of PV+ neurons and the hippocampal CA1 stratum radiatum area where most pyramidal neurons form excitatory synapses. Both the size and the signal intensity of Shank1 puncta are significantly higher in PV+ neurons (averaged size of Shank1 puncta: dendritic segment of PV+ neurons, 0.55 ± 0.05 µm^2, hippocampal stratum radiatum area, 0.26 ± 0.02, $p < 0.0001$, Wilcoxon signed rank *t-test*; averaged Shank1 signal intensity: dendritic segment of PV+ neurons, 2195.4 ± 108.8 arbitrary units; hippocampal stratum radiatum area, 2050.6 ± 100.5; $p < 0.001$, paired *t-test*. N = 28 PV neurons/3 mice). In addition, we observed strong VGluT1 signals, a marker

of glutamatergic terminals, proximal to Shank1 puncta in PV+ neurons (**Fig 3.1C**). These results suggest that Shank1 may play a key role at excitatory synapses in PV+ interneurons. These prominent Shank1 signals were not co-localized with other interneuronal markers, including Calb- and Calr-expressing inhibitory interneurons (**Fig 3.1 D, E**).

We also measured the expression of SHANK genes in PV+ neurons. PV+ neurons in PV-RFP mouse hippocampi (which specifically express red fluorescent protein in PV+ neurons) were dissected by LCM, and, using qPCR, we confirmed that all SHANK genes are expressed in both PV+ and pyramidal neurons (**Fig 3.1F**).

Altered PSD protein expression in PV+ neurons lacking Shank1

Shank1 protein exclusively localizes at excitatory synapses in excitatory neurons and regulates spine structure (Sala et al., 2001). However, the role of Shank1 in non-spiny neurons, such as PV+ inhibitory interneurons, has not been addressed. We next examined the expression of synaptic proteins in PV+ interneurons in dissociated hippocampal neurons cultured from wild-type or Shank1$^{-/-}$ mice. Shank1 was easily detectable in wild-type interneurons, but, as expected, was not observed in PV+ interneurons from mutant mice (**Fig 3.2 A, B**).

Wild-type Shank1 is partially co-localized at dendritic clusters with the excitatory synapse marker PSD-95 (**Fig 3.2A**). Similar to excitatory neurons where 45.2 ± 10.8% of Shank1 puncta co-localized with PSD-95 clusters (n = 15 neurons,

image not shown), the Shank1 puncta in PV+ neurons also co-localized with PSD-95 (32.1 ± 9.8%; n = 10 neurons). It should be noted that the population of neurons with co-localized Shank1 and PSD-95 is much smaller than that in other reports because of the fixation method used in this study (see Materials and Methods) (Hung et al., 2008). In Shank1$^{-/-}$ PV+ neurons, the density of Shank puncta (labeled with pan-Shank antibody) along the dendrite was reduced to ≈ 50% (**Fig 3.2 B, C**). The remaining Shank staining, presumably from Shank2 and Shank3 proteins, still localized at excitatory synapses. Furthermore, immunoreactivity against GKAP, PSD-95 and GluA1 were significantly reduced in Shank1$^{-/-}$ PV+ neurons compared with wild-type neurons (**Fig 3.2C**). There was no difference between cultured wild-type and Shank1$^{-/-}$ PV+ interneurons in cluster density or staining pattern of Homer and Bassoon. These results indicate that Shank1 is important for the assembly of the excitatory postsynaptic structure in PV+ neurons.

PV+ basket cells in Shank1$^{-/-}$ mice exhibit reduced basal excitatory synaptic transmission

To study the function of Shank1 in PV+ neurons, we generated Shank1 wild-type and Shank1$^{-/-}$ mice that express RFP in PV+ neurons, and measured basal excitatory synaptic transmission from RFP-positive neurons. We chose PV+ basket neurons, one of the major PV+ cell-types in CA1 *stratum pyramidale*, and performed whole-cell recordings to measure AMPAR-mediated spontaneous and miniature EPSCs (sEPSCs and mEPSCs) (**Fig 3.3 A-F**). The amplitudes and

frequencies of both sEPSCs and mEPSCs in PV+ Shank1$^{-/-}$ basket cells were lower than those of wild-type mice (**Fig 3.3 B, E**). In addition, sEPSCs in PV+ Shank1$^{-/-}$ basket cells exhibited slower rise times compared with that of wild-type mice (**Fig 3.3 C, F**). The AMPA receptor-mediated paired-pulse facilitation (PPF), a type of short-term synaptic plasticity that measures the change of presynaptic release probability, was similar in wild-type and Shank1$^{-/-}$ slices [PPF induced by 50 ms of inter-stimulus interval: wild-type, 1.57 ± 0.19 (n = 8); Shank1$^{-/-}$, 1.60 ± 0.13 (n = 7); $p > 0.8$, Student *t-test*], implying that the change in sEPSC frequency in Shank1$^{-/-}$ PV+ neurons is due to the reduction of the number of functional excitatory synapses. These results are consistent with our immunocytochemical studies indicating a reduction in the expression of the excitatory postsynaptic markers GKAP, PSD-95 and GluA1 in Shank1$^{-/-}$ PV+ neurons (**Fig 3.2 B, C**). GluA1 is one of the major AMPAR subunits in PV+ neurons and regulates excitatory synaptic transmission in hippocampal PV+ neurons (Fuchs et al., 2007) while PSD-95 is critical for AMPAR trafficking at synapses (Elias and Nicoll, 2007). Therefore, it is possible that the reduced GluA1 and PSD-95 signals in Shank1$^{-/-}$ PV+ neurons caused the changes in amplitude and kinetics of sEPSCs. These results highlight that Shank1 in PV+ neurons has a different role in regulating excitatory synapses compared with that in pyramidal neurons, since CA1 pyramidal neurons exhibited only reduced miniature EPSC frequency (Hung et al., 2008).

Shank1$^{-/-}$ mice display normal membrane excitability in PV+ neurons

It has been reported that Shank1 and Shank3 directly bind to Ca$_v$1.3, L-type Ca^{2+} channel subunits (Zhang et al., 2005). In addition, Shank1 regulates Ca^{2+}-sensitive Big K$^+$-channel activity (Sala et al., 2005) that shapes the width of action potentials by regulating after-hyperpolarization of action potentials at presynaptic and postsynaptic sites (Hu et al., 2001; Matthews et al., 2008; Sailer et al., 2006). Thus, Shank1 may regulate not only excitatory synaptic transmission but also intrinsic membrane excitability in PV+ neurons.

One of the most prominent membrane properties of PV+ neurons is their firing capability, which underlies their characterization as "fast-spiking" neurons. Therefore, we compared the firing patterns of CA1 PV+ neurons in wild-type and Shank1$^{-/-}$ mice. We performed whole-cell current clamp recordings from RFP-positive PV+ neurons and injected a series of current pulses into the neurons. All recorded RFP-positive neurons displayed fast-spiking properties. Neither the firing frequencies (**Fig 3.3G**) nor the basic membrane properties of FS-interneurons in Shank1$^{-/-}$ mice were different from those of wild-type PV+ neurons [resting membrane potentials: wild-type, −61.0 ± 1.1 (n = 8); Shank1$^{-/-}$, −59.9 ± 0.7 mV (n = 7); series resistance: wild-type, 20.6 ± 1.3; Shank1$^{-/-}$, 21.1 ± 1.6 MΩ; input resistance: wild-type, 122.6 ± 21.1; Shank1$^{-/-}$, 109.7 ± 9.7 MΩ; *p* > 0.3, Student *t-test*]. These results indicate that Shank1 does not play a major role in the membrane excitability of PV+ neurons.

Shank1-/- mice show reduced PV+ neuron-mediated inhibitory synaptic transmission

The reduced excitatory synaptic transmission in Shank1$^{-/-}$ PV+ neurons may decrease basal activity in these cells. We therefore performed cell-attached patch-clamp recordings and measured PV+ neuronal excitability in hippocampal CA1 area (**Fig 3.4A**). Interestingly, PV+ neurons in Shank1$^{-/-}$ slices exhibited lower firing rates compared with those of wild-type slices. This result suggests that the reduced excitatory synaptic transmission in PV+ neurons (**Fig 3.3 A-F**) causes a decrease in their firing rates in Shank1$^{-/-}$ slices.

Do the reduced firing rates of PV+ neurons in Shank1$^{-/-}$ mice change the inhibitory outputs onto postsynaptic pyramidal neurons? It has been reported that glutamatergic inputs to GABAergic neurons modulate their inhibitory outputs (Chang et al., 2014). Chronic reduction of PV+ neuronal activity may decrease their inhibitory outputs onto CA1 pyramidal neurons. To address this question, we performed simultaneous pre- and postsynaptic dual whole-cell voltage-clamp recordings from RFP-positive presynaptic CA1 PV+ neurons and postsynaptic pyramidal neurons located within 50 μm of PV+ neurons in wild-type and Shank1$^{-/-}$ mice (**Fig 3.4 C, D**). PV+ neurons were identified by RFP fluorescence (**Fig 3.4C**, left). Presynaptic GABA release was evoked by applying single or double depolarization commands (**Fig 3.4C**, middle and right). The amplitude of PV+ neuron-mediated inhibitory synaptic transmission and connective frequency were reduced in Shank1$^{-/-}$ mice compared with that of wild-type mice (**Fig 3.4D**,

left and middle). Shank1$^{-/-}$ PV+ neurons exhibited essentially similar levels of paired-pulse ratio as wild-type (**Fig 3.4D**, right), suggesting that the reduced inhibitory synaptic transmission and connective frequency are not attributable to a difference in presynaptic release probability. These results suggest that reduced excitatory synaptic transmission in PV+ neurons weakens the inhibitory outputs of PV+ neurons to pyramidal neurons, although it is possible that the null knockout of Shank1 can indirectly change synaptic function in hippocampus.

Shank1$^{-/-}$ mice show increased excitatory and inhibitory ratio

What is the consequence of reduced PV+ neuron-mediated inhibitory synaptic transmission in the hippocampal CA1 circuit? The *E-I balance* plays a critical role in cognitive behavior (Zikopoulos and Barbas, 2013). Abnormal *E-I balance,* as caused by the dysfunction or loss of inhibitory interneurons, has been suggested as a pathophysiological hallmark in ASD, schizophrenia and animal models of these disorders (Gatto and Broadie, 2010; LeBlanc and Fagiolini, 2011; Markram and Markram, 2010; Rubenstein and Merzenich, 2003; Yizhar et al., 2011). To address whether the abnormal PV+ neuron-mediated inhibitory transmission in Shank1$^{-/-}$ mice leads to an *E-I imbalance*, we measured the *E-I balance* in hippocampal CA1 pyramidal neurons using an approach previously described (Futai et al., 2013). We divided the amplitude of AMPAR-mediated excitatory postsynaptic currents (AMPAR-EPSCs) by GABA$_A$R-mediated inhibitory

postsynaptic currents (GABA$_A$R-IPSCs) in the same cells and refer to this as the *E-I ratio*.

Interestingly, the *E-I ratio* of Shank1$^{-/-}$ mice was significantly higher than that of wild-type animals (**Fig 3.5A**). It has been reported that excitatory synaptic strength is moderately reduced in Shank1$^{-/-}$ hippocampal CA1 pyramidal neurons (Hung et al., 2008); therefore, the degree of IPSC reduction in Shank1$^{-/-}$ mice must be more severe than the decrease of excitatory synaptic transmission to account for the *E-I imbalance* that we detected. Shank1$^{-/-}$ mice showed essentially the same paired-pulse depression (PPD) induced by the double stimulation of synaptic inputs with 50 ms of inter-pulse interval as wild-type (wild-type: 0.64 ± 0.03, n = 20 from 6 mice; Shank1$^{-/-}$: 0.67 ± 0.02, n = 24/6; *p* = 0.36, Student *t-test*). Paired-pulse depression is one form of short-term synaptic plasticity that reflects the change of presynaptic release probability. Therefore, this result indicates that Shank1 knockout does not change the inhibitory presynaptic release probability.

We next examined the amplitudes and frequencies of the GABA$_A$R-mediated miniature IPSCs (**Fig 3.5B**). The frequencies, but not the amplitudes, of the mIPSCs from Shank1$^{-/-}$ mice were significantly reduced, suggesting that the increased *E-I ratio* is caused in large part by a reduction in the number of functional inhibitory synapses.

Gephyrin expression is down-regulated in Shank1$^{-/-}$ mice

To further investigate the mechanisms underlying the shift of *E-I balance*, we compared the expression of synaptic proteins in membrane fractions of Shank1$^{-/-}$ and wild-type mice. Interestingly, expression of gephyrin, a scaffold molecule of inhibitory synapses, was significantly reduced in Shank1$^{-/-}$ membrane fractions (**Fig 3.5C**), consistent with the impairment of inhibitory transmission in Shank1$^{-/-}$ mice. We next examined expression of gephyrin histochemically in the hippocampal CA1 area. Consistent with our western blot data, the size of gephyrin immunoreactivity in CA1 *stratum radiatum* (SR) and *pyramidale* (SP) in Shank1$^{-/-}$ mice are reduced compared with Shank1 wild-type mice (averaged size of gephyrin puncta: wild-type, 0.09 ± 0.01 µm^2; Shank1$^{-/-}$, 0.05 ± 0.002 µm^2, *p* < 0.01; averaged puncta densities: wild-type, 13.73 ± 0.15 puncta / 100 µm^2; Shank1$^{-/-}$, 13.18 ± 0.39, *p* = 0.49, Student *t-test*. N = 4 brains from each genotype). (**Fig 3.5D**). The density of gephyrin puncta in Shank1$^{-/-}$ mice was comparable to that of wild-type mice, which is not consistent with our mIPSC results that showed that Shank1 KO mice exhibit normal mIPSC amplitudes (**Fig 3.5B)**. In this regard, it is interesting to note that gephyrin knockout moderately reduces mIPSC amplitude compared with wild-type, and further, that knockdown of gephyrin reduces the number of GABA$_A$R clusters (Jacob et al., 2005; Lévi et al., 2004). Thus, a subtle reduction of gephyrin may have more impact on the number of active synapses rather than the number of GABA$_A$R per synapse.

Discussion

Molecular architecture of excitatory synapses in inhibitory neurons

Shank proteins serve as scaffolds for a variety of postsynaptic molecules, including GKAP, Homer, L-type Ca^{2+} channels and actin regulatory molecules, such as cortactin, Sharpin, α-fodrin, Abp1 and β-Pix (Jiang and Ehlers, 2013). Shank proteins are targeted to postsynaptic sites in spiny neurons and regulate spine size, which determines the number of AMPA receptors expressed at the synapses (Matsuzaki et al., 2001; Naisbitt et al., 1999). Ectopic expression of Shanks enlarges spines in excitatory spiny neurons and induces spinogenesis in non-spiny neurons (Roussignol et al., 2005; Sala et al., 2001). Questions remain what physiological and structural roles Shanks have in non-spiny inhibitory neurons.

To address this, we first demonstrated that Shank1 is highly expressed in PV+ neurons. Furthermore, we confirmed the expression of major synaptic molecules, such as PSD-95, GKAP and Homer, in PV+ neurons, indicating that the composition of the postsynaptic architecture in inhibitory neurons is similar to that of excitatory neurons. However, the consequences of Shank1 knockout in PV+ basket cells are more severe than that in pyramidal neurons. Shank1 deficit reduced spine size and the frequency of mEPSCs in pyramidal neurons, while the expression of other postsynaptic molecules is comparable to that in wild-type neurons (Hung et al., 2008). In contrast, the absence of Shank1 protein in PV+ interneurons caused reduced expression of PSD-95, GKAP and GluA1, and led to

abnormal frequency, amplitude and kinetics of sEPSCs and mEPSCs (**Fig 3.2 and 3.3**). While the possibility that conventional Shank1 knockout can dysregulate PV+ neuronal function through non-cell autonomous fashion cannot be excluded, our results suggest that Shank1 plays an important role in the assembly of synaptic molecules at postsynaptic membranes in PV+ neurons. It is possible that the differential impact of Shank1 knockout between excitatory and PV+ neurons is a consequence of the distinct structures of the excitatory synapses in these two classes of neurons. The spine structure in excitatory neurons may act as a barrier that prevents diffusion of postsynaptic proteins, thus minimizing the knockout effect of Shank1. In contrast, excitatory synapses in inhibitory interneurons, which mostly form directly on the dendritic shaft, may rely on the scaffold proteins to maintain synaptic structure (Douglas and Martin, 1998).

Roles of Shank scaffolds in *E-I balance*

We have demonstrated that Shank1 is highly expressed in PV+ neurons and regulates excitatory synaptic transmission in PV+ basket cells. Furthermore, Shank1$^{-/-}$ mice display increased *E-I balance* in hippocampal CA1 pyramidal neurons due to the reduction of inhibitory synaptic transmission and reduced gephyrin expression. Since knockout or knockdown of gephyrin reduces GABA$_A$R-mediated currents by disrupting receptor function without changing the total expression of GABA$_A$Rs (Jacob et al., 2005; Kneussel et al., 1999; Lévi et al., 2004), these results complement each other. However, it is unclear how a Shank1

deficit causes abnormal inhibitory synaptic transmission as Shank1 is exclusively localized to excitatory postsynaptic sites. We found that Shank1$^{-/-}$ PV+ neurons display reduced excitatory synaptic transmission and diminished firing rates. Neuronal activity is critical for synaptogenesis in the brain (Lu et al., 2009a) and excitatory inputs modulate the properties of synaptic outputs in GABAergic neurons (Chang et al., 2014). It is possible that the weakened PV+ neuronal activity reduces inhibitory synaptic output on pyramidal neurons, and this may lead to a subsequent decrease in gephyrin expression. Generating a PV+ neuron-specific Shank1 knockout would allow us to directly address the roles of Shank1 protein in PV+ neurons on *E-I balance*. An alternative possibility that explains the reduction of inhibition in Shank1$^{-/-}$ mice is the contribution of neuronal homeostasis. It has been reported that excitatory synaptic transmission in pyramidal neurons is slightly reduced in Shank1$^{-/-}$ mice (Hung et al., 2008). Therefore, reduced excitatory synaptic transmission in pyramidal neurons may cause a homeostatic reduction of inhibition, including a reduced number of active inhibitory synapses and reduced expression of gephyrin, in a cell autonomous manner.

We evaluated *E-I ratio* in pyramidal neurons by taking the ratio of evoked EPSC and IPSC responses that are derived from non-specific synaptic inputs from different types of neurons, and observed increased *E-I ratio* in Shank1$^{-/-}$ pyramidal neurons (**Fig 3.5A**). In addition, we detected reduced inhibition in Shank1$^{-/-}$ pyramidal neurons by recording mIPSCs that measures the activity of all GABAergic synapses in pyramidal neurons (**Fig 3.5B**). Therefore,

reduced inhibitory synaptic transmission may not be solely due to abnormal inhibition through PV+ neurons. Other interneuronal types that exhibit lower clustering of Shank1 compared with PV+ neurons may also be dysregulated by Shank1 knockout.

Detailed behavioral tests have shown that Shank1$^{-/-}$ mice exhibit better performance in radial maze task, impaired memory retention, impaired contextual fear memory, abnormal ultrasonic vocalization and scent marking behavior (Hung et al., 2008; Silverman et al., 2011; Wöhr et al., 2011). In contrast to these intriguing phenotypes, the physiological characteristics previously observed in this mouse line were only subtly perturbed: moderately reduced basal excitatory synaptic transmission in CA1 pyramidal neurons, normal NMDAR-dependent long-term potentiation (LTP) and long term depression, and intact protein synthesis-dependent LTP.

Our data suggest that abnormal *E-I balance* can be a pathophysiological hallmark of Shank1$^{-/-}$ mice exhibiting abnormal behavioral phenotypes reminiscent of neuropsychiatric disorders. Importantly, Shank3 transgenic mice also exhibit dysregulation of *E-I balance*, reduced gephyrin expression and normal Hebbian type of synaptic plasticity (Han et al., 2013). The similarities of physiological phenotypes between Shank1$^{-/-}$ and Shank3 transgenic mice highlight the potential significance of Shank-mediated *E-I balance* in neuropsychiatric disorders.

SHANK2 and SHANK3 have also been characterized as disease-associated genes (Guilmatre et al., 2014; Jiang and Ehlers, 2013) and their transcripts are expressed in hippocampal CA1 PV+ neurons (**Fig 3.1E**). It is of paramount interest to elucidate the roles of Shank2 and Shank3 proteins in PV+ interneurons in hippocampus and cortex.

Materials and methods

Animals

All animal protocols were approved by the Institutional Animal Care and Use Committee (IACUC) of the University of Massachusetts Medical School. Shank1 mutant mice were generated previously and backcrossed with C57BL/6 and 129SvJae strains (gift from M. Sheng and R. Jaenisch, Massachusetts Institute of Technology, Cambridge, MA) (Hung et al., 2008). The animals used in this study were in a 129SvJae/C57BL/6 hybrid genetic background. We generated PV-RFP mice by crossing PV-Cre mice (Carlén et al., 2012) with a Cre-reporter mouse line carrying tdTomato (variant of red fluorescent protein, JAX: 007905) (Madisen et al., 2010). To generate Shank1$^{-/-}$/PV-RFP mice, we first crossed Shank1 heterozygous (C57BL/6 background) mutants with PV-RFP mice for at least three generations to transmit the cre recombinase and RFP genes [Shank1BL6$^{+/-}$/PV-RFP]. Shank1$^{-/-}$/PV-RFP and wild-type mice were generated by crossing Shank1BL6$^{+/-}$/PV-RFP and Shank1$^{+/-}$ (129SvJae) mutant mice. This mouse line expresses RFP in 80% of PV+ neurons with over 99% of the RFP-expressing cells

exhibiting PV immunoreactivity in the hippocampus (confirmed in two PV-RFP brains, 748 out of 903 PV-positive neurons expressed RFP and 7 out of 748 RFP-positive neurons were negative to PV immunoreactivity).

Antibodies and Biochemistry

The following antibodies were used (dilution used for immunochemistry are indicated in parentheses): rabbit/mouse anti-calbindin, -parvalbumin and -calretinin (1:1000, SWANT); goat/mouse anti-parvalbumin (1:2000, SWANT); rabbit anti-GKAP (1:1000, gift from Dr. Morgan Sheng); rabbit anti-GABA$_A$R α1 (1:1000, EMD Millipore); mouse anti-GABA$_A$R β2/3 and -Synaptophysin (1:1000, EMD Millipore); mouse anti-pan-Shank (1:3000, Neuromab); rabbit anti-Shank1a [western blotting: 1:1000 Shank1_1356 (gift from Dr. E. Kim, Korea Advanced Institute of Science and Technology, Korea), immunohistochemistry and immunocytochemistry: 1:10000, Abcam (ab66315) and Synaptic Systems (162013)]; mouse anti-PSD95 (1:2000, Neuromab); rabbit/mouse anti-Gephyrin (1:1000-3000, Synaptic Systems); mouse anti-Bassoon (1:3000, Synaptic Systems); mouse anti-VGAT and -VGluT1 (1:2000, Synaptic Systems); mouse anti-Homer (1:1000, Transduction Laboratories); secondary Alexa dye-conjugated anti-mouse (Alexa 488, 647), anti-rabbit (Alexa 488, 594, 647), anti-goat (Alexa 405, 488, 594), anti-guinea pig (Alexa 488, 647) antibodies (Invitrogen or Jackson ImmunoResearch Labs); HRP-conjugated anti-mouse and anti-rabbit antibodies (GE Healthcare, 1:2000). Fab fragment goat Anti-Mouse IgG (H+L) (Jackson

ImmunoResearch Labs) was applied prior to the application of primary mouse antibodies. The Triton-extracted P2 fraction was purified from the hippocampi of 5–7 week old mice, as described previously (Cho et al., 1992; Futai et al., 2013).

Immunohistochemistry

Mice (5–7 weeks old) were deeply anesthetized under isofluorane and transcardially perfused with heparin/saline and 4% paraformaldehyde in 0.1 M phosphate buffered saline (PBS), pH 7.4. The brains were removed and post-fixed in the same fixative for 24 hours at 4°C. The fixed brains were sectioned in the coronal plane at 10 and 30 μm thicknesses on a microslicer (VT1200 S; Leica, Germany) to perform staining for gephyrin and Shank1, respectively. The sections were washed with PBS and then blocked with GDB buffer (30 mM phosphate buffer, pH 7.4, containing 0.2% gelatin, 0.5% Triton X-100, and 0.45 M NaCl) for 2 hours at room temperature. Sections were then incubated overnight at 4°C with primary antibodies against interneuronal markers, Shank1 or gephyrin. Following PBS washes, the sections were incubated at room temperature for 1.5 hours with secondary antibodies. Following a third round of PBS washes, the sections were mounted on slides with Vectashield mounting medium (Vector Laboratories, Inc.).

Primary hippocampal neuron culture, immunocytochemistry

Hippocampal primary cultures were prepared from the brains of individual mice at postnatal day 0–3 as described previously (Futai et al., 2013). Cells were plated

onto coverslips (Matsunami, Japan) coated with poly-D-lysine (80 µg/ml, BD) and laminin (2 µg/ml, BD) at a density of 200 cells/mm^2 in Neurobasal medium supplemented with 2% B27 supplement (Invitrogen). For immunocytochemistry against synaptic proteins in PV+ cells, hippocampal cultures were fixed at days *in vitro* 14 (DIV14) with 4% paraformaldehyde in PBS. The methanol fixation approach, a standard procedure to stain molecules in postsynaptic densities (Kim et al., 2007), was not used in this study as this treatment dramatically reduced immunoreactivity against PV. Primary and secondary antibodies were applied in GDB buffer using the dilutions of antibodies described above. Primary neurons were incubated with primary and secondary antibodies for two and one hours at room temperature, respectively. The coverslips washed with PBS were mounted on slides with Vectashield (Vector Labs) mounting medium.

Neuronal Imaging

A spinning disk confocal microscope (Nikon TE-2000E2 and Leica TCS SP5 II; University of Massachusetts Medical School Imaging Core Facility) was used for imaging. The confocal images (512 × 512 or 1024 × 1024 pixels) of primary hippocampal cultures and slices were taken using 40X, 60X, 63X or 100X objective lenses. Each image was a *Z*-series projection of *x-y* images, and taken at 0.2 – 1 µm depth intervals. The size, intensity and density of immunopositive signals were evaluated by MetaMorph software (Molecular Devices). Shank1 signals in the dendritic segments of PV+ neurons and in the *stratum radiatum* region were

obtained from the same images (**Fig 3.1A**). Neurons that exhibited immunoreactivity against Shank1 antibody in the cell body and dendritic segments were classified as Shank1-decorated neurons. All measurements in Fig 3.2 and Fig 3.5 were carried out in a "blind" manner.

Laser Capture Microdissection (LCM) and Real-time PCR

Adult (5 – 7 week old, either sex) PV-RFP mice were euthanized and the brains were immediately frozen in dry ice-cooled 2-methylbutane (−60°C) and stored at −80°C. Coronal serial sections (10 µm) of the hippocampi were prepared using a cryostat (Leica, Germany) and mounted on pre-cleaned glass slides (Fisher Scientific). The sections were stored at −80°C until use. A Veritas Microdissection System Model 704 (Arcturus Bioscience) was used for LCM. Approximately 1000 – 2000 RFP-positive neurons (PV+ inhibitory interneurons) were obtained from the hippocampal CA1 region of each animal. The same number of RFP-negative neurons in CA1 stratum pyramidale was obtained as pyramidal neurons. Five to seven different mice were used for each test. Neurons were captured on CapSure MacroLCMcaps (Arcturus Bioscience) for mRNA isolation.

Total RNA was extracted from individual replicate samples using an RNAqueous-Micro Kit (Ambion). RNA samples extracted from hippocampal CA1 PV+ and pyramidal neurons were reverse-transcribed into cDNA using TaqMan Gene Expression Cells-to-CT Kit (Ambion).

Polymerase chain reactions (PCRs) were set up in 10-μl reaction mixtures using TaqMan Gene Expression Assays (SHANK1: Mm01206737_m1, SHANK2: Mm01163731_m1, SHANK3: Mm00498775_m1, PV: Mm00443100_m1, Slc17a7 (VGluT1): Mm00812886_m1, GAPDH: Mm99999915_g1, Applied Biosystems). GAPDH transcript was used as an internal control to normalize gene expression levels. The expression of PV and Slc17a7, a marker of excitatory neurons, transcripts were measured against the samples that targeted PV+ and excitatory neurons to evaluate the quality of samples harvested by LCM. The expression of PV and Slc17a7 in two different cell-types are; PV: PV+ neurons, 0.18 ± 0.06, excitatory neurons, 0.02 ± 0.01; Slc17a7: PV+ neurons, 0.19 ± 0.01, excitatory neurons, 0.78 ± 0.06, N = 4 mice. These results indicate that our LCM approach collected the specific cell types we expected. PCRs were performed using an ABI PRISM 7500 Sequence Detection System (Applied Biosystems). All reactions were performed in duplicate or triplicate. Relative amplicon quantification was calculated as the difference between Ct values of GAPDH and that of Shank1, Shank2 and Shank3.

Electrophysiology

Transverse hippocampal slices (400 μm thickness) were prepared from 3- to 5-week-old mice (either sex) in ice-cold dissection buffer (in mM: 238 sucrose, 2.5 KCl, 1 $CaCl_2$, 5 $MgCl_2$, 26 $NaHCO_3$, 1 NaH_2PO_4, 11 glucose, gassed with 5% CO_2/95% O_2, pH 7.4) as described (Hung et al., 2008; Ryu et al., 2008). Slices

were incubated in an interface or submersion incubation chamber containing extracellular artificial cerebrospinal fluid (aCSF; in mM: 119 NaCl, 2.5 KCl, 2.5 $CaCl_2$, 1.3 $MgCl_2$, 26 $NaHCO_3$, 1 NaH_2PO_4, 11 glucose, gassed with 5%CO_2/95%O_2, pH 7.4) and allowed to recover for 30 min at 28°C and then maintained at room temperature (24–26°C) for at least 30 min. Slices were then transferred to a submerged recording chamber and continuously perfused with aCSF.

For whole-cell recordings, thick-walled borosilicate glass pipettes (Warner Instruments) were pulled to a resistance of 3–5 MΩ. For current-clamp recordings, pipettes were filled with internal solution containing the following (in mM): 115 potassium methanesulfonate, 20 CsCl, 10 HEPES, 2.5 $MgCl_2$, 4 adenosine triphosphate disodium salt, 0.4 guanosine triphosphate trisodium salt, 10 sodium phosphocreatine, and 0.6 EGTA, pH 7.25, with KOH. For voltage-clamp recordings, the potassium was replaced by cesium. To measure $GABA_AR$-mediated inhibitory postsynaptic current (IPSC) and AMPAR-mediated excitatory postsynaptic current (EPSC), NMDAR antagonist (D-APV, 0.05 mM; Ascent Scientific) dissolved in aCSF was present throughout the recording. A tungsten bipolar electrode (Frederick Haer Company, Bowdoin, ME) was placed in the *stratum radiatum* proximal to the *stratum pyramidale,* and the Schaffer collateral/commissural fibers and inhibitory inputs were stimulated at 0.1 Hz. $GABA_AR$-IPSC was first measured at Vhold = 0 mV. After obtaining forty to fifty consecutive stable IPSC responses, picrotoxin (0.10 mM; Sigma-Aldrich) was

added to aCSF to eliminate the IPSC. Then, AMPAR-EPSCs were evoked at Vhold = −60 mV without changing the stimulus strength. Stimulus strength was set to produce an IPSC amplitude of ~ 1000 pA which leads to ~50 pA of AMPAR-EPSC. Measurements of $GABA_AR$-mediated miniature IPSCs (mIPSCs) were performed in the presence of D-APV, NBQX and tetrodotoxin (0.001 mM; Ascent Scientific). AMPAR-mediated miniature and spontaneous EPSCs (mEPSCs and sEPSCs) in PV+ neurons were measured in the presence of picrotoxin and with or without tetrodotoxin, respectively. In Figure 3.3, all recorded PV+ neurons were filled with biocytin in order to identify PV+ basket cells. The measurement of firing activity was performed against PV+ neurons that established gigaohm seals (> 2 GΩ) under cell-attached voltage-clamp mode. Miniature and spontaneous synaptic events were analyzed using Mini Analysis software (Synaptosoft, Decatur, GA). Approximately three hundred events were sampled from each experiment; only events >5 pA were analyzed.

Dual whole-cell recordings were performed to monitor PV+ neuron-mediated unitary inhibitory synaptic transmission. RFP-positive neurons that were proximal to hippocampal CA1 stratum pyramidale, presumably basket and axo-axonic PV+ neurons, were chosen as presynaptic neurons. The neighboring CA1 pyramidal neurons (within 50 μm radius from PV+ neurons) were selected as postsynaptic neurons. Cesium-based internal solution was used for double whole-cell recordings of presynaptic interneurons. Pre- and postsynaptic neurons were voltage-clamped under −70 and 0 mV, respectively. Inhibitory synaptic

transmission was evoked by applying one or two 70 mV depolarization pulses (2–3 ms duration, 50 ms interval) at 0.1 Hz. Consecutive paired stimuli (25 – 50 times) were applied to presynaptic neurons, and responses larger than 10 pA observed within 5 ms after the onset of depolarization pulses were considered as evoked unitary IPSCs. If any evoked response was observed during this period, the pair was considered synaptically connected.

All experiments and the analysis of data were performed in a blind manner. Recordings were performed using a MultiClamp 700B amplifier and Digidata 1440, while data were acquired and analyzed using Clampex 10 and Clampfit 10 (Molecular Devices, Union City, CA).

Statistical analyses

Results are reported as mean ± SEM. The statistical significance was evaluated by two-way ANOVA for multiple comparison, and by Student's *t-test*, paired *t-test* or Wilcoxon signed rank *t-test* with equal variance test for two-group comparison. Statistical significance was set at $p < 0.05$.
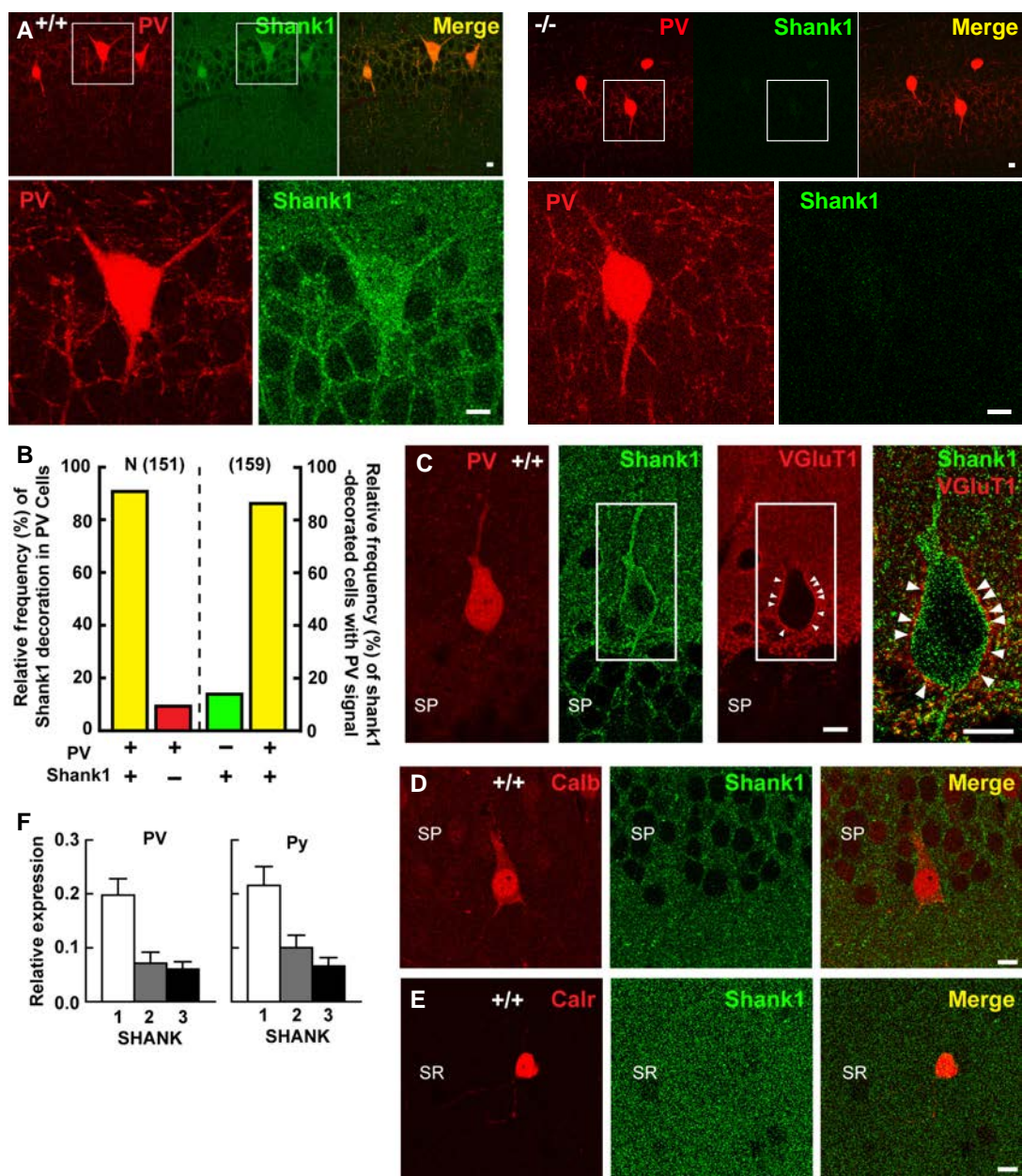
Figure 3.1

Figure 3.1 Shank1 is highly expressed in Parvalbumin-expressing interneurons

(A, B) Confocal images of double-labeled immunofluorescence staining against parvalbumin (PV, red) and Shank1 (green) from the hippocampal CA1 pyramidal cell layer of wild-type (+/+) (left) and Shank1$^{-/-}$ (−/−) (right) mice. Note that the immunoreactivity of Shank1 in Shank1$^{-/-}$ tissue is minimal, confirming the specificity of the antibody. Enlargements of the indicated rectangular fields are shown at bottom. (B) Relative proportion of hippocampal CA1 PV+ neurons as a fraction of neurons decorated by Shank1 signals (left), and that of Shank1-decorated neurons as a fraction of PV+ neurons (right). Numbers of neurons obtained from 4 wild-type mice were: Shank1-decorated PV+ neurons, 137; PV+ and Shank1 non-decorated neurons, 14; PV negative and Shank1 positive decorated neurons, 22. Note that the majority of PV+ neurons were immunopositive for Shank1. (C) Confocal images of triple-labeled immunofluorescence staining against PV (red), Shank1 (green) and VGluT1 (red) from the proximal region of hippocampal CA1 stratum pyramidale (SP) of a wild-type mouse. Note that the dense VGluT1 signals (arrow heads) were localized close to Shank1 puncta in PV+ neurons. (D, E) Confocal images of double-labeled immunofluorescence staining against calbindin (Calb, D, red), calretinin (Calr, E, red) and Shank1 (green) from hippocampal CA1 stratum pyramidale (SP) and radiatum (SR) regions of wild-type (+/+) mice. (F) Relative expression of SHANK genes (SHANK1, SHANK2 and SHANK3) in PV+ and pyramidal (Py) neurons in adult mouse hippocampus. The expression level was normalized to that of GAPDH. Approximately 1000 PV+ and pyramidal neurons in hippocampal CA1 pyramidal cell layer per mouse were cut from one PV-RFP mouse (N = 6–8 mice). Scale bars: 10 μm.
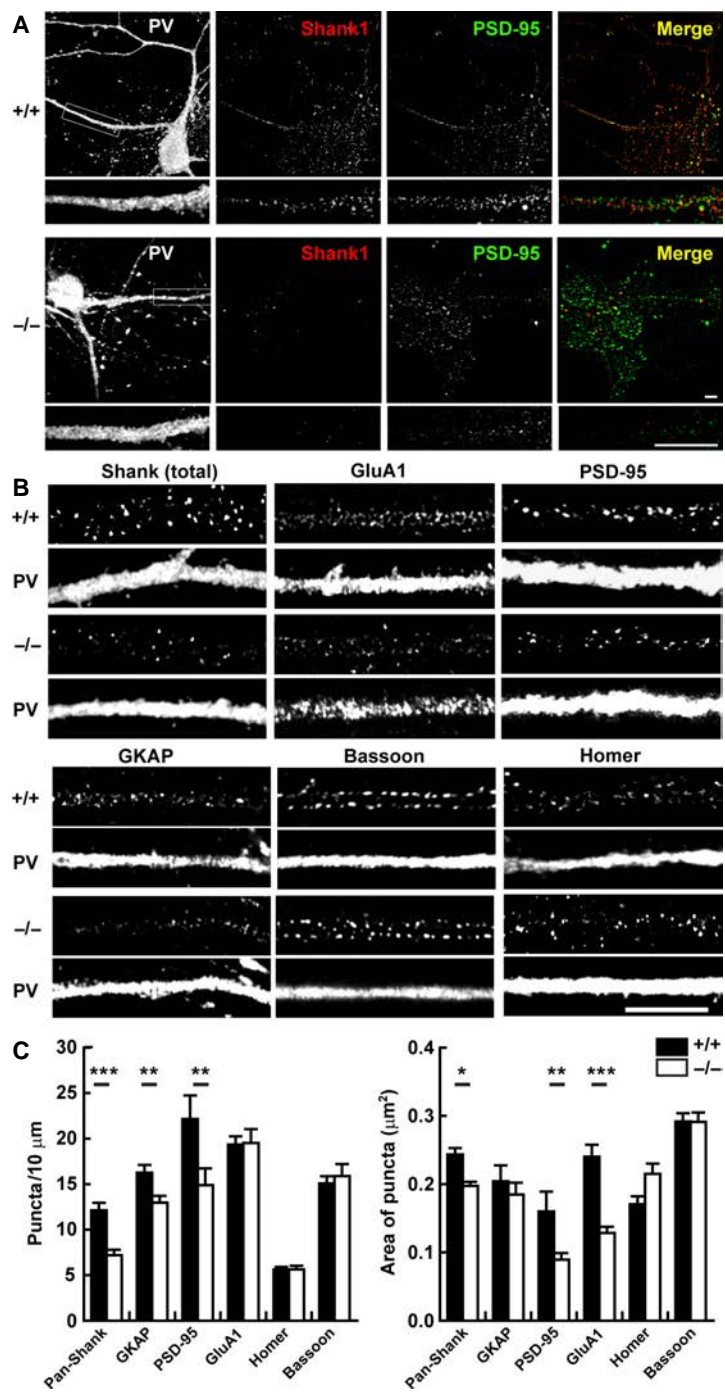
Figure 3.2

Figure 3.2 Altered expression of postsynaptic proteins in Shank1-deficient PV+ neurons

Triple- or double-labeled immunofluorescence staining for PV and synaptic proteins in hippocampal primary cultures (14 DIV) prepared from wild-type (+/+) or Shank1$^{-/-}$ (−/−) mice. (A) PV+ interneurons in wild-type and Shank1$^{-/-}$ cultures were triple-stained for PV, Shank1 and PSD-95. (B) Double-immunostaining for pan-Shank, PSD-95, GKAP, Homer, GluA1, or Bassoon, and PV. (C) Quantification of puncta density per 10 µm dendrite length (left) and puncta area (right) for the indicated proteins. Shank1$^{-/-}$ dendrites show a significant reduction in pan-Shank, PSD-95, GKAP and GluA1 (n = 10 cells from 3 mice, 3 independent cultures) signals. The error bars show standard error. Scale bars, 10 µm. *, $p < 0.05$; **, $p < 0.01$; ***, $p < 0.001$, *student t-test.*

Figure 3.3

Figure 3.3 Shank1 regulates excitatory synaptic transmission in Parvalbumin-expressing basket cells

(A, D) *Top*, Consecutive sample sEPSC (A) and mEPSC (D) traces of PV+ basket cells in wild-type (black traces) and Shank1$^{-/-}$ (grey traces) mice. *Bottom*, Averaged and n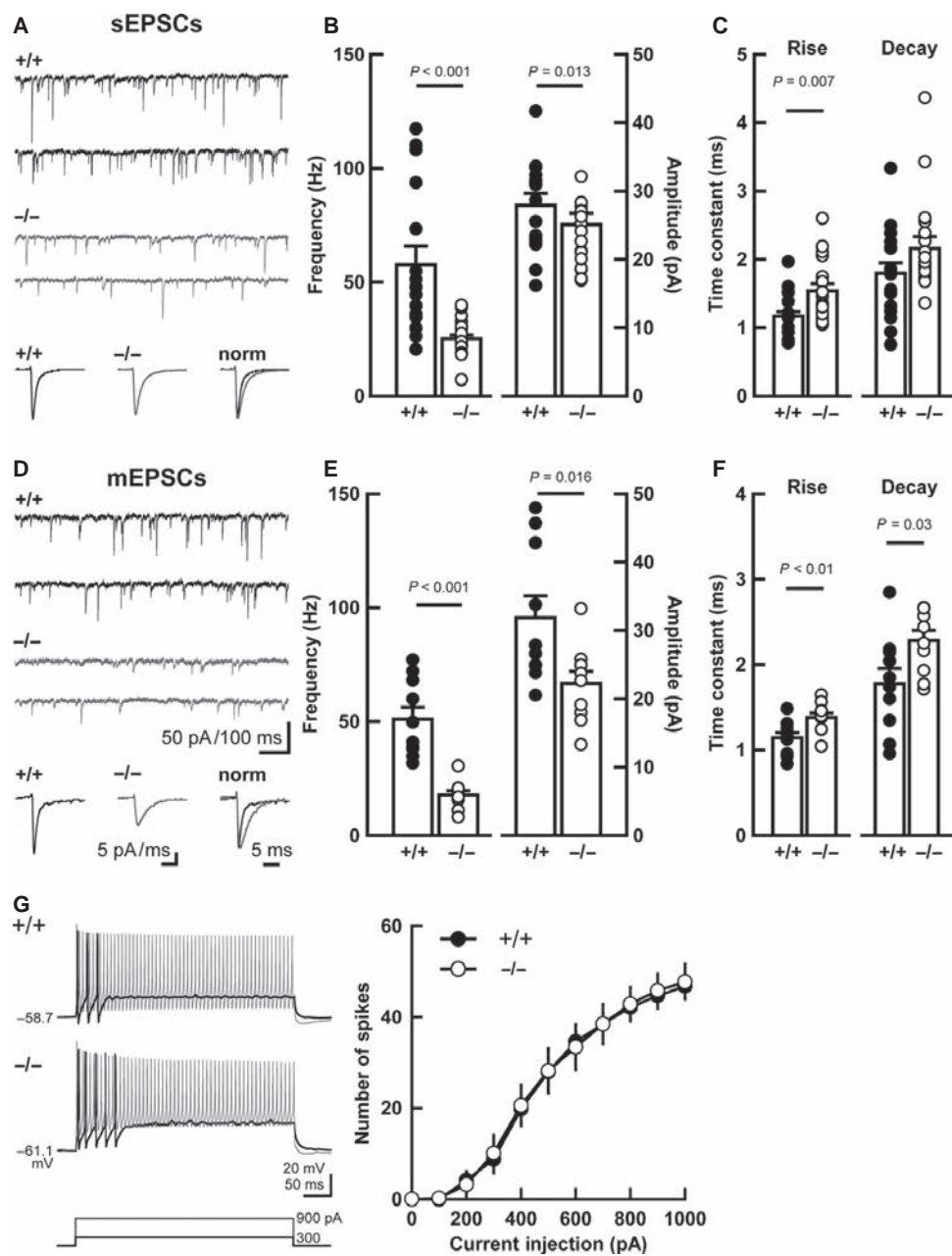ormalized sample sEPSC (A) and mEPSC (D) traces in PV+ basket cells. (B, C, E and F) Summary of the frequency and amplitude (B and E), and kinetics (C and F) of sEPSCs and mEPSCs in wild-type (+/+) and Shank1$^{-/-}$ (−/−) animals. The averaged EPSC frequency and amplitude for each cell were superimposed as circles while the bar graphs indicate the means ± SEM. Number of cells: sEPSC: wild-type, 16 cells from 7 mice; Shank1$^{-/-}$, 19 / 11; mEPSC: wild-type, 10 cells from 5 mice; Shank1$^{-/-}$, 10 / 4. (G) *Left*, Sample traces from CA1 fast-spiking PV+ basket cells in wild-type and Shank1$^{-/-}$ hippocampal slices showing spikes elicited by current injections of 300 pA (black) and 900 pA (grey) for 400 ms. *Right,* Summary graph of the frequency of action potentials in wild-type and Shank1$^{-/-}$ animals. Input-output relationship [number of spikes elicited versus amount of current injection (400 ms duration)] was plotted for wild-type and Shank1$^{-/-}$ animals. Neurons were held at the indicated resting membrane potentials. Number of cells: wild-type, 10 cells from 7 mice; Shank1$^{-/-}$, 11 / 6.

Figure 3.4
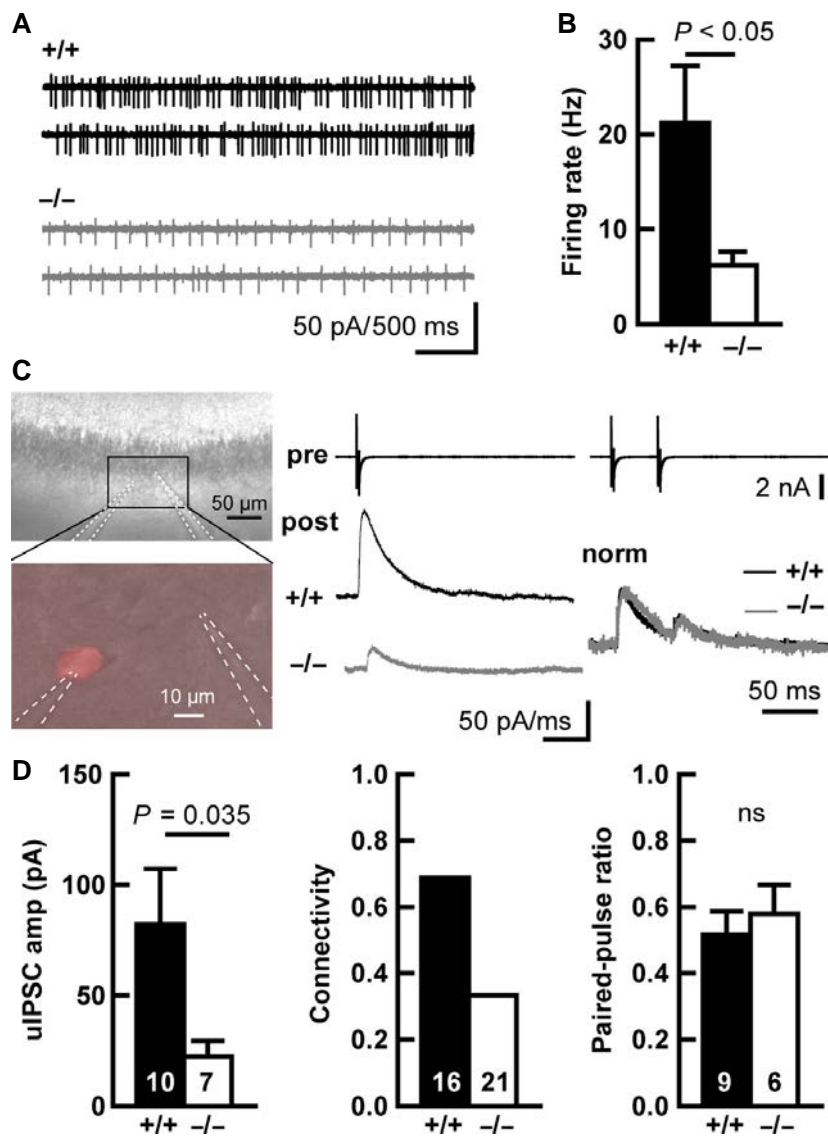
Figure 3.4 Shank1 deficit causes reduced basal firing rate in PV+ neurons and PV neuron-mediated inhibitory synaptic output onto CA1 pyramidal neurons

(A) Sample traces of PV+ neurons in wild-type (black traces) and Shank1$^{-/-}$ (gray traces) mice. (B) Summary graph of the firing rates measured by cell-attached recordings of PV+ neurons in wild-type and Shank1$^{-/-}$ animals. Number of cells: wild-type, 7 cells from 7 mice; Shank1$^{-/-}$, 6 / 5. (C–D) Effect of Shank1 deficiency on unitary inhibitory synaptic transmission between hippocampal CA1 PV+ and pyramidal neurons. (C) Left, superimposed fluorescent and Nomarski images. Averaged sample unitary IPSC (uIPSC) traces by one (middle) and double (right) presynaptically applied depolarization commands. (D) Summary of uIPSC amplitude (left), connectivity (middle) and paired-pulse ratio (right). Number in each bar represents the number of synaptically connected cell pairs (left and right), total number of cell pairs tested (middle).

Figure 3.5

Figure 3.5 Shank1 deficit causes increased *E-I ratio* by reducing inhibitory synaptic function and gephyrin expression

(A) Shank1$^{-/-}$ mice display increased *E-I ratio* compared with wild-type mice. *Left*, Sample traces (average of 10 consecutive responses) mediated by GABA$_A$R (upward) and AMPAR (downward) from wild-type (+/+) or Shank1$^{-/-}$ (−/−) hippocampal slice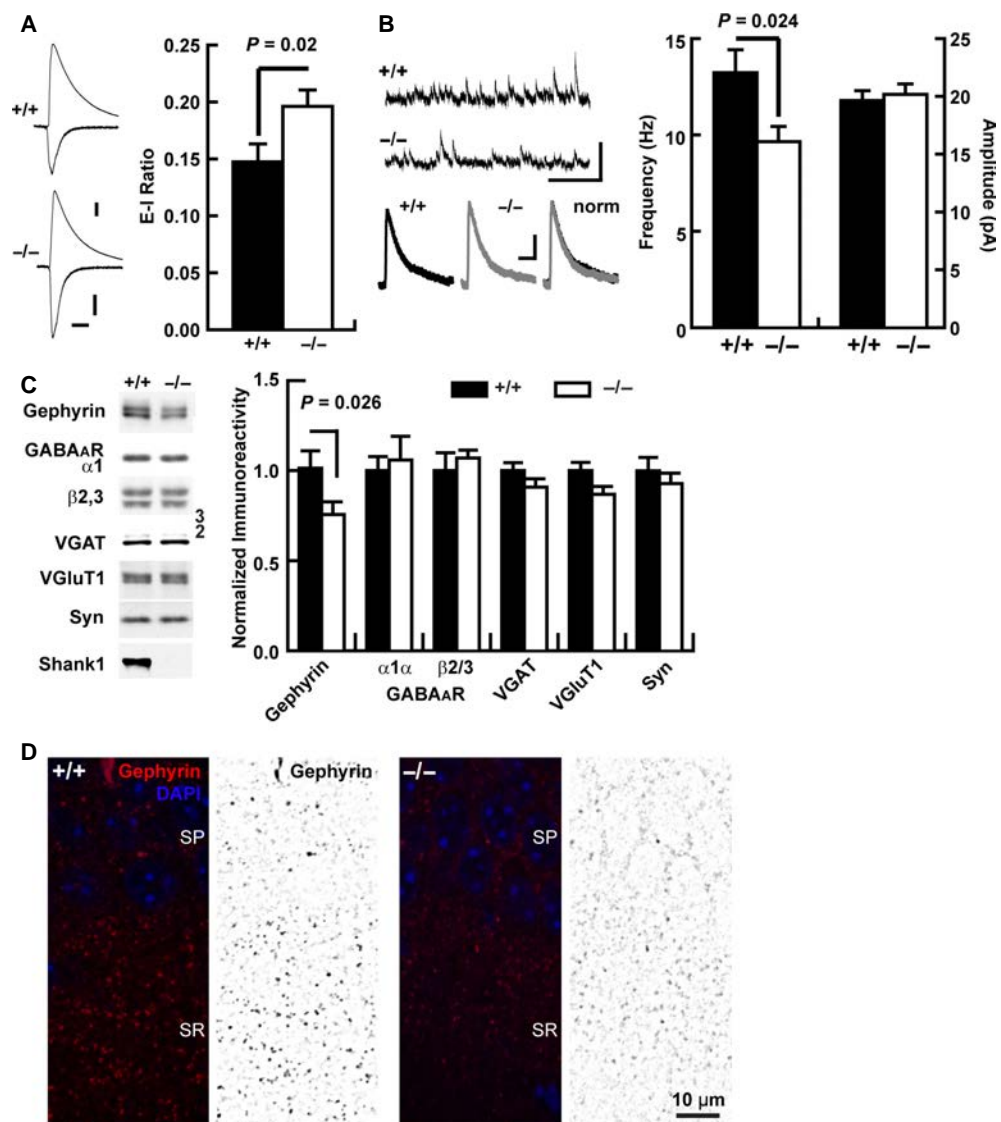s. Stimulus artifacts were truncated. Calibration, 200 and 50 pA, 20 msec. *Right*, Summary graph of *E-I ratio* of wild-type (total n = 20 cells from 6 mice) and Shank1$^{-/-}$ mice (n = 24 / 6, student *t-test*) (see text for definition). (B) Shank1$^{-/-}$ mice reduce inhibitory synaptic transmission. *Left*, Sample traces of mIPSC events (top) and the average traces of mIPSC traces (bottom) obtained from wild-type (+/+) or Shank1$^{-/-}$ (−/−) hippocampal slices. The averaged traces scaled to match the amplitude and aligned at the onset of response are shown at the bottom right (norm). Note that the time course of events is the same. Calibration, 40 pA, 500 msec (top), 5 pA, 20 msec (bottom). *Right,* Summary graphs of the frequency (left) and amplitude (right) of mIPSCs in wild-type (+/+) and Shank1$^{-/-}$ (−/−) animals. Number of cells: wild-type, total 9 cells from 3 mice; Shank1$^{-/-}$, 9 / 3. (C, D, E) Shank1$^{-/-}$ mice exhibit reduced expression of gephyrin. (C) *Left,* Immunoblot analysis of membrane (P2) fractions from individual wild-type (+/+) and Shank1$^{-/-}$ (−/−) mice for the indicated proteins. *Right,* Quantitation of various proteins in membrane fractions. Syn: Synaptophysin. (D) Confocal images of gephyrin puncta in hippocampal CA1 stratum pyramidale (SP) and radiatum (SR) areas from wild-type and Shank1$^{-/-}$ mice. *Left,* double-labeled staining for gephyrin and DAPI. *Right,* the gephyrin images were deconvoluted and quantified after thresholding of fluorescence intensity (grey images).

CHAPTER IV

Discussion

CHAPTER IV

DISCUSSION

Summary

Research presented in this dissertation demonstrated two aspects of preserving excitatory and inhibitory balance in the brain: the homeostatic control of neurotransmitter receptor abundance (Chapter II) and the modulation of excitatory synapses onto inhibitory interneurons (Chapter III). In Chapter II, we set out to identify epigenetic regulators in synaptic compensation. We first showed that chromatin reader L3mbtl1 is downregulated by neuronal activity elevation. We next investigated its role in synaptic functions and found that L3mbtl1 knockout exhibited reduced basal excitatory synaptic transmission and disrupted synaptic downscaling of AMPA receptors. The TTX-induced synaptic upscaling is unaffected. The bidirectional scaling of $GABA_A$ receptor-mediated inhibitory synaptic transmission is also unperturbed. Furthermore, by genome-wide analysis, we showed that L3mbtl1 is associated with transcriptional regulation and binds to the promotors of Ctnnb1 and Gabra2, two genes previously identified to be involved in homeostatic plasticity. Finally, we confirmed that Ctnnb1 knockdown by itself prevents activity-induced synaptic downscaling and also exhibits weakened basal synaptic transmission, mimicking the effect of L3mbtl1 knockout and knockdown. In Chapter III, we addressed the role of scaffold protein Shank1 in excitatory synapses onto inhibitory interneurons. We showed that Shank1 is

expressed in parvalbumin-expressing (PV+) interneurons and regulates the steady-state excitatory synaptic transmission, which in turn affects inhibitory outputs of PV+ neurons to CA1 pyramidal neurons. In addition, we observed that loss of Shank1 caused a shift of the E/I balance towards excitation, due to significantly weakened inhibitory synaptic transmission. This is accompanied by reduced expression of gephyrin, a scaffold protein at inhibitory synapses. Overall, these results are important because they continue the identification and characterization of molecular players involved in preserving excitatory and inhibitory balance in the brain, but they also raise questions that warrant further investigations. In this chapter, I will address the challenges in interpreting the results and the implications for future studies.

Is L3mbtl1 a scaling factor?

Sustained changes in neuronal activity induce transcriptional regulatory events that alter chromatin structure and composition, which in turn has a long-lasting effect on gene expression. This is especially important for terminally differentiated neurons in the face of chronic activity perturbations, where neurons initiate homeostatic control of synaptic transmission to maintain the proper levels of neuronal activity over a time course of days. A question remains whether the involvement of these chromatin modifications merely reflects a general transcriptional control pathway in any cellular system, or that a chromatin regulator is a central component playing a specific role in this context. The study presented

in Chapter II provides several lines of evidence suggesting a highly specific role for the chromatin reader L3mbtl1, a member of the MBT protein family, in transcriptional control of synaptic scaling.

First, we showed that expression of L3mbtl1 mRNA in the brain is highest in hippocampus, particularly in the pyramidal cell layer. We further demonstrated specific expression of L3mbtl1 in neurons, but not in non-neuronal cells such as astrocytes, oligodendrocytes or microglia, suggesting a cell-type specific function. Importantly, the transcript and protein levels of L3mbtl1 are tightly regulated by activity. We observed a drop of L3mbtl1 mRNA level four hours after PTX application, followed by protein reduction 24 hours after PTX application. Interestingly, we also noted a correlated downregulation of the L3mbtl1 target gene Ctnnb1, shown to be an effector protein for L3mbtl1-mediated transcriptional regulation at synapses. Note that this time course loosely correlates with the timing for the expression of homeostatic synaptic scaling (O'Brien et al., 1998; Sutton et al., 2006; Turrigiano et al., 1998). Further characterization determined that the activity-induced downregulation of L3mbtl1 is dependent on Ca^{2+} influx, which is established as a prerequisite to triggering synaptic scaling (Goold and Nicoll, 2010; Ibata et al., 2008) .

Additional piece of evidence for a role of L3mbtl1 in synaptic scaling is the specificity of L3mbtl1's functions in PTX-induced synaptic downscaling of AMPA receptors. We found that L3mbtl1 is not required in TTX-induced excitatory synaptic upscaling and does not affect bidirectional scaling at inhibitory synapses.

Moreover, L3mbtl1 knockout mice express normal Hebbian-type hippocampal LTP, LTD and mGluR-LTD (data not shown). Based on these results, the lack of synaptic downscaling in L3mbtl1 knockout mice is not likely due to a general defect in plasticity; rather, it's tempting to speculate that elevated activity triggers a highly regulated process involving L3mbtl1 and its transcriptional regulation of target genes, needed for expression of synaptic downscaling. Indeed, while activation of Ca^{2+}/calmodulin-dependent signaling has been established as necessary for both scaling up and scaling down (Goold and Nicoll, 2010; Ibata et al., 2008), there are likely divergent downstream pathways involved, indicated by studies showing molecular players specifically involved in unidirectional synaptic scaling. For instance, Arc/Arg3.1 knockout mice fail to induce scaling up of AMPA receptors but continue to display activity induced-scaling down, suggesting that Arc is dispensable for synaptic downscaling (Shepherd et al., 2006). In contrast, synaptic downscaling can be triggered by a separate Ca^{2+}-dependent pathway which involves Plk2/Cdk5-dependent phosphorylation of SPAR and subsequent AMPA receptor endocytosis (Seeburg and Sheng, 2008; Seeburg et al., 2008). Whether these pathways converge, and if so at what point, remains an open question. This study places L3mbtl1 between Ca^{2+} sensing and the expression of divergent effector proteins at synapses.

One complication to interpret L3mbtl1 functions is that the synaptic phenotype in primary dissociated cultures is different from that in organotypic slice cultures. L3mbtl1 knockout or sparse knockdown in CA3 neurons in slice cultures

caused a failure to induce synaptic downscaling, without affecting basal synaptic transmission. In contrast, in primary cultured neurons, L3mbtl1 knockout led to a reduction in basal excitatory synaptic transmission, on top of disruption of synaptic downscaling. An important question rises whether these two aspects of L3mbtl1 functions (basal synaptic transmission and synaptic plasticity) represent multifold effects from parallel pathway, or are mechanistically linked. For example, L3mbtl1 may be a regulator for general maintenance of steady-state AMPA receptor abundance at synapses and may not be related to scaling; the failure to scale down in L3mbtl1 knockout could be attributed to a floor-effect, where there is a limit to the degree of downscaling that can occur under reduced levels of basal synaptic transmission. However, arguments could be made that the activity-regulated L3mbtl1 transcript and protein levels, and the activity-dependent dissociation of chromatin-bound L3mbtl1 from its target promoters strongly suggest a tightly controlled signaling pathway specifically activated during activity elevation. On the premise that L3mbtl1 is in fact a plasticity gene, what could be the reason for reduced basal synaptic transmission in L3mbtl1 knockout primary cultures? In this study, we showed that Gabra2, encoding the GABA$_A$ receptor subunit α2, is also a target for L3mbtl1. In L3mbtl1 knockout primary cultures, we indeed observed reduced expression levels of Gabra2 and decreased inhibitory synaptic transmission, raising the possibility that a homeostatic mechanism could be responsible for the reduction of excitatory synaptic transmission. Why is it induced in primary cultures but not in slice cultures? One explanation is that high-density

dissociated cultures which we used are known to have high levels of neuronal network activity, thus are more readily prone to overexcitation by Gabra2 deficit, triggering a secondary homeostatic response in excitatory synaptic transmission. Ultimately, separating the effects of basal transmission from plasticity requires careful considerations, and which category L3mbtl1 falls into remains open to interpretation.

Activity-dependent gene expression and L3mbtl1-mediated transcription

Synaptic scaling is generally considered to require activity-dependent transcription (Goold and Nicoll, 2010; Ibata et al., 2008; Meadows et al., 2015). In Chapter II, we utilized an unbiased transcriptome screen in dissociated primary neuronal cultures to identify genes that are up- and down-regulated during synaptic downscaling. Not surprisingly, genes with known functions in regulating neuronal excitability were shown to respond to activity. The top functional enriched categories include protein kinases, calcium signaling pathway, synapse, sequence-specific DNA binding (transcription factors). Note that genes previously implicated in synaptic scaling showed changes in expression in our study, including Arc, Bdnf, Camk4, Casp3, Cdk5, Epha4, Grip1, Homer1, Itgb3, Nptx1, Nptx2, Plk2, etc. (reviewed in Chen et al., 2014; Pozo and Goda, 2010; Rich and Wenner, 2007; Turrigiano, 2012). The caveat of this approach is that dissociated cultures are extremely heterogeneous, which may reduce the sensitivity to detect cell-type specific scaling factors involved in synaptic plasticity (Feldman, 2009). To

overcome this challenge, future studies could employ cell sorting approaches prior to RNA-seq, for example by fluorescence-activated cell sorting (FACS) for cells expressing GFP-tagged histone H2B under control of a cell-type specific promoter (Jiang et al., 2008), or by affinity purification-based INTACT (isolation of nuclei tagged in specific cell types) approach (Deal and Henikoff, 2010; Steiner et al., 2012).

Since we established roles for the chromatin reader L3mbtl1 in synaptic downscaling and synaptic transmission, we next asked through what mechanisms L3mbtl1 affects changes at the synapse. In other words, what are the target genes for L3mbtl1-mediated transcriptional regulation? We identified L3mbtl1 chromatin binding sites *in vivo* by ChIP-seq from P7 hippocampus. Because L3mbtl1 regulates synaptic downscaling likely through transcriptional regulation, we would expect a significant overlap between L3mbtl1-bound genes and genes that respond to activity elevation. We performed analyses to test for any enrichment of L3mbtl1 putative targets in activity-deregulated genes. We found that 16% of upregulated and 12% of downregulated genes are putative L3mbtl1 targets. However, since 3,188 L3mbtl1 target genes comprise ~16% of all expressed genes detected in the RNA-seq experiment, there is no significant enrichment. Two possibilities could contribute to the poor correlation. (1) Different experimental systems were used. The ChIP-seq experiment was conducted in P7 pups whereas RNA-seq data were obtained from P0 primary neuronal cultures at *days in vitro* 14. Besides the difference in developmental stages, the heterogenous cell populations

in primary cultures (discussed above) could mask potential L3mbtl1-mediated transcriptional changes. Notably, both the Ctnnb1 and Gabra2 genes, retrospectively confirmed by RT-qPCR to be regulated by activity, fell below our detection threshold in the RNA-seq experiment. (2) Chromatin binding does not necessarily facilitate transcriptional regulation. In fact, it has been shown that a substantial number of transcription factor binding sites are non-functional and do not influence gene expression (Cusanovich et al., 2014). Among the 16 L3mbtl1-bound genes we tested by RT-qPCR, only 2 genes show differential expression in L3mbtl1 knockout neurons. If only a small portion of L3mbtl1 binding sites are functional, we cannot expect a direct correlation between ChIP-seq and RNA-seq data. Therefore, in the current study, we decided to focus on a subset of L3mbtl1-bound genes that have known functions in synaptic scaling and synaptic transmission, and subsequently identified Ctnnb1 and Gabra2 as L3mbtl1 target genes. Note that this approach will not identify uncharacterized genes that have not been previously implicated in synaptic scaling. For example, among the 3,188 L3mbtl putative target genes, the top significantly enriched functional categories include transcriptional regulation and nucleosome assembly, suggesting that L3mbtl1-mediated transcriptional regulation could occur at multiple levels, for instance through regulating regulators of gene expression, influencing chromatin structures, and other secondary mechanisms. Future studies could coordinately perform expression analysis and chromatin binding analysis from sorted cells of the same cell-type (discussed above) in an attempt to shed light on the broader

picture of L3mbtl1-mediated synaptic scaling.

How does L3mbtl1 affect synaptic scaling and transmission through Ctnnb1 and Gabra2? Ctnnb1 encodes β-catenin, which forms adherent junctions with N-cadherin at synaptic clefts and postsynaptic densities (Uchida et al., 1996). The cadherin/catenin complex is known to be critical for synaptic efficacy and spine morphology (Bozdagi et al., 2004; Murase et al., 2002; Okuda et al., 2007; Togashi et al., 2002), axon outgrowth (Riehl et al., 1996), cell-cell contact and recognition (Fannon and Colman, 1996). One group showed that N-cadherin/β-catenin cell-autonomously controls the abundance of postsynaptic AMPA receptors; ablation of postsynaptic β-catenin reduced synaptic transmission and abolished bidirectional homeostatic synaptic scaling (Okuda et al., 2007). Interestingly, they also found that N-cadherin affects presynaptic release under basal conditions, whereas β-catenin disrupts activity blockade-induced upregulation of presynaptic release without affecting the basal level (Vitureira et al., 2012). In Chapter II, we identified Ctnnb1 (β-catenin) as one of the putative target genes of L3mbtl1 and validated that L3mbtl1 binds to the Ctnnb1 promoter in an activity-dependent manner, and acts as a transcriptional activator. We further demonstrated by a knockdown experiment that a reduction in β-catenin levels is sufficient to weaken synaptic transmission and prevent synaptic downscaling in a cell-autonomous manner. We observed a change in AMPA receptor-mediated mEPSC amplitude but not frequency, consistent with previous findings that β-catenin mediates postsynaptic but not presynaptic mechanisms under basal conditions. Taken

together, these results present a model where a constitutive reduction in Ctnnb1 levels caused by L3mbtl1 knockout is responsible for the deficits in basal synaptic transmission and synaptic scaling (**Fig 4.1**). However, this does not rule out possible roles for other molecules regulated by L3mbtl1 in synaptic scaling.

To address this possibility, one could perform rescue experiments, for example, by overexpressing Ctnnb1 in L3mbtl1 knockout cultures, and test if synaptic transmission and synaptic scaling can be restored. Overexpression of exogenous protein, however, often leads to adverse effects. Recently, with the discovery of the CRISPR-Cas9 system, many approaches have been developed to recruit chromatin regulators or transcription factors endogenously to specific genomic sequences (Braun et al., 2017; Enríquez, 2016; Gaj et al., 2013; Tanenbaum et al., 2014; Zetsche et al., 2015). For future experiments, we could tether L3mbtl1 to a dCas9 sgRNA complex using the FIRE-Cas9 system (Braun et al., 2017), with a sgRNA sequence designed to target the Ctnnb1 promoter loci, and specifically activate Ctnnb1 expression in L3mbtl1 knockout neurons. This will bypass any epigenetic regulation by L3mbtl1 on other genes, and directly examine the role for L3mbtl1-mediated Ctnnb1 expression in synaptic transmission and synaptic scaling.

Another target gene regulated by L3mbtl1 is Gabra2, which encodes the α2 subunit of $GABA_A$ receptors. During early development, GABA initially exerts excitatory effects due to a high intracellular chloride concentration, and gradually switches to an inhibitory function by the end of the first postnatal week in rodents

(Valeeva et al., 2013), a process commonly referred to as the "GABA switch" (Ben-Ari et al., 1989; Luhmann and Prince, 1991; Mueller et al., 1984). GABA switching is accompanied by a receptor subunit composition change from α2/α3-containing receptors to α1-containing receptors (Fritschy et al., 1994). The change in subunit compositions is functionally linked to acquisition of the mature type of IPSCs with a shorter duration (Bosman et al., 2005; Okada et al., 2000). The timing of the "GABA switch" is interesting because it coincides with the peak of L3mbtl1 expression at postnatal day 7 in hippocampus. Whether L3mbtl1 affects the switch *in vivo* has not been tested. However, we observed in primary hippocampal cultures that basal inhibitory synaptic transmission is reduced in L3mbtl1 knockout compared to that in wild type, likely due to decreased Gabra2 gene expression (**Fig 4.1**).

While we showed that L3mbtl1 binds to target gene loci and likely mediates transcriptional activation, we still do not know how it performs this function. For example, how is L3mbtl1 recruited to chromatin? To address this question, we first compared L3mbtl1 occupancy to histone modification signals across the genome. With the caveat that the datasets for histone PTMs are from cortical neurons, we were able to establish a positive correlation between L3mbtl1 binding and H3K4me3/H3K27ac signals, generally associated with active transcription; and a negative correlation between L3mbtl1 binding and H3K27me3 signals, a mark for transcription repression. This genome-wide correlation is also observed at specific target gene loci. For example, both the Ctnnb1 and Gabra2 promoters are enriched
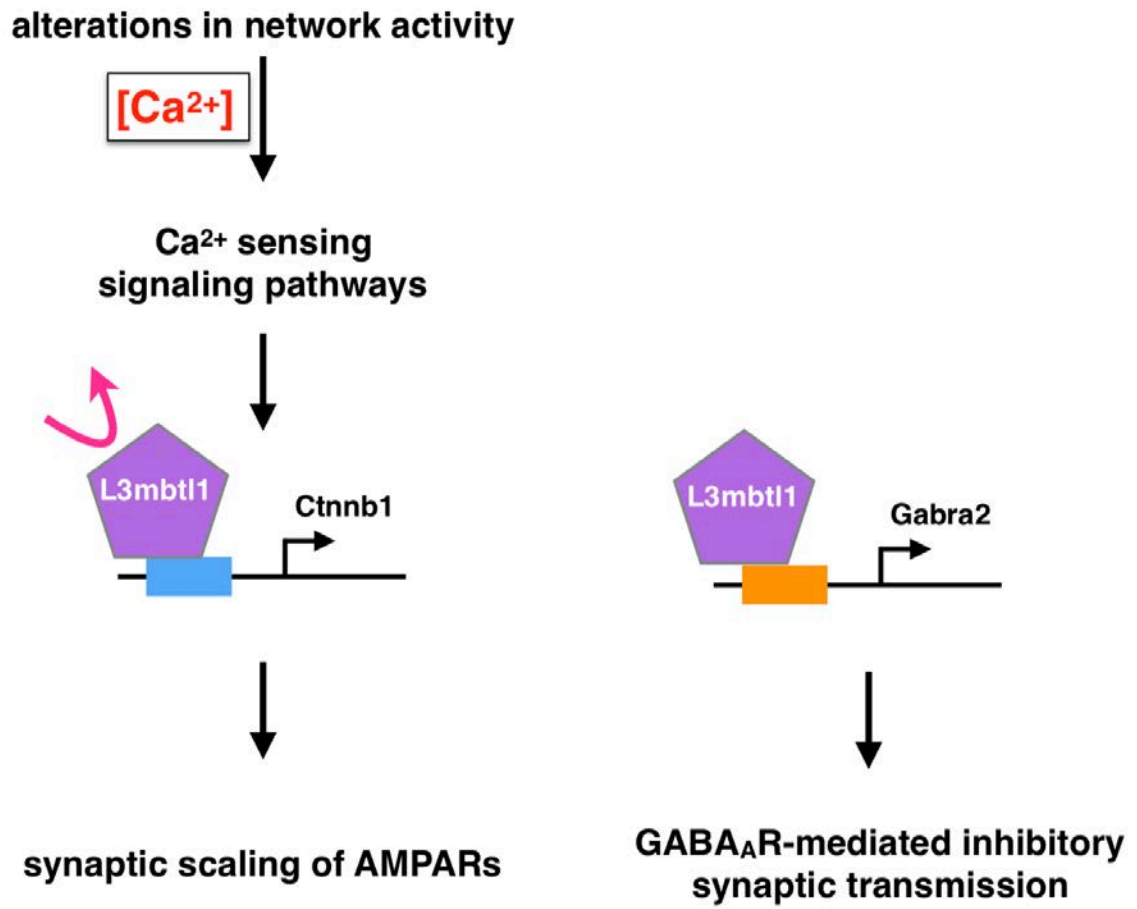
Figure 4.1

Figure 4.1 Models for L3mbtl1-mediated control of synaptic strength and synaptic plasticity.

L3mbtl1 regulates synaptic scaling of AMPARs through target gene Ctnnb1; L3mbtl1 regulates inhibitory synaptic transmission through target gene Gabra2.

for L3mbtl1, H3K4me3 and H3K27ac. This is consistent with the result that both Ctnnb1 and Gabra2 display reduced expression in L3mbtl1 knockout. We note that our data contrasts previous findings that L3mbtl1 represses transcription in heterologous cell lines (Boccuni et al., 2003; Kalakonda et al., 2008; Perna et al., 2015; Trojer et al., 2007). This is not surprising, however, because the functional outcomes for chromatin binding factors are context-dependent, and can have opposing effects in a loci-specific and cell-type specific manner. For example, multiple MBT proteins including L3mbtl2, Scml2, Sfmbt1 and Sfmbt2 work in conjunction with Polycomb Repressive Complex (PRC) (Bonasio et al., 2014; Trojer et al., 2011; Zhang et al., 2013). PRC2 has been shown to regulate the methylation status of H3K27 in a spatially defined manner, which leads to opposing transcriptional outcomes (Ferrari et al., 2014). PRC1 can also mediate gene activation through the action of protein kinases in a tissue-specific manner (Frangini et al., 2013; Gao et al., 2014; Kondo et al., 2014). This does not exclude the possibility that L3mbtl1 may mediate repression of other target genes. It will be interesting to explore the effects of L3mbtl1 regulation on a global scale and assess the transcriptional outcome against the histone disposition of underlying genes. We showed that L3mbtl1-occupied regions are enriched with active histone marks, but whether these histone marks themselves are sufficient to recruit L3mbtl1 still needs to be determined.

Another interesting question to address is what other proteins are included in the L3mbtl1 complex. One candidate may be the E2F/Rb complex. L3mbtl1 has

been shown to interact with E2F/Rb in cell lines through binding to methylated Rb via its MBT domain (Saddic et al., 2010). Our motif analysis identified an E2F transcription factor consensus sequence among the top L3mbtl1 binding motifs, suggesting that L3mbtl1 may be recruited to E2F/Rb target sites *in vivo*. Mass spectrometry analysis of L3mbtl1-immunoprecipitated samples from cultures or hippocampus can help to elucidate protein components in L3mbtl1-containing chromatin complexes.

Animal behavior associated with synaptic scaling deficit

What is the biological relevance of the observed alterations in homeostatic synaptic downscaling by L3mbtl1 knockout? Previously, we reported (published as Shen et al., 2015) that L3mbtl1 knockout mice exhibit decreased anxiety in some behavior paradigms, such as the light-dark box and open-field test, but not in others, such as the elevated plus maze. In addition, decreased depression is observed in the forced swim and tail suspension tests. Spatial working memory, fear conditioning retrieval and locomotor activity are normal. Interestingly, social isolation stress induced a reduction in general locomotor activity in L3mbtl1 knockout mice, which is a depression-related phenotype. Overall, we observed that L3mbtl1 loss caused subtle changes in behavior but that the changes were not consistent across all tests applied.

One important caveat is that all animals tested above are 3-6 months of age. However, in the study presented in Chapter 2, we demonstrated that L3mbtl1

expression peaks at postnatal day 7 and downregulates significantly afterwards into adulthood. Therefore, it will be interesting to test behaviors in infant or juvenile mice. Although multiple studies have demonstrated the importance of synaptic scaling in visual cortex development *in vivo* (Desai et al., 2002; Gainey et al., 2009; Goel and Lee, 2007; Goel et al., 2011; Keck et al., 2013; Maffei and Turrigiano, 2008), to date no animal behavior has been directly associated with synaptic scaling deficit. In L3mbtl1 knockouts, we reported a lack of excitatory synaptic downscaling and reduced inhibitory synaptic transmission caused by decreased Gabra2 levels. It is therefore likely that L3mbtl1 knockout may exhibit disrupted E/I balance and manifest seizure-like behavior. For future studies, it will be interesting to test PTX or PTZ (pentylenetetrazole)-induced epileptic seizures in young animals. We expect to see increased susceptibility to epileptic stress in L3mbtl1 knockouts.

Role of Shank1 in E/I balance

Shank family proteins are a core component of the postsynaptic density (PSD) of excitatory synapses. They interact with other scaffolding molecules such as GKAP (Boeckers et al., 1999; Naisbitt et al., 1999), GRIP (Brückner et al., 1999; Dong et al., 1997), Homer (Tu et al., 1998; Xiao et al., 1998) and Cortactin (Du et al., 1998; Wu and Parsons, 1993) at synapses, thus indirectly affecting the expression, function or distribution of AMPA receptors, NMDA receptors and mGluRs. Overexpression or knockdown studies have found that Shank proteins contribute

to the formation of new synapses, maturation of spine structure and mediate excitatory synaptic transmission (Grabrucker et al., 2011; Haeckel et al., 2008; Roussignol et al., 2005; Sala et al., 2001; Verpelli et al., 2011). In the study presented in Chapter III, we used a Shank1 mutant mouse line with a deletion in its PDZ domain (Hung et al., 2008). Multiple studies have characterized the behavior phenotypes in Shank1 knockout mice, including increased anxiety, decreased locomotor activity, enhanced spatial learning but impaired memory retention, abnormal ultrasonic vocalization and scent marking behaviors indicating impaired social behavior responses (Hung et al., 2008; Silverman et al., 2011; Wöhr et al., 2011), reminiscent of autistic-like behaviors. Indeed, microdeletions of the Shank1 gene has been found in male patients with mild ASD (Sato et al., 2012). Hung et al. demonstrated a role for Shank1 at excitatory synapses onto pyramidal neurons. They observed a moderately altered PSD composition: GKAP and Homer were reduced, while no changes in AMPARs, NMDARs, mGluR5, GRIP, PSD95, Cortactin, CaMKII and β-PIX were observed. This was accompanied by smaller spine sizes, thinner PSDs, and decreased excitatory synaptic transmission (Hung et al., 2008). In Chapter III, we asked what role Shank1 plays at excitatory synapses onto inhibitory interneurons.

We first showed that the expression of Shank1 in PV+ interneurons is comparable to that in pyramidal neurons. Shank1 puncta in PV+ neurons were observed proximal to vesicular glutamate transporter VGluT1, a glutamatergic terminal marker, demonstrating a highly specific localization of Shank1 at

excitatory synapses. Notably, calretinin- and calbindin-expressing interneurons do not exhibit prominent Shank1 signals, suggesting that divergent scaffolding compositions may exist in different interneuron types.

What properties are affected in PV+ interneurons by loss of Shank1? We further reported alterations of several PSD scaffold molecules, reduced basal excitatory synaptic input due to decreases in postsynaptic AMPAR abundance and functional excitatory synapse number, reduced firing rate, and reduced unitary inhibitory synaptic output. Finally, we measured the E/I ratio in pyramidal neurons, and observed a shift of E/I balance towards excitation in Shank1 knockouts. Given the previous finding that basal excitatory transmission is reduced in Shank1 knockouts, we conclude that this shift of E/I balance is due to a larger decrease in inhibition. Consistent with this speculation, we found that $GABA_AR$-mediated mIPSC frequency is reduced, and an inhibitory synaptic scaffold molecule gephyrin is also reduced in Shank1 knockouts. These results are summarized in **Fig 4.2**.

A major complication in interpreting the results from this study is that Shank1 protein is knocked out in all cell types. Without future studies using PV+ neuron specific conditional Shank1 knockout or knockdown, it is difficult to separate cell-autonomous functions of Shank1 in PV+ neurons from secondary effects due to loss of Shank1 in pyramidal cells and other cell types. For example, we showed a reduction of several synaptic scaffold proteins at excitatory synapses onto PV+ neurons in Shank1 knockout mice. This could be a direct consequence of the loss of Shank1 scaffold protein at postsynaptic densities in PV+ neurons. However,
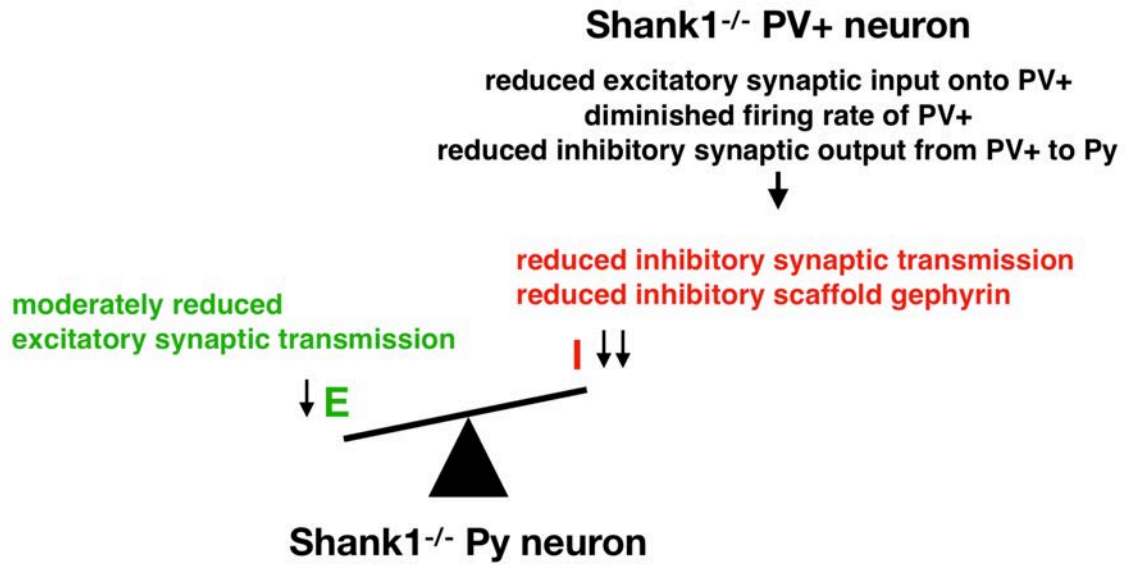
Figure 4.2

Figure 4.2 Summary for Shank1$^{-/-}$ phenotypes.

Shank1$^{-/-}$ pyramidal neurons show increased E/I ratio due to moderate reduction in excitation (E) and strong reduction in inhibition (I).

Shank1-deficient pyramidal neurons could affect postsynaptic PV+ neurons indirectly, for instance by altered excitatory synaptic output. In addition, we found that Shank1 deficient PV+ neurons display reduced firing rates and decreased inhibitory outputs onto pyramidal neurons. If this is indeed cell-autonomous, how does synaptically localized Shank1 affect inhibitory output? Two studies reported that selective disruption of postsynaptic receptors at excitatory synapses onto PV+ interneurons leads to changes in their inhibitory outputs onto pyramidal neurons (Korotkova et al., 2010; Rácz et al., 2009), which is similar to what we observed in this study by knocking out Shank1. An alternative possibility is due to homeostatic mechanisms. Pyramidal neurons have the ability to change their inhibitory synaptic strength cell-autonomously when activity is chronically perturbed (Peng et al., 2010). In this context, reduced excitatory synaptic transmission in pyramidal neurons (Hung et al., 2008) could be the cause of a homeostatic reduction of inhibitory transmission. Indeed, we detected a reduction of mIPSCs in pyramidal neurons, which is a sum for all GABAergic inhibitory synaptic events, and therefore does not necessarily point to abnormal inhibition by PV+ interneurons. The same applies to reduction of gephyrin expression. In summary, the cause and effect of physiologic changes in pyramidal cells and interneurons in Shank1 knockout mice can be difficult to discern. Future studies employing cell-type specific knockout or knockdown approaches will be able to isolate the effects of Shank1 in specific cell types.

Bibliography

Aaron, G.B., and Dichter, M.A. (2001). Excitatory synapses from CA3 pyramidal cells onto neighboring pyramidal cells differ from those onto inhibitory interneurons. Synapse *42*, 199–202.

Abidi, F.E., Miano, M.G., Murray, J.C., and Schwartz, C.E. (2007). A novel mutation in the PHF8 gene is associated with X-linked mental retardation with cleft lip/cleft palate. Clin. Genet. *72*, 19–22.

Abraham, W.C., and Bear, M.F. (1996). Metaplasticity: the plasticity of synaptic plasticity. Trends Neurosci. *19*, 126–130.

Abraham, W.C., and Goddard, G.V. (1983). Asymmetric relationships between homosynaptic long-term potentiation and heterosynaptic long-term depression. Nature *305*, 717–719.

Acs, K., Luijsterburg, M.S., Ackermann, L., Salomons, F.A., Hoppe, T., and Dantuma, N.P. (2011). The AAA-ATPase VCP/p97 promotes 53BP1 recruitment by removing L3MBTL1 from DNA double-strand breaks. Nat. Struct. Mol. Biol. *18*, 1345–1350.

Adams-Cioaba, M., and Min, J. (2009). Structure and function of histone methylation binding proteinsThis paper is one of a selection of papers published in this Special Issue, entitled CSBMCB's 51st Annual Meeting – Epigenetics and Chromatin Dynamics, and has undergone the Journal's usual peer review process. Biochem. Cell Biol. *87*, 93–105.

Adegbola, A., Gao, H., Sommer, S., and Browning, M. (2008). A novel mutation in JARID1C/SMCX in a patient with autism spectrum disorder (ASD). Am. J. Med. Genet. A. *146A*, 505–511.

Akgul, G., and Wollmuth, L.P. (2013). Synapse-associated protein 97 regulates the membrane properties of fast-spiking parvalbumin interneurons in the visual cortex. J. Neurosci. Off. J. Soc. Neurosci. *33*, 12739–12750.

Amaral, D.G., and Witter, M.P. (1989). The three-dimensional organization of the hippocampal formation: a review of anatomical data. Neuroscience *31*, 571–591.

Amir, R.E., Van den Veyver, I.B., Wan, M., Tran, C.Q., Francke, U., and Zoghbi, H.Y. (1999). Rett syndrome is caused by mutations in X-linked MECP2, encoding methyl-CpG-binding protein 2. Nat. Genet. *23*, 185–188.

Anders, S., Pyl, P.T., and Huber, W. (2015). HTSeq—a Python framework to work with high-throughput sequencing data. Bioinformatics *31*, 166–169.

Anggono, V., Clem, R.L., and Huganir, R.L. (2011). PICK1 loss of function occludes homeostatic synaptic scaling. J. Neurosci. Off. J. Soc. Neurosci. *31*, 2188–2196.

Angulo, M.C., Lambolez, B., Audinat, E., Hestrin, S., and Rossier, J. (1997). Subunit composition, kinetic, and permeation properties of AMPA receptors in single neocortical nonpyramidal cells. J. Neurosci. Off. J. Soc. Neurosci. *17*, 6685–6696.

Aoto, J., Nam, C.I., Poon, M.M., Ting, P., and Chen, L. (2008). Synaptic signaling by all-trans retinoic acid in homeostatic synaptic plasticity. Neuron *60*, 308–320.

Asaka, Y., Jugloff, D.G.M., Zhang, L., Eubanks, J.H., and Fitzsimonds, R.M. (2006). Hippocampal synaptic plasticity is impaired in the Mecp2-null mouse model of Rett syndrome. Neurobiol. Dis. *21*, 217–227.

Aziz, A., Baxter, E.J., Edwards, C., Cheong, C.Y., Ito, M., Bench, A., Kelley, R., Silber, Y., Beer, P.A., Chng, K., et al. (2013). Cooperativity of imprinted genes inactivated by acquired chromosome 20q deletions. J. Clin. Invest. *123*, 2169–2182.

Barski, A., Cuddapah, S., Cui, K., Roh, T.-Y., Schones, D.E., Wang, Z., Wei, G., Chepelev, I., and Zhao, K. (2007). High-resolution profiling of histone methylations in the human genome. Cell *129*, 823–837.

Ben-Ari, Y., Cherubini, E., Corradetti, R., and Gaiarsa, J.L. (1989). Giant synaptic potentials in immature rat CA3 hippocampal neurones. J. Physiol. *416*, 303–325.

Bender, V.A., Bender, K.J., Brasier, D.J., and Feldman, D.E. (2006). Two coincidence detectors for spike timing-dependent plasticity in somatosensory cortex. J. Neurosci. Off. J. Soc. Neurosci. *26*, 4166–4177.

Benevento, M., Iacono, G., Selten, M., Ba, W., Oudakker, A., Frega, M., Keller, J., Mancini, R., Lewerissa, E., Kleefstra, T., et al. (2016). Histone Methylation by the Kleefstra Syndrome Protein EHMT1 Mediates Homeostatic Synaptic Scaling. Neuron *91*, 341–355.

Berkel, S., Tang, W., Treviño, M., Vogt, M., Obenhaus, H.A., Gass, P., Scherer, S.W., Sprengel, R., Schratt, G., and Rappold, G.A. (2012). Inherited and de novo SHANK2 variants associated with autism spectrum disorder impair neuronal morphogenesis and physiology. Hum. Mol. Genet. *21*, 344–357.

Bharadwaj, R., Jiang, Y., Mao, W., Jakovcevski, M., Dincer, A., Krueger, W., Garbett, K., Whittle, C., Tushir, J.S., Liu, J., et al. (2013). Conserved Chromosome 2q31 Conformations Are Associated with Transcriptional Regulation of GAD1 GABA Synthesis Enzyme and Altered in Prefrontal Cortex of Subjects with Schizophrenia. J. Neurosci. *33*, 11839–11851.

Bi, G.Q., and Poo, M.M. (1998). Synaptic modifications in cultured hippocampal neurons: dependence on spike timing, synaptic strength, and postsynaptic cell type. J. Neurosci. Off. J. Soc. Neurosci. *18*, 10464–10472.

Blackman, M.P., Djukic, B., Nelson, S.B., and Turrigiano, G.G. (2012). A Critical and Cell-Autonomous Role for MeCP2 in Synaptic Scaling Up. J. Neurosci. *32*, 13529–13536.

Bliss, T.V., and Lomo, T. (1973). Long-lasting potentiation of synaptic transmission in the dentate area of the anaesthetized rabbit following stimulation of the perforant path. J. Physiol. *232*, 331–356.

Boccuni, P., MacGrogan, D., Scandura, J.M., and Nimer, S.D. (2003). The Human L(3)MBT Polycomb Group Protein Is a Transcriptional Repressor and

Interacts Physically and Functionally with TEL (ETV6). J. Biol. Chem. *278*, 15412–15420.

Boeckers, T.M., Winter, C., Smalla, K.H., Kreutz, M.R., Bockmann, J., Seidenbecher, C., Garner, C.C., and Gundelfinger, E.D. (1999). Proline-rich synapse-associated proteins ProSAP1 and ProSAP2 interact with synaptic proteins of the SAPAP/GKAP family. Biochem. Biophys. Res. Commun. *264*, 247–252.

Bonasio, R., Lecona, E., and Reinberg, D. (2010). MBT domain proteins in development and disease. Semin. Cell Dev. Biol. *21*, 221–230.

Bonasio, R., Lecona, E., Narendra, V., Voigt, P., Parisi, F., Kluger, Y., and Reinberg, D. (2014). Interactions with RNA direct the Polycomb group protein SCML2 to chromatin where it represses target genes. ELife *3*.

Bosman, L.W.J., Heinen, K., Spijker, S., and Brussaard, A.B. (2005). Mice lacking the major adult GABAA receptor subtype have normal number of synapses, but retain juvenile IPSC kinetics until adulthood. J. Neurophysiol. *94*, 338–346.

Boulter, J., Hollmann, M., O'Shea-Greenfield, A., Hartley, M., Deneris, E., Maron, C., and Heinemann, S. (1990). Molecular cloning and functional expression of glutamate receptor subunit genes. Science *249*, 1033–1037.

Bozdagi, O., Valcin, M., Poskanzer, K., Tanaka, H., and Benson, D.L. (2004). Temporally distinct demands for classic cadherins in synapse formation and maturation. Mol. Cell. Neurosci. *27*, 509–521.

Braun, S.M.G., Kirkland, J.G., Chory, E.J., Husmann, D., Calarco, J.P., and Crabtree, G.R. (2017). Rapid and reversible epigenome editing by endogenous chromatin regulators. Nat. Commun. *8*, 560.

Brewer, G.J., Torricelli, J.R., Evege, E.K., and Price, P.J. (1993). Optimized survival of hippocampal neurons in B27-supplemented Neurobasal, a new serum-free medium combination. J. Neurosci. Res. *35*, 567–576.

Brückner, K., Pablo Labrador, J., Scheiffele, P., Herb, A., Seeburg, P.H., and Klein, R. (1999). EphrinB ligands recruit GRIP family PDZ adaptor proteins into raft membrane microdomains. Neuron *22*, 511–524.

Buonanno, A. (2010). The Neuregulin Signaling Pathway and Schizophrenia: From Genes to Synapses and Neural Circuits. Brain Res. Bull. *83*, 122–131.

Burrone, J., O'Byrne, M., and Murthy, V.N. (2002). Multiple forms of synaptic plasticity triggered by selective suppression of activity in individual neurons. Nature *420*, 414–418.

Cajal, S.R. (1913). Degeneration and regeneration of the nervous system. (Madrid: Moya). (Translated and edited by Raoul M., 1928, London: Oxford University Press). (Reprinted and edited with additional translations by DeFelipe, J. and Jones, E.G., 1991, New York: Oxford University Press)

Carlén, M., Meletis, K., Siegle, J.H., Cardin, J.A., Futai, K., Vierling-Claassen, D., Rühlmann, C., Jones, S.R., Deisseroth, K., Sheng, M., et al. (2012). A critical role for NMDA receptors in parvalbumin interneurons for gamma rhythm induction and behavior. Mol. Psychiatry *17*, 537–548.

Catania, M.V., Tölle, T.R., and Monyer, H. (1995). Differential expression of AMPA receptor subunits in NOS-positive neurons of cortex, striatum, and hippocampus. J. Neurosci. Off. J. Soc. Neurosci. *15*, 7046–7061.

Chahrour, M., and Zoghbi, H.Y. (2007). The story of Rett syndrome: from clinic to neurobiology. Neuron *56*, 422–437.

Chang, C.-L., Trimbuch, T., Chao, H.-T., Jordan, J.-C., Herman, M.A., and Rosenmund, C. (2014). Investigation of synapse formation and function in a glutamatergic-GABAergic two-neuron microcircuit. J. Neurosci. Off. J. Soc. Neurosci. *34*, 855–868.

Chang, M.C., Park, J.M., Pelkey, K.A., Grabenstatter, H.L., Xu, D., Linden, D.J., Sutula, T.P., McBain, C.J., and Worley, P.F. (2010). Narp regulates homeostatic scaling of excitatory synapses on parvalbumin-expressing interneurons. Nat. Neurosci. *13*, 1090–1097.

Chen, L., Lau, A.G., and Sarti, F. (2014). Synaptic retinoic acid signaling and homeostatic synaptic plasticity. Neuropharmacology *78*, 3–12.

Cho, K.O., Hunt, C.A., and Kennedy, M.B. (1992). The rat brain postsynaptic density fraction contains a homolog of the Drosophila discs-large tumor suppressor protein. Neuron *9*, 929–942.

Cingolani, L.A., and Goda, Y. (2008). Differential involvement of beta3 integrin in pre- and postsynaptic forms of adaptation to chronic activity deprivation. Neuron Glia Biol. *4*, 179–187.

Cingolani, L.A., Thalhammer, A., Yu, L.M.Y., Catalano, M., Ramos, T., Colicos, M.A., and Goda, Y. (2008). Activity-Dependent Regulation of Synaptic AMPA Receptor Composition and Abundance by β3 Integrins. Neuron *58*, 749–762.

Cobb, S.R., Buhl, E.H., Halasy, K., Paulsen, O., and Somogyi, P. (1995). Synchronization of neuronal activity in hippocampus by individual GABAergic interneurons. Nature *378*, 75–78.

Colino, A., Huang, Y.Y., and Malenka, R.C. (1992). Characterization of the integration time for the stabilization of long-term potentiation in area CA1 of the hippocampus. J. Neurosci. Off. J. Soc. Neurosci. *12*, 180–187.

Collins, A.L., Ma, D., Whitehead, P.L., Martin, E.R., Wright, H.H., Abramson, R.K., Hussman, J.P., Haines, J.L., Cuccaro, M.L., Gilbert, J.R., et al. (2006). Investigation of autism and GABA receptor subunit genes in multiple ethnic groups. Neurogenetics *7*, 167–174.

Crowe, S.L., Movsesyan, V.A., Jorgensen, T.J., and Kondratyev, A. (2006). Rapid Phosphorylation of Histone H2A.X Following Ionotropic Glutamate Receptor Activation. Eur. J. Neurosci. *23*, 2351–2361.

Crowe, S.L., Tsukerman, S., Gale, K., Jorgensen, T.J., and Kondratyev, A.D. (2011). Phosphorylation of Histone H2A.X as an Early Marker of Neuronal Endangerment following Seizures in the Adult Rat Brain. J. Neurosci. *31*, 7648–7656.

Cusanovich, D.A., Pavlovic, B., Pritchard, J.K., and Gilad, Y. (2014). The Functional Consequences of Variation in Transcription Factor Binding. PLOS Genet. *10*, e1004226.

Davis, G.W. (2006). Homeostatic control of neural activity: from phenomenology to molecular design. Annu Rev Neurosci *29*, 307–323.

Deal, R.B., and Henikoff, S. (2010). A simple method for gene expression and chromatin profiling of individual cell types within a tissue. Dev. Cell *18*, 1030–1040.

Debanne, D., Gähwiler, B.H., and Thompson, S.M. (1998). Long-term synaptic plasticity between pairs of individual CA3 pyramidal cells in rat hippocampal slice cultures. J. Physiol. *507 (Pt 1)*, 237–247.

Deisseroth, K., Bito, H., Schulman, H., and Tsien, R.W. (1995). Synaptic plasticity: A molecular mechanism for metaplasticity. Curr. Biol. CB *5*, 1334–1338.

Desai, N., Cudmore, R., Nelson, S., and Turrigiano, G.G. (2002). Critical period for experience-dependent synaptic scaling in visual cortex. Nat. Neurosci.

Desai, N.S., Rutherford, L.C., and Turrigiano, G.G. (1999). BDNF regulates the intrinsic excitability of cortical neurons. Learn. Mem. Cold Spring Harb. N *6*, 284–291.

Di Croce, L., and Helin, K. (2013). Transcriptional regulation by Polycomb group proteins. Nat. Struct. Mol. Biol. *20*, 1147–1155.

Diering, G.H., Nirujogi, R.S., Roth, R.H., Worley, P.F., Pandey, A., and Huganir, R.L. (2017). Homer1a drives homeostatic scaling-down of excitatory synapses during sleep. Science *355*, 511–515.

Dong, H., O'Brien, R.J., Fung, E.T., Lanahan, A.A., Worley, P.F., and Huganir, R.L. (1997). GRIP: a synaptic PDZ domain-containing protein that interacts with AMPA receptors. Nature *386*, 279–284.

Douglas, R., and Martin, K.A. (1998). The Synaptic Organization of the Brain. Neocortex 459–509.

Du, Y., Weed, S.A., Xiong, W.C., Marshall, T.D., and Parsons, J.T. (1998). Identification of a novel cortactin SH3 domain-binding protein and its localization to growth cones of cultured neurons. Mol. Cell. Biol. *18*, 5838–5851.

Ehlers, M.D. (2003). Activity level controls postsynaptic composition and signaling via the ubiquitin-proteasome system. Nat. Neurosci. *6*, 231–242.

Elias, G.M., and Nicoll, R.A. (2007). Synaptic trafficking of glutamate receptors by MAGUK scaffolding proteins. Trends Cell Biol. *17*, 343–352.

Engert, F., and Bonhoeffer, T. (1999). Dendritic spine changes associated with hippocampal long-term synaptic plasticity. Nature *399*, 19978.

Enríquez, P. (2016). CRISPR-Mediated Epigenome Editing. Yale J. Biol. Med. *89*, 471–486.

Fannon, A.M., and Colman, D.R. (1996). A Model for Central Synaptic Junctional Complex Formation Based on the Differential Adhesive Specificities of the Cadherins. Neuron *17*, 423–434.

Fatemi, S.H., Halt, A.R., Stary, J.M., Kanodia, R., Schulz, S.C., and Realmuto, G.R. (2002). Glutamic acid decarboxylase 65 and 67 kDa proteins are reduced in autistic parietal and cerebellar cortices. Biol. Psychiatry *52*, 805–810.

Fatemi, S.H., Reutiman, T.J., Folsom, T.D., and Thuras, P.D. (2009). GABA(A) receptor downregulation in brains of subjects with autism. J. Autism Dev. Disord. *39*, 223–230.

Fatemi, S.H., Folsom, T.D., Rooney, R.J., and Thuras, P.D. (2013). mRNA and protein expression for novel GABAA receptors θ and ρ2 are altered in schizophrenia and mood disorders; relevance to FMRP-mGluR5 signaling pathway. Transl. Psychiatry *3*, e271.

Fazzari, P., Paternain, A.V., Valiente, M., Pla, R., Luján, R., Lloyd, K., Lerma, J., Marín, O., and Rico, B. (2010). Control of cortical GABA circuitry development by Nrg1 and ErbB4 signalling. Nature *464*, 1376–1380.

Feldman, D.E. (2009). Synaptic Mechanisms for Plasticity in Neocortex. Annu. Rev. Neurosci. *32*, 33–55.

Ferrari, K.J., Scelfo, A., Jammula, S., Cuomo, A., Barozzi, I., Stützer, A., Fischle, W., Bonaldi, T., and Pasini, D. (2014). Polycomb-dependent H3K27me1 and H3K27me2 regulate active transcription and enhancer fidelity. Mol. Cell *53*, 49–62.

Fino, E., and Yuste, R. (2011). Dense inhibitory connectivity in neocortex. Neuron *69*, 1188–1203.

Frangini, A., Sjöberg, M., Roman-Trufero, M., Dharmalingam, G., Haberle, V., Bartke, T., Lenhard, B., Malumbres, M., Vidal, M., and Dillon, N. (2013). The aurora B kinase and the polycomb protein ring1B combine to regulate active promoters in quiescent lymphocytes. Mol. Cell *51*, 647–661.

Freund, T.F., and Katona, I. (2007). Perisomatic inhibition. Neuron *56*, 33–42.

Fritschy, J.M., Paysan, J., Enna, A., and Mohler, H. (1994). Switch in the expression of rat GABAA-receptor subtypes during postnatal development: an immunohistochemical study. J. Neurosci. *14*, 5302–5324.

Fu, A.K.Y., Hung, K.-W., Fu, W.-Y., Shen, C., Chen, Y., Xia, J., Lai, K.-O., and Ip, N.Y. (2011). APC(Cdh1) mediates EphA4-dependent downregulation of AMPA receptors in homeostatic plasticity. Nat. Neurosci. *14*, 181–189.

Fuchs, E.C., Zivkovic, A.R., Cunningham, M.O., Middleton, S., Lebeau, F.E.N., Bannerman, D.M., Rozov, A., Whittington, M.A., Traub, R.D., Rawlins, J.N.P., et al. (2007). Recruitment of parvalbumin-positive interneurons determines hippocampal function and associated behavior. Neuron *53*, 591–604.

Futai, K., Doty, C.D., Baek, B., Ryu, J., and Sheng, M. (2013). Specific Trans-Synaptic Interaction with Inhibitory Interneuronal Neurexin Underlies Differential Ability of Neuroligins to Induce Functional Inhibitory Synapses. J. Neurosci. *33*, 3612–3623.

Gainey, M.A., Hurvitz-Wolff, J.R., Lambo, M.E., and Turrigiano, G.G. (2009). Synaptic Scaling Requires the GluR2 Subunit of the AMPA Receptor. J. Neurosci. Off. J. Soc. Neurosci. *29*, 6479–6489.

Gainey, M.A., Tatavarty, V., Nahmani, M., Lin, H., and Turrigiano, G.G. (2015). Activity-dependent synaptic GRIP1 accumulation drives synaptic scaling up in response to action potential blockade. Proc. Natl. Acad. Sci. U. S. A. *112*, E3590-3599.

Gaj, T., Gersbach, C.A., and Barbas, C.F. (2013). ZFN, TALEN, and CRISPR/Cas-based methods for genome engineering. Trends Biotechnol. *31*, 397–405.

Gao, Z., Lee, P., Stafford, J.M., von Schimmelmann, M., Schaefer, A., and Reinberg, D. (2014). An AUTS2-Polycomb complex activates gene expression in the CNS. Nature *516*, 349–354.

Garcia, R.A., Vasudevan, K., and Buonanno, A. (2000). The neuregulin receptor ErbB-4 interacts with PDZ-containing proteins at neuronal synapses. Proc. Natl. Acad. Sci. U. S. A. *97*, 3596–3601.

Gatto, C.L., and Broadie, K. (2010). Genetic controls balancing excitatory and inhibitory synaptogenesis in neurodevelopmental disorder models. Front. Synaptic Neurosci. *2*, 4.

Geiger, J.R., Melcher, T., Koh, D.S., Sakmann, B., Seeburg, P.H., Jonas, P., and Monyer, H. (1995). Relative abundance of subunit mRNAs determines gating and Ca2+ permeability of AMPA receptors in principal neurons and interneurons in rat CNS. Neuron *15*, 193–204.

Ghosh, A., Carnahan, J., and Greenberg, M.E. (1994). Requirement for BDNF in activity-dependent survival of cortical neurons. Science *263*, 1618–1623.

Goel, A., and Lee, H.-K. (2007). Persistence of experience-induced homeostatic synaptic plasticity through adulthood in superficial layers of mouse visual cortex. J. Neurosci. Off. J. Soc. Neurosci. *27*, 6692–6700.

Goel, A., Xu, L.W., Snyder, K.P., Song, L., Goenaga-Vazquez, Y., Megill, A., Takamiya, K., Huganir, R.L., and Lee, H.-K. (2011). Phosphorylation of AMPA receptors is required for sensory deprivation-induced homeostatic synaptic plasticity. PloS One *6*, e18264.

Goldberg, J.H., Yuste, R., and Tamas, G. (2003). Ca2+ imaging of mouse neocortical interneurone dendrites: contribution of Ca2+-permeable AMPA and NMDA receptors to subthreshold Ca2+dynamics. J. Physiol. *551*, 67–78.

Goold, C.P., and Nicoll, R.A. (2010). Single-Cell Optogenetic Excitation Drives Homeostatic Synaptic Depression. Neuron *68*, 512–528.

Grabrucker, A.M., Knight, M.J., Proepper, C., Bockmann, J., Joubert, M., Rowan, M., Nienhaus, G.U., Garner, C.C., Bowie, J.U., Kreutz, M.R., et al. (2011). Concerted action of zinc and ProSAP/Shank in synaptogenesis and synapse maturation. EMBO J. *30*, 569–581.

Greer, P.L., Hanayama, R., Bloodgood, B.L., Mardinly, A.R., Lipton, D.M., Flavell, S.W., Kim, T.-K., Griffith, E.C., Waldon, Z., Maehr, R., et al. (2010). The Angelman Syndrome protein Ube3A regulates synapse development by ubiquitinating arc. Cell *140*, 704–716.

Guan, J.-S., Haggarty, S.J., Giacometti, E., Dannenberg, J.-H., Joseph, N., Gao, J., Nieland, T.J.F., Zhou, Y., Wang, X., Mazitschek, R., et al. (2009). HDAC2 negatively regulates memory formation and synaptic plasticity. Nature *459*, 55–60.

Guan, Z., Giustetto, M., Lomvardas, S., Kim, J.-H., Miniaci, M.C., Schwartz, J.H., Thanos, D., and Kandel, E.R. (2002). Integration of Long-Term-Memory-

Related Synaptic Plasticity Involves Bidirectional Regulation of Gene Expression and Chromatin Structure. Cell *111*, 483–493.

Guilmatre, A., Huguet, G., Delorme, R., and Bourgeron, T. (2014). The emerging role of SHANK genes in neuropsychiatric disorders. Dev. Neurobiol. *74*, 113–122.

Gupta, S., Kim, S.Y., Artis, S., Molfese, D.L., Schumacher, A., Sweatt, J.D., Paylor, R.E., and Lubin, F.D. (2010). Histone Methylation Regulates Memory Formation. J. Neurosci. *30*, 3589–3599.

Gurvich, N., Perna, F., Farina, A., Voza, F., Menendez, S., Hurwitz, J., and Nimer, S.D. (2010). L3MBTL1 polycomb protein, a candidate tumor suppressor in del(20q12) myeloid disorders, is essential for genome stability. Proc. Natl. Acad. Sci. *107*, 22552–22557.

Guy, J., Gan, J., Selfridge, J., Cobb, S., and Bird, A. (2007). Reversal of Neurological Defects in a Mouse Model of Rett Syndrome. Science *315*, 1143–1147.

Haeckel, A., Ahuja, R., Gundelfinger, E.D., Qualmann, B., and Kessels, M.M. (2008). The actin-binding protein Abp1 controls dendritic spine morphology and is important for spine head and synapse formation. J. Neurosci. Off. J. Soc. Neurosci. *28*, 10031–10044.

Han, K., Holder, J.L., Schaaf, C.P., Lu, H., Chen, H., Kang, H., Tang, J., Wu, Z., Hao, S., Cheung, S.W., et al. (2013). SHANK3 overexpression causes manic-like behaviour with unique pharmacogenetic properties. Nature *503*, 72–77.

Harada, M., Taki, M.M., Nose, A., Kubo, H., Mori, K., Nishitani, H., and Matsuda, T. (2011). Non-invasive evaluation of the GABAergic/glutamatergic system in autistic patients observed by MEGA-editing proton MR spectroscopy using a clinical 3 tesla instrument. J. Autism Dev. Disord. *41*, 447–454.

Hartman, K.N., Pal, S.K., Burrone, J., and Murthy, V.N. (2006). Activity-dependent regulation of inhibitory synaptic transmission in hippocampal neurons. Nat. Neurosci. *9*, 642–649.

Hebb, D.O. (1949). The organization of behavior: a neuropsychological theory (New York: Wiley).

Heinz, S., Benner, C., Spann, N., Bertolino, E., Lin, Y.C., Laslo, P., Cheng, J.X., Murre, C., Singh, H., and Glass, C.K. (2010). Simple Combinations of Lineage-Determining Transcription Factors Prime cis-Regulatory Elements Required for Macrophage and B Cell Identities. Mol. Cell *38*, 576–589.

Hengen, K.B., Torrado Pacheco, A., McGregor, J.N., Van Hooser, S.D., and Turrigiano, G.G. (2016). Neuronal Firing Rate Homeostasis Is Inhibited by Sleep and Promoted by Wake. Cell *165*, 180–191.

Hensch, T.K. (2004). Critical period regulation. Annu. Rev. Neurosci. *27*, 549–579.

Hou, Q., Zhang, D., Jarzylo, L., Huganir, R.L., and Man, H.-Y. (2008). Homeostatic regulation of AMPA receptor expression at single hippocampal synapses. Proc. Natl. Acad. Sci. U. S. A. *105*, 775–780.

Hu, H., Shao, L.R., Chavoshy, S., Gu, N., Trieb, M., Behrens, R., Laake, P., Pongs, O., Knaus, H.G., Ottersen, O.P., et al. (2001). Presynaptic Ca2+-activated K+ channels in glutamatergic hippocampal terminals and their role in spike repolarization and regulation of transmitter release. J. Neurosci. Off. J. Soc. Neurosci. *21*, 9585–9597.

Hu, J.-H., Park, J.M., Park, S., Xiao, B., Dehoff, M.H., Kim, S., Hayashi, T., Schwarz, M.K., Huganir, R.L., Seeburg, P.H., et al. (2010). Homeostatic scaling requires group I mGluR activation mediated by Homer1a. Neuron *68*, 1128–1142.

Huang, D.W., Sherman, B.T., and Lempicki, R.A. (2009a). Bioinformatics enrichment tools: paths toward the comprehensive functional analysis of large gene lists. Nucleic Acids Res. *37*, 1–13.

Huang, D.W., Sherman, B.T., and Lempicki, R.A. (2009b). Systematic and integrative analysis of large gene lists using DAVID bioinformatics resources. Nat. Protoc. *4*, 44–57.

Huang, H.-S., Matevossian, A., Whittle, C., Kim, S.Y., Schumacher, A., Baker, S.P., and Akbarian, S. (2007). Prefrontal dysfunction in schizophrenia involves mixed-lineage leukemia 1-regulated histone methylation at GABAergic gene promoters. J. Neurosci. Off. J. Soc. Neurosci. *27*, 11254–11262.

Huang, Y.Z., Won, S., Ali, D.W., Wang, Q., Tanowitz, M., Du, Q.S., Pelkey, K.A., Yang, D.J., Xiong, W.C., Salter, M.W., et al. (2000). Regulation of neuregulin signaling by PSD-95 interacting with ErbB4 at CNS synapses. Neuron *26*, 443–455.

Hung, A.Y., Futai, K., Sala, C., Valtschanoff, J.G., Ryu, J., Woodworth, M.A., Kidd, F.L., Sung, C.C., Miyakawa, T., Bear, M.F., et al. (2008). Smaller dendritic spines, weaker synaptic transmission, but enhanced spatial learning in mice lacking Shank1. J. Neurosci. Off. J. Soc. Neurosci. *28*, 1697–1708.

Ibata, K., Sun, Q., and Turrigiano, G.G. (2008). Rapid synaptic scaling induced by changes in postsynaptic firing. Neuron *57*, 819–826.

Jaaro-Peled, H., Hayashi-Takagi, A., Seshadri, S., Kamiya, A., Brandon, N.J., and Sawa, A. (2009). Neurodevelopmental mechanisms of schizophrenia: understanding disturbed postnatal brain maturation through neuregulin-1-ErbB4 and DISC1. Trends Neurosci. *32*, 485–495.

Jacob, T.C., Bogdanov, Y.D., Magnus, C., Saliba, R.S., Kittler, J.T., Haydon, P.G., and Moss, S.J. (2005). Gephyrin regulates the cell surface dynamics of synaptic GABAA receptors. J. Neurosci. Off. J. Soc. Neurosci. *25*, 10469–10478.

Jiang, Y.-H., and Ehlers, M.D. (2013). Modeling autism by SHANK gene mutations in mice. Neuron *78*, 8–27.

Jiang, Y., Matevossian, A., Huang, H.-S., Straubhaar, J., and Akbarian, S. (2008). Isolation of neuronal chromatin from brain tissue. BMC Neurosci. *9*, 42.

Jonas, P., Racca, C., Sakmann, B., Seeburg, P.H., and Monyer, H. (1994). Differences in Ca2+ permeability of AMPA-type glutamate receptor channels

in neocortical neurons caused by differential GluR-B subunit expression. Neuron *12*, 1281–1289.

Ju, W., Morishita, W., Tsui, J., Gaietta, G., Deerinck, T.J., Adams, S.R., Garner, C.C., Tsien, R.Y., Ellisman, M.H., and Malenka, R.C. (2004). Activity-dependent regulation of dendritic synthesis and trafficking of AMPA receptors. Nat. Neurosci. *7*, nn1189.

Kalakonda, N., Fischle, W., Boccuni, P., Gurvich, N., Hoya-Arias, R., Zhao, X., Miyata, Y., MacGrogan, D., Zhang, J., Sims, J.K., et al. (2008). Histone H4 lysine 20 monomethylation promotes transcriptional repression by L3MBTL1. Oncogene *27*, 4293–4304.

Keck, T., Keller, G.B., Jacobsen, R.I., Eysel, U.T., Bonhoeffer, T., and Hübener, M. (2013). Synaptic Scaling and Homeostatic Plasticity in the Mouse Visual Cortex In Vivo. Neuron *80*, 327–334.

Kilman, V., van Rossum, M.C., and Turrigiano, G.G. (2002). Activity deprivation reduces miniature IPSC amplitude by decreasing the number of postsynaptic GABAA receptors clustered at neocortical synapses. J. Neurosci. *22*, 1328–1337.

Kim, J., Tsien, R.W., and Alger, B.E. (2012). An improved test for detecting multiplicative homeostatic synaptic scaling. PloS One *7*, e37364.

Kim, M.J., Futai, K., Jo, J., Hayashi, Y., Cho, K., and Sheng, M. (2007). Synaptic accumulation of PSD-95 and synaptic function regulated by phosphorylation of serine-295 of PSD-95. Neuron *56*, 488–502.

Kleefstra, T., Kramer, J.M., Neveling, K., Willemsen, M.H., Koemans, T.S., Vissers, L.E.L.M., Wissink-Lindhout, W., Fenckova, M., van den Akker, W.M.R., Kasri, N.N., et al. (2012). Disruption of an EHMT1-associated chromatin-modification module causes intellectual disability. Am. J. Hum. Genet. *91*, 73–82.

Kneussel, M., Brandstätter, J.H., Laube, B., Stahl, S., Müller, U., and Betz, H. (1999). Loss of postsynaptic GABA(A) receptor clustering in gephyrin-deficient mice. J. Neurosci. Off. J. Soc. Neurosci. *19*, 9289–9297.

Koivisto, A.M., Ala-Mello, S., Lemmelä, S., Komu, H.A., Rautio, J., and Järvelä, I. (2007). Screening of mutations in the PHF8 gene and identification of a novel mutation in a Finnish family with XLMR and cleft lip/cleft palate. Clin. Genet. *72*, 145–149.

Kondo, M., Sumino, R., and Okado, H. (1997). Combinations of AMPA receptor subunit expression in individual cortical neurons correlate with expression of specific calcium-binding proteins. J. Neurosci. Off. J. Soc. Neurosci. *17*, 1570–1581.

Kondo, T., Isono, K., Kondo, K., Endo, T.A., Itohara, S., Vidal, M., and Koseki, H. (2014). Polycomb Potentiates Meis2 Activation in Midbrain by Mediating Interaction of the Promoter with a Tissue-Specific Enhancer. Dev. Cell *28*, 94–101.

Korotkova, T., Fuchs, E.C., Ponomarenko, A., von Engelhardt, J., and Monyer, H. (2010). NMDA receptor ablation on parvalbumin-positive interneurons

impairs hippocampal synchrony, spatial representations, and working memory. Neuron *68*, 557–569.

Kouzarides, T. (2007). Chromatin modifications and their function. Cell *128*, 693–705.

Kudo, T., Uchigashima, M., Miyazaki, T., Konno, K., Yamasaki, M., Yanagawa, Y., Minami, M., and Watanabe, M. (2012). Three Types of Neurochemical Projection from the Bed Nucleus of the Stria Terminalis to the Ventral Tegmental Area in Adult Mice. J. Neurosci. *32*, 18035–18046.

Kühnle, S., Mothes, B., Matentzoglu, K., and Scheffner, M. (2013). Role of the ubiquitin ligase E6AP/UBE3A in controlling levels of the synaptic protein Arc. Proc. Natl. Acad. Sci. U. S. A. *110*, 8888–8893.

Lamsa, K., Irvine, E.E., Giese, K.P., and Kullmann, D.M. (2007a). NMDA receptor-dependent long-term potentiation in mouse hippocampal interneurons shows a unique dependence on Ca2+/calmodulin-dependent kinases. J. Physiol. *584*, 885–894.

Lamsa, K.P., Heeroma, J.H., Somogyi, P., Rusakov, D.A., and Kullmann, D.M. (2007b). Anti-Hebbian long-term potentiation in the hippocampal feedback inhibitory circuit. Science *315*, 1262–1266.

Langmead, B., Trapnell, C., Pop, M., and Salzberg, S.L. (2009). Ultrafast and memory-efficient alignment of short DNA sequences to the human genome. Genome Biol. *10*, R25.

Laumonnier, F., Holbert, S., Ronce, N., Faravelli, F., Lenzner, S., Schwartz, C.E., Lespinasse, J., Van Esch, H., Lacombe, D., Goizet, C., et al. (2005). Mutations in PHF8 are associated with X linked mental retardation and cleft lip/cleft palate. J. Med. Genet. *42*, 780–786.

LeBlanc, J.J., and Fagiolini, M. (2011). Autism: a "critical period" disorder? Neural Plast. *2011*, 921680.

Lee, K.J., Queenan, B.N., Rozeboom, A.M., Bellmore, R., Lim, S.T., Vicini, S., and Pak, D.T.S. (2013). Mossy Fiber-CA3 Synapses Mediate Homeostatic Plasticity in Mature Hippocampal Neurons. Neuron *77*, 99–114.

Lein, E.S., Hawrylycz, M.J., Ao, N., Ayres, M., Bensinger, A., Bernard, A., Boe, A.F., Boguski, M.S., Brockway, K.S., Byrnes, E.J., et al. (2007). Genome-wide atlas of gene expression in the adult mouse brain. Nature *445*, 168–176.

Lévi, S., Logan, S.M., Tovar, K.R., and Craig, A.M. (2004). Gephyrin is critical for glycine receptor clustering but not for the formation of functional GABAergic synapses in hippocampal neurons. J. Neurosci. Off. J. Soc. Neurosci. *24*, 207–217.

Li, H., Fischle, W., Wang, W., Duncan, E.M., Liang, L., Murakami-Ishibe, S., Allis, C.D., and Patel, D.J. (2007). Structural Basis for Lower Lysine Methylation State-Specific Readout by MBT Repeats of L3MBTL1 and an Engineered PHD Finger. Mol. Cell *28*, 677–691.

Li, Q., Brown, J.B., Huang, H., and Bickel, P.J. (2011). Measuring reproducibility of high-throughput experiments. Ann. Appl. Stat. *5*, 1752–1779.

Lisman, J. (1989). A mechanism for the Hebb and the anti-Hebb processes underlying learning and memory. Proc. Natl. Acad. Sci. U. S. A. *86*, 9574–9578.

Lissin, D.V., Gomperts, S.N., Carroll, R.C., Christine, C.W., Kalman, D., Kitamura, M., Hardy, S., Nicoll, R.A., Malenka, R.C., and von Zastrow, M. (1998). Activity differentially regulates the surface expression of synaptic AMPA and NMDA glutamate receptors. Proc. Natl. Acad. Sci. U. S. A. *95*, 7097–7102.

Livak, K.J., and Schmittgen, T.D. (2001). Analysis of relative gene expression data using real-time quantitative PCR and the 2(-Delta Delta C(T)) Method. Methods San Diego Calif *25*, 402–408.

Lois, C., Hong, E.J., Pease, S., Brown, E.J., and Baltimore, D. (2002). Germline Transmission and Tissue-Specific Expression of Transgenes Delivered by Lentiviral Vectors. Science *295*, 868–872.

Love, M.I., Huber, W., and Anders, S. (2014). Moderated estimation of fold change and dispersion for RNA-seq data with DESeq2. Genome Biol. *15*, 550.

Lu, B., Wang, K.H., and Nose, A. (2009a). Molecular mechanisms underlying neural circuit formation. Curr. Opin. Neurobiol. *19*, 162–167.

Lu, W., Shi, Y., Jackson, A.C., Bjorgan, K., During, M.J., Sprengel, R., Seeburg, P.H., and Nicoll, R.A. (2009b). Subunit composition of synaptic AMPA receptors revealed by a single-cell genetic approach. Neuron *62*, 254–268.

Luhmann, H.J., and Prince, D.A. (1991). Postnatal maturation of the GABAergic system in rat neocortex. J. Neurophysiol. *65*, 247–263.

Lynch, G.S., Dunwiddie, T., and Gribkoff, V. (1977). Heterosynaptic depression: a postsynaptic correlate of long-term potentiation. Nature *266*, 737–739.

Mabb, A.M., Je, H.S., Wall, M.J., Robinson, C.G., Larsen, R.S., Qiang, Y., Corrêa, S.A.L., and Ehlers, M.D. (2014). Triad3A Regulates Synaptic Strength by Ubiquitination of Arc. Neuron *82*, 1299–1316.

Maccaferri, G., and McBain, C.J. (1995). Passive propagation of LTD to stratum oriens-alveus inhibitory neurons modulates the temporoammonic input to the hippocampal CA1 region. Neuron *15*, 137–145.

Maccaferri, G., Tóth, K., and McBain, C.J. (1998). Target-specific expression of presynaptic mossy fiber plasticity. Science *279*, 1368–1370.

Madisen, L., Zwingman, T.A., Sunkin, S.M., Oh, S.W., Zariwala, H.A., Gu, H., Ng, L.L., Palmiter, R.D., Hawrylycz, M.J., Jones, A.R., et al. (2010). A robust and high-throughput Cre reporting and characterization system for the whole mouse brain. Nat. Neurosci. *13*, 133–140.

Maffei, A., and Turrigiano, G.G. (2008). Multiple Modes of Network Homeostasis in Visual Cortical Layer 2/3. J. Neurosci. Off. J. Soc. Neurosci. *28*, 4377–4384.

Magee, J.C., and Johnston, D. (1997). A synaptically controlled, associative signal for Hebbian plasticity in hippocampal neurons. Science *275*, 209–213.

Markram, K., and Markram, H. (2010). The intense world theory - a unifying theory of the neurobiology of autism. Front. Hum. Neurosci. *4*, 224.

Markram, H., Lübke, J., Frotscher, M., and Sakmann, B. (1997). Regulation of synaptic efficacy by coincidence of postsynaptic APs and EPSPs. Science *275*, 213–215.

Markram, H., Toledo-Rodriguez, M., Wang, Y., Gupta, A., Silberberg, G., and Wu, C. (2004). Interneurons of the neocortical inhibitory system. Nat. Rev. Neurosci. *5*, nrn1519.

Matsuzaki, M., Ellis-Davies, G.C., Nemoto, T., Miyashita, Y., Iino, M., and Kasai, H. (2001). Dendritic spine geometry is critical for AMPA receptor expression in hippocampal CA1 pyramidal neurons. Nat. Neurosci. *4*, 1086–1092.

Matthews, E.A., Weible, A.P., Shah, S., and Disterhoft, J.F. (2008). The BK-mediated fAHP is modulated by learning a hippocampus-dependent task. Proc. Natl. Acad. Sci. U. S. A. *105*, 15154–15159.

Maurer-Stroh, S., Dickens, N.J., Hughes-Davies, L., Kouzarides, T., Eisenhaber, F., and Ponting, C.P. (2003). The Tudor domain "Royal Family": Tudor, plant Agenet, Chromo, PWWP and MBT domains. Trends Biochem. Sci. *28*, 69–74.

Maze, I., Covington, H.E., Dietz, D.M., LaPlant, Q., Renthal, W., Russo, S.J., Mechanic, M., Mouzon, E., Neve, R.L., Haggarty, S.J., et al. (2010). Essential Role of the Histone Methyltransferase G9a in Cocaine-induced Plasticity. Science *327*, 213.

McMahon, L.L., and Kauer, J.A. (1997). Hippocampal interneurons express a novel form of synaptic plasticity. Neuron *18*, 295–305.

Meadows, J.P., Guzman-Karlsson, M.C., Phillips, S., Holleman, C., Posey, J.L., Day, J.J., Hablitz, J.J., and Sweatt, J.D. (2015). DNA methylation regulates neuronal glutamatergic synaptic scaling. Sci Signal *8*, ra61-ra61.

Mei, L., and Xiong, W.-C. (2008). Neuregulin 1 in neural development, synaptic plasticity and schizophrenia. Nat. Rev. Neurosci. *9*, 437–452.

Min, J., Allali-Hassani, A., Nady, N., Qi, C., Ouyang, H., Liu, Y., MacKenzie, F., Vedadi, M., and Arrowsmith, C.H. (2007). L3MBTL1 recognition of mono- and dimethylated histones. Nat. Struct. Mol. Biol. *14*, 1229–1230.

Mitra, A., Mitra, S.S., and Tsien, R.W. (2012). Heterogeneous reallocation of presynaptic efficacy in recurrent excitatory circuits adapting to inactivity. Nat. Neurosci. *15*, 250–257.

Mo, A., Mukamel, E.A., Davis, F.P., Luo, C., Henry, G.L., Picard, S., Urich, M.A., Nery, J.R., Sejnowski, T.J., Lister, R., et al. (2015). Epigenomic Signatures of Neuronal Diversity in the Mammalian Brain. Neuron *86*, 1369–1384.

Moretti, P. (2006). Learning and Memory and Synaptic Plasticity Are Impaired in a Mouse Model of Rett Syndrome. J. Neurosci. *26*, 319–327.

Mosimann, C., Hausmann, G., and Basler, K. (2009). β-Catenin hits chromatin: regulation of Wnt target gene activation. Nat. Rev. Mol. Cell Biol. *10*, 276–286.

Mueller, A.L., Taube, J.S., and Schwartzkroin, P.A. (1984). Development of hyperpolarizing inhibitory postsynaptic potentials and hyperpolarizing response to gamma-aminobutyric acid in rabbit hippocampus studied in vitro. J. Neurosci. Off. J. Soc. Neurosci. *4*, 860–867.

Murase, S., Mosser, E., and Schuman, E.M. (2002). Depolarization Drives β-Catenin into Neuronal Spines Promoting Changes in Synaptic Structure and Function. Neuron *35*, 91–105.

Murthy, V.N., Schikorski, T., Stevens, C.F., and Zhu, Y. (2001). Inactivity produces increases in neurotransmitter release and synapse size. Neuron *32*, 673–682.

Nägerl, U.V., Eberhorn, N., Cambridge, S.B., and Bonhoeffer, T. (2004). Bidirectional activity-dependent morphological plasticity in hippocampal neurons. Neuron *44*, 759–767.

Naisbitt, S., Kim, E., Tu, J.C., Xiao, B., Sala, C., Valtschanoff, J., Weinberg, R.J., Worley, P.F., and Sheng, M. (1999). Shank, a novel family of postsynaptic density proteins that binds to the NMDA receptor/PSD-95/GKAP complex and cortactin. Neuron *23*, 569–582.

Naldini, L., Blömer, U., Gallay, P., Ory, D., Mulligan, R., Gage, F.H., Verma, I.M., and Trono, D. (1996). In vivo gene delivery and stable transduction of nondividing cells by a lentiviral vector. Science *272*, 263–267.

O'Brien, R.J., Kamboj, S., Ehlers, M.D., Rosen, K.R., Fischbach, G.D., and Huganir, R.L. (1998). Activity-dependent modulation of synaptic AMPA receptor accumulation. Neuron *21*, 1067–1078.

Okada, M., Onodera, K., Van Renterghem, C., Sieghart, W., and Takahashi, T. (2000). Functional correlation of GABA(A) receptor alpha subunits expression with the properties of IPSCs in the developing thalamus. J. Neurosci. Off. J. Soc. Neurosci. *20*, 2202–2208.

Okuda, T., Lily, M.Y., Cingolani, L.A., Kemler, R., and Goda, Y. (2007). β-Catenin regulates excitatory postsynaptic strength at hippocampal synapses. Proc. Natl. Acad. Sci. *104*, 13479–13484.

Ouardouz, M., and Lacaille, J.C. (1995). Mechanisms of selective long-term potentiation of excitatory synapses in stratum oriens/alveus interneurons of rat hippocampal slices. J. Neurophysiol. *73*, 810–819.

Pastalkova, E., Serrano, P., Pinkhasova, D., Wallace, E., Fenton, A.A., and Sacktor, T.C. (2006). Storage of spatial information by the maintenance mechanism of LTP. Science *313*, 1141–1144.

Pastuzyn, E.D., and Shepherd, J.D. (2017). Activity-Dependent Arc Expression and Homeostatic Synaptic Plasticity Are Altered in Neurons from a Mouse Model of Angelman Syndrome. Front. Mol. Neurosci. *10*.

Peça, J., Feliciano, C., Ting, J.T., Wang, W., Wells, M.F., Venkatraman, T.N., Lascola, C.D., Fu, Z., and Feng, G. (2011). Shank3 mutant mice display autistic-like behaviours and striatal dysfunction. Nature *472*, 437–442.

Pelka, G.J., Watson, C.M., Radziewic, T., Hayward, M., Lahooti, H., Christodoulou, J., and Tam, P.P.L. (2006). Mecp2 deficiency is associated with learning and cognitive deficits and altered gene activity in the hippocampal region of mice. Brain *129*, 887–898.

Peng, Y.-R., Zeng, S.-Y., Song, H.-L., Li, M.-Y., Yamada, M.K., and Yu, X. (2010). Postsynaptic Spiking Homeostatically Induces Cell-Autonomous

Regulation of Inhibitory Inputs via Retrograde Signaling. J. Neurosci. *30*, 16220–16231.

Perna, F., Gurvich, N., Hoya-Arias, R., Abdel-Wahab, O., Levine, R.L., Asai, T., Voza, F., Menendez, S., Wang, L., Liu, F., et al. (2010). Depletion of L3MBTL1 promotes the erythroid differentiation of human hematopoietic progenitor cells: possible role in 20q− polycythemia vera. Blood *116*, 2812–2821.

Perna, F., Vu, L.P., Themeli, M., Kriks, S., Hoya-Arias, R., Khanin, R., Hricik, T., Mansilla-Soto, J., Papapetrou, E.P., Levine, R.L., et al. (2015). The Polycomb Group Protein L3MBTL1 Represses a SMAD5-Mediated Hematopoietic Transcriptional Program in Human Pluripotent Stem Cells. Stem Cell Rep. *4*, 658–669.

Plant, K., Pelkey, K.A., Bortolotto, Z.A., Morita, D., Terashima, A., McBain, C.J., Collingridge, G.L., and Isaac, J.T.R. (2006). Transient incorporation of native GluR2-lacking AMPA receptors during hippocampal long-term potentiation. Nat. Neurosci. *9*, 602–604.

Qin, J., Van Buren, D., Huang, H.-S., Zhong, L., Mostoslavsky, R., Akbarian, S., and Hock, H. (2010). Chromatin Protein L3MBTL1 Is Dispensable for Development and Tumor Suppression in Mice. J. Biol. Chem. *285*, 27767–27775.

Qin, J., Whyte, W.A., Anderssen, E., Apostolou, E., Chen, H.-H., Akbarian, S., Bronson, R.T., Hochedlinger, K., Ramaswamy, S., Young, R.A., et al. (2012). The Polycomb Group Protein L3mbtl2 Assembles an Atypical PRC1-Family Complex that Is Essential in Pluripotent Stem Cells and Early Development. Cell Stem Cell *11*, 319–332.

Qiu, Z., Sylwestrak, E.L., Lieberman, D.N., Zhang, Y., Liu, X.-Y., and Ghosh, A. (2012). The Rett Syndrome Protein MeCP2 Regulates Synaptic Scaling. J. Neurosci. Off. J. Soc. Neurosci. *32*, 989–994.

Rácz, A., Ponomarenko, A.A., Fuchs, E.C., and Monyer, H. (2009). Augmented hippocampal ripple oscillations in mice with reduced fast excitation onto parvalbumin-positive cells. J. Neurosci. Off. J. Soc. Neurosci. *29*, 2563–2568.

Ramocki, M.B., and Zoghbi, H.Y. (2008). Failure of neuronal homeostasis results in common neuropsychiatric phenotypes. Nature *455*, 912–918.

Rich, M.M., and Wenner, P. (2007). Sensing and expressing homeostatic synaptic plasticity. Trends Neurosci. *30*, 119–125.

Riehl, R., Johnson, K., Bradley, R., Grunwald, G.B., Cornel, E., Lilienbaum, A., and Holt, C.E. (1996). Cadherin Function Is Required for Axon Outgrowth in Retinal Ganglion Cells In Vivo. Neuron *17*, 837–848.

Rossignol, E. (2011). Genetics and function of neocortical GABAergic interneurons in neurodevelopmental disorders. Neural Plast. *2011*, 649325.

Roussignol, G., Ango, F., Romorini, S., Tu, J.C., Sala, C., Worley, P.F., Bockaert, J., and Fagni, L. (2005). Shank expression is sufficient to induce functional dendritic spine synapses in aspiny neurons. J. Neurosci. Off. J. Soc. Neurosci. *25*, 3560–3570.

Rubenstein, J.L.R., and Merzenich, M.M. (2003). Model of autism: increased ratio of excitation/inhibition in key neural systems. Genes Brain Behav. *2*, 255–267.

Rutherford, L.C., Nelson, S.B., and Turrigiano, G.G. (1998). BDNF has opposite effects on the quantal amplitude of pyramidal neuron and interneuron excitatory synapses. Neuron *21*, 521–530.

Ryu, J., Futai, K., Feliu, M., Weinberg, R., and Sheng, M. (2008). Constitutively active Rap2 transgenic mice display fewer dendritic spines, reduced extracellular signal-regulated kinase signaling, enhanced long-term depression, and impaired spatial learning and fear extinction. J. Neurosci. Off. J. Soc. Neurosci. *28*, 8178–8188.

Saddic, L.A., West, L.E., Aslanian, A., Yates, J.R., Rubin, S.M., Gozani, O., and Sage, J. (2010). Methylation of the Retinoblastoma Tumor Suppressor by SMYD2. J. Biol. Chem. *285*, 37733–37740.

Sailer, C.A., Kaufmann, W.A., Kogler, M., Chen, L., Sausbier, U., Ottersen, O.P., Ruth, P., Shipston, M.J., and Knaus, H.-G. (2006). Immunolocalization of BK channels in hippocampal pyramidal neurons. Eur. J. Neurosci. *24*, 442–454.

Sala, C., Piëch, V., Wilson, N.R., Passafaro, M., Liu, G., and Sheng, M. (2001). Regulation of dendritic spine morphology and synaptic function by Shank and Homer. Neuron *31*, 115–130.

Sala, C., Roussignol, G., Meldolesi, J., and Fagni, L. (2005). Key role of the postsynaptic density scaffold proteins Shank and Homer in the functional architecture of Ca2+ homeostasis at dendritic spines in hippocampal neurons. J. Neurosci. Off. J. Soc. Neurosci. *25*, 4587–4592.

Saliba, R.S., Michels, G., Jacob, T.C., Pangalos, M.N., and Moss, S.J. (2007). Activity-Dependent Ubiquitination of GABAA Receptors Regulates Their Accumulation at Synaptic Sites. J. Neurosci. *27*, 13341–13351.

Sathyamurthy, A., Allen, M.D., Murzin, A.G., and Bycroft, M. (2003). Crystal structure of the malignant brain tumor (MBT) repeats in Sex Comb on Midleg-like 2 (SCML2). J. Biol. Chem. *278*, 46968–46973.

Sato, D., Lionel, A.C., Leblond, C.S., Prasad, A., Pinto, D., Walker, S., O'Connor, I., Russell, C., Drmic, I.E., Hamdan, F.F., et al. (2012). SHANK1 Deletions in Males with Autism Spectrum Disorder. Am. J. Hum. Genet. *90*, 879–887.

Schanzenbächer, C.T., Sambandan, S., Langer, J.D., and Schuman, E.M. (2016). Nascent Proteome Remodeling following Homeostatic Scaling at Hippocampal Synapses. Neuron *92*, 358–371.

Schaukowitch, K., Reese, A.L., Kim, S.-K., Kilaru, G., Joo, J.-Y., Kavalali, E.T., and Kim, T.-K. (2017). An Intrinsic Transcriptional Program Underlying Synaptic Scaling during Activity Suppression. Cell Rep. *18*, 1512–1526.

Schmeisser, M.J., Ey, E., Wegener, S., Bockmann, J., Stempel, A.V., Kuebler, A., Janssen, A.-L., Udvardi, P.T., Shiban, E., Spilker, C., et al. (2012). Autistic-like behaviours and hyperactivity in mice lacking ProSAP1/Shank2. Nature *486*, 256–260.

Seeburg, D.P., and Sheng, M. (2008). Activity-Induced Polo-Like Kinase 2 Is Required for Homeostatic Plasticity of Hippocampal Neurons during Epileptiform Activity. J. Neurosci. *28*, 6583–6591.

Seeburg, D.P., Feliu-Mojer, M., Gaiottino, J., Pak, D.T.S., and Sheng, M. (2008). Critical role of CDK5 and Polo-like kinase 2 in homeostatic synaptic plasticity during elevated activity. Neuron *58*, 571–583.

Shahbazian, M.D., Young, J.I., Yuva-Paylor, L.A., Spencer, C.M., Antalffy, B.A., Noebels, J.L., Armstrong, D.L., Paylor, R., and Zoghbi, H.Y. (2002). Mice with Truncated MeCP2 Recapitulate Many Rett Syndrome Features and Display Hyperacetylation of Histone H3. Neuron *35*, 243–254.

Shen, E.Y., Jiang, Y., Mao, W., Futai, K., Hock, H., and Akbarian, S. (2015). Cognition and Mood-Related Behaviors in L3mbtl1 Null Mutant Mice. PLOS ONE *10*, e0121252.

Shepherd, J.D., Rumbaugh, G., Wu, J., Chowdhury, S., Plath, N., Kuhl, D., Huganir, R.L., and Worley, P.F. (2006). Arc/Arg3.1 Mediates Homeostatic Synaptic Scaling of AMPA Receptors. Neuron *52*, 475–484.

Shin, S.M., Zhang, N., Hansen, J., Gerges, N.Z., Pak, D.T.S., Sheng, M., and Lee, S.H. (2012). GKAP orchestrates activity-dependent postsynaptic protein remodeling and homeostatic scaling. Nat. Neurosci. *15*, 1655–1666.

Silverman, J.L., Turner, S.M., Barkan, C.L., Tolu, S.S., Saxena, R., Hung, A.Y., Sheng, M., and Crawley, J.N. (2011). Sociability and motor functions in Shank1 mutant mice. Brain Res. *1380*, 120–137.

Sims, J.K., and Rice, J.C. (2008). PR-Set7 Establishes a Repressive trans-Tail Histone Code That Regulates Differentiation. Mol. Cell. Biol. *28*, 4459–4468.

Sjöström, P.J., Turrigiano, G.G., and Nelson, S.B. (2003). Neocortical LTD via Coincident Activation of Presynaptic NMDA and Cannabinoid Receptors. Neuron *39*, 641–654.

Song, S., Sjöström, P.J., Reigl, M., Nelson, S., and Chklovskii, D.B. (2005). Highly nonrandom features of synaptic connectivity in local cortical circuits. PLoS Biol. *3*, e68.

Steiner, F.A., Talbert, P.B., Kasinathan, S., Deal, R.B., and Henikoff, S. (2012). Cell-type-specific nuclei purification from whole animals for genome-wide expression and chromatin profiling. Genome Res. *22*, 766–777.

Stellwagen, D., and Malenka, R.C. (2006). Synaptic scaling mediated by glial TNF-alpha. Nature *440*, 1054–1059.

Suberbielle, E., Sanchez, P.E., Kravitz, A.V., Wang, X., Ho, K., Eilertson, K., Devidze, N., Kreitzer, A.C., and Mucke, L. (2013). Physiologic brain activity causes DNA double-strand breaks in neurons, with exacerbation by amyloid-β. Nat. Neurosci. *16*, 613–621.

Sun, Q., and Turrigiano, G.G. (2011). PSD-95 and PSD-93 play critical but distinct roles in synaptic scaling up and down. J. Neurosci. Off. J. Soc. Neurosci. *31*, 6800–6808.

Sun, H.Y., Lyons, S.A., and Dobrunz, L.E. (2005). Mechanisms of target-cell specific short-term plasticity at Schaffer collateral synapses onto interneurones versus pyramidal cells in juvenile rats. J. Physiol. *568*, 815–840.

Sutton, M.A., Ito, H.T., Cressy, P., Kempf, C., Woo, J.C., and Schuman, E.M. (2006). Miniature Neurotransmission Stabilizes Synaptic Function via Tonic Suppression of Local Dendritic Protein Synthesis. Cell *125*, 785–799.

Swanwick, C.C., Murthy, N.R., and Kapur, J. (2006). Activity-dependent scaling of GABAergic synapse strength is regulated by brain-derived neurotrophic factor. Mol. Cell. Neurosci. *31*, 481–492.

Takahashi, N., Sasaki, T., Matsumoto, W., Matsuki, N., and Ikegaya, Y. (2010). Circuit topology for synchronizing neurons in spontaneously active networks. Proc. Natl. Acad. Sci. *107*, 10244–10249.

Takeichi, M. (2007). The cadherin superfamily in neuronal connections and interactions. Nat. Rev. Neurosci. *8*, 11–20.

Tamás, G., Buhl, E.H., Lörincz, A., and Somogyi, P. (2000). Proximally targeted GABAergic synapses and gap junctions synchronize cortical interneurons. Nat. Neurosci. *3*, 366–371.

Tan, H.L., Queenan, B.N., and Huganir, R.L. (2015). GRIP1 is required for homeostatic regulation of AMPAR trafficking. Proc. Natl. Acad. Sci. U. S. A. *112*, 10026–10031.

Tanenbaum, M.E., Gilbert, L.A., Qi, L.S., Weissman, J.S., and Vale, R.D. (2014). A protein-tagging system for signal amplification in gene expression and fluorescence imaging. Cell *159*, 635–646.

Taverna, S.D., Li, H., Ruthenburg, A.J., Allis, C.D., and Patel, D.J. (2007). How chromatin-binding modules interpret histone modifications: lessons from professional pocket pickers. Nat. Struct. Mol. Biol. *14*, 1025–1040.

Teichert, M., Liebmann, L., Hübner, C.A., and Bolz, J. (2017). Homeostatic plasticity and synaptic scaling in the adult mouse auditory cortex. Sci. Rep. *7*, 17423.

Thiagarajan, T.C., Piedras-Renteria, E.S., and Tsien, R.W. (2002). alpha- and betaCaMKII. Inverse regulation by neuronal activity and opposing effects on synaptic strength. Neuron *36*, 1103–1114.

Thiagarajan, T.C., Lindskog, M., and Tsien, R.W. (2005). Adaptation to synaptic inactivity in hippocampal neurons. Neuron *47*, 725–737.

Togashi, H., Abe, K., Mizoguchi, A., Takaoka, K., Chisaka, O., and Takeichi, M. (2002). Cadherin regulates dendritic spine morphogenesis. Neuron *35*, 77–89.

Trapnell, C., Pachter, L., and Salzberg, S.L. (2009). TopHat: discovering splice junctions with RNA-Seq. Bioinformatics *25*, 1105–1111.

Trojer, P., and Reinberg, D. (2008). Beyond histone methyl-lysine binding: How malignant brain tumor (MBT) protein L3MBTL1 impacts chromatin structure. Cell Cycle *7*, 578–585.

Trojer, P., Li, G., Sims, R.J., Vaquero, A., Kalakonda, N., Boccuni, P., Lee, D., Erdjument-Bromage, H., Tempst, P., Nimer, S.D., et al. (2007). L3MBTL1, a Histone-Methylation-Dependent Chromatin Lock. Cell *129*, 915–928.

Trojer, P., Cao, A.R., Gao, Z., Li, Y., Zhang, J., Xu, X., Li, G., Losson, R., Erdjument-Bromage, H., Tempst, P., et al. (2011). L3MBTL2 Protein Acts in Concert with PcG Protein-Mediated Monoubiquitination of H2A to Establish a Repressive Chromatin Structure. Mol. Cell *42*, 438–450.

Tsankova, N.M., Berton, O., Renthal, W., Kumar, A., Neve, R.L., and Nestler, E.J. (2006). Sustained hippocampal chromatin regulation in a mouse model of depression and antidepressant action. Nat. Neurosci. *9*, 519–525.

Tu, J.C., Xiao, B., Yuan, J.P., Lanahan, A.A., Leoffert, K., Li, M., Linden, D.J., and Worley, P.F. (1998). Homer binds a novel proline-rich motif and links group 1 metabotropic glutamate receptors with IP3 receptors. Neuron *21*, 717–726.

Tuchman, R., and Rapin, I. (2002). Epilepsy in autism. Lancet Neurol. *1*, 352–358.

Turrigiano, G. (2011). Too Many Cooks? Intrinsic and Synaptic Homeostatic Mechanisms in Cortical Circuit Refinement. Annu. Rev. Neurosci. *34*, 89–103.

Turrigiano, G. (2012). Homeostatic Synaptic Plasticity: Local and Global Mechanisms for Stabilizing Neuronal Function. Cold Spring Harb. Perspect. Biol. *4*.

Turrigiano, G.G., and Nelson, S.B. (2004). Homeostatic plasticity in the developing nervous system. Nat. Rev. Neurosci. *5*, 97–107.

Turrigiano, G.G., Leslie, K.R., Desai, N.S., Rutherford, L.C., and Nelson, S.B. (1998). Activity-dependent scaling of quantal amplitude in neocortical neurons. Nature *391*, 892–896.

Uchida, N., Honjo, Y., Johnson, K.R., Wheelock, M.J., and Takeichi, M. (1996). The catenin/cadherin adhesion system is localized in synaptic junctions bordering transmitter release zones. J. Cell Biol. *135*, 767–779.

Vakoc, C.R., Sachdeva, M.M., Wang, H., and Blobel, G.A. (2006). Profile of Histone Lysine Methylation across Transcribed Mammalian Chromatin. Mol. Cell. Biol. *26*, 9185–9195.

Valeeva, G., Valiullina, F., and Khazipov, R. (2013). Excitatory actions of GABA in the intact neonatal rodent hippocampus in vitro. Front. Cell. Neurosci. *7*.

Verkerk, A.J., Pieretti, M., Sutcliffe, J.S., Fu, Y.H., Kuhl, D.P., Pizzuti, A., Reiner, O., Richards, S., Victoria, M.F., and Zhang, F.P. (1991). Identification of a gene (FMR-1) containing a CGG repeat coincident with a breakpoint cluster region exhibiting length variation in fragile X syndrome. Cell *65*, 905–914.

Verpelli, C., Dvoretskova, E., Vicidomini, C., Rossi, F., Chiappalone, M., Schoen, M., Di Stefano, B., Mantegazza, R., Broccoli, V., Böckers, T.M., et al. (2011). Importance of Shank3 protein in regulating metabotropic glutamate receptor 5 (mGluR5) expression and signaling at synapses. J. Biol. Chem. *286*, 34839–34850.

Vitureira, N., Letellier, M., White, I.J., and Goda, Y. (2012). Differential control of presynaptic efficacy by postsynaptic N-cadherin and β-catenin. Nat. Neurosci. *15*, 81–89.

Vogel-Ciernia, A., and Wood, M.A. (2014). Neuron-specific chromatin remodeling: A missing link in epigenetic mechanisms underlying synaptic plasticity, memory, and intellectual disability disorders. Neuropharmacology *80*, 18–27.

Vullhorst, D., Neddens, J., Karavanova, I., Tricoire, L., Petralia, R.S., McBain, C.J., and Buonanno, A. (2009). Selective expression of ErbB4 in interneurons, but not pyramidal cells, of the rodent hippocampus. J. Neurosci. Off. J. Soc. Neurosci. *29*, 12255–12264.

Wang, C.-C., Held, R.G., and Hall, B.J. (2013). SynGAP regulates protein synthesis and homeostatic synaptic plasticity in developing cortical networks. PloS One *8*, e83941.

Wang, W.K., Tereshko, V., Boccuni, P., MacGrogan, D., Nimer, S.D., and Patel, D.J. (2003). Malignant brain tumor repeats: a three-leaved propeller architecture with ligand/peptide binding pockets. Struct. Lond. Engl. 1993 *11*, 775–789.

Wang, X., McCoy, P.A., Rodriguiz, R.M., Pan, Y., Je, H.S., Roberts, A.C., Kim, C.J., Berrios, J., Colvin, J.S., Bousquet-Moore, D., et al. (2011). Synaptic dysfunction and abnormal behaviors in mice lacking major isoforms of Shank3. Hum. Mol. Genet. *20*, 3093–3108.

West, L.E., Roy, S., Lachmi-Weiner, K., Hayashi, R., Shi, X., Appella, E., Kutateladze, T.G., and Gozani, O. (2010). The MBT Repeats of L3MBTL1 Link SET8-mediated p53 Methylation at Lysine 382 to Target Gene Repression. J. Biol. Chem. *285*, 37725–37732.

Whitlock, J.R., Heynen, A.J., Shuler, M.G., and Bear, M.F. (2006). Learning induces long-term potentiation in the hippocampus. Science *313*, 1093–1097.

Whittington, M.A., Traub, R.D., and Jefferys, J.G. (1995). Synchronized oscillations in interneuron networks driven by metabotropic glutamate receptor activation. Nature *373*, 612–615.

Wierenga, C.J., Ibata, K., and Turrigiano, G.G. (2005). Postsynaptic Expression of Homeostatic Plasticity at Neocortical Synapses. J. Neurosci. *25*, 2895–2905.

Williams, C.A., Beaudet, A.L., Clayton-Smith, J., Knoll, J.H., Kyllerman, M., Laan, L.A., Magenis, R.E., Moncla, A., Schinzel, A.A., Summers, J.A., et al. (2006). Angelman syndrome 2005: updated consensus for diagnostic criteria. Am. J. Med. Genet. A. *140*, 413–418.

Wismar, J., Löffler, T., Habtemichael, N., Vef, O., Geissen, M., Zirwes, R., Altmeyer, W., Sass, H., and Gateff, E. (1995). The Drosophila melanogaster tumor suppressor gene lethal(3)malignant brain tumor encodes a proline-rich protein with a novel zinc finger. Mech. Dev. *53*, 141–154.

Wöhr, M., Roullet, F.I., Hung, A.Y., Sheng, M., and Crawley, J.N. (2011). Communication impairments in mice lacking Shank1: reduced levels of ultrasonic vocalizations and scent marking behavior. PloS One *6*, e20631.

Won, H., Lee, H.-R., Gee, H.Y., Mah, W., Kim, J.-I., Lee, J., Ha, S., Chung, C., Jung, E.S., Cho, Y.S., et al. (2012). Autistic-like social behaviour in Shank2-

mutant mice improved by restoring NMDA receptor function. Nature *486*, 261–265.

Wu, H., and Parsons, J.T. (1993). Cortactin, an 80/85-kilodalton pp60src substrate, is a filamentous actin-binding protein enriched in the cell cortex. J. Cell Biol. *120*, 1417–1426.

Xiao, B., Tu, J.C., Petralia, R.S., Yuan, J.P., Doan, A., Breder, C.D., Ruggiero, A., Lanahan, A.A., Wenthold, R.J., and Worley, P.F. (1998). Homer regulates the association of group 1 metabotropic glutamate receptors with multivalent complexes of homer-related, synaptic proteins. Neuron *21*, 707–716.

Yamasaki, M., Matsui, M., and Watanabe, M. (2010). Preferential Localization of Muscarinic M1 Receptor on Dendritic Shaft and Spine of Cortical Pyramidal Cells and Its Anatomical Evidence for Volume Transmission. J. Neurosci. *30*, 4408–4418.

Yang, M., Bozdagi, O., Scattoni, M.L., Wöhr, M., Roullet, F.I., Katz, A.M., Abrams, D.N., Kalikhman, D., Simon, H., Woldeyohannes, L., et al. (2012). Reduced excitatory neurotransmission and mild autism-relevant phenotypes in adolescent Shank3 null mutant mice. J. Neurosci. Off. J. Soc. Neurosci. *32*, 6525–6541.

Yang, S.N., Tang, Y.G., and Zucker, R.S. (1999). Selective induction of LTP and LTD by postsynaptic [Ca2+]i elevation. J. Neurophysiol. *81*, 781–787.

Yip, J., Soghomonian, J.-J., and Blatt, G.J. (2007). Decreased GAD67 mRNA levels in cerebellar Purkinje cells in autism: pathophysiological implications. Acta Neuropathol. (Berl.) *113*, 559–568.

Yizhar, O., Fenno, L.E., Prigge, M., Schneider, F., Davidson, T.J., O'Shea, D.J., Sohal, V.S., Goshen, I., Finkelstein, J., Paz, J.T., et al. (2011). Neocortical excitation/inhibition balance in information processing and social dysfunction. Nature *477*, 171–178.

Zetsche, B., Volz, S.E., and Zhang, F. (2015). A split-Cas9 architecture for inducible genome editing and transcription modulation. Nat. Biotechnol. *33*, 139–142.

Zhang, H., and Macara, I.G. (2006). The polarity protein PAR-3 and TIAM1 cooperate in dendritic spine morphogenesis. Nat. Cell Biol. *8*, 227–237.

Zhang, W., and Linden, D.J. (2003). The other side of the engram: experience-driven changes in neuronal intrinsic excitability. Nat. Rev. Neurosci. *4*, 885–900.

Zhang, H., Maximov, A., Fu, Y., Xu, F., Tang, T.-S., Tkatch, T., Surmeier, D.J., and Bezprozvanny, I. (2005). Association of CaV1.3 L-type calcium channels with Shank. J. Neurosci. Off. J. Soc. Neurosci. *25*, 1037–1049.

Zhang, J., Bonasio, R., Strino, F., Kluger, Y., Holloway, J.K., Modzelewski, A.J., Cohen, P.E., and Reinberg, D. (2013). SFMBT1 functions with LSD1 to regulate expression of canonical histone genes and chromatin-related factors. Genes Dev. *27*, 749–766.

Zhang, W., Vazquez, L., Apperson, M., and Kennedy, M.B. (1999). Citron binds to PSD-95 at glutamatergic synapses on inhibitory neurons in the hippocampus. J. Neurosci. Off. J. Soc. Neurosci. *19*, 96–108.

Zhang, Y., Chen, K., Sloan, S.A., Bennett, M.L., Scholze, A.R., O'Keeffe, S., Phatnani, H.P., Guarnieri, P., Caneda, C., Ruderisch, N., et al. (2014). An RNA-Sequencing Transcriptome and Splicing Database of Glia, Neurons, and Vascular Cells of the Cerebral Cortex. J. Neurosci. *34*, 11929–11947.

Zhong, X., Li, H., and Chang, Q. (2012). MeCP2 phosphorylation is required for modulating synaptic scaling through mGluR5. J. Neurosci. Off. J. Soc. Neurosci. *32*, 12841–12847.

Zhou, Q., Homma, K.J., and Poo, M. (2004). Shrinkage of dendritic spines associated with long-term depression of hippocampal synapses. Neuron *44*, 749–757.

Zikopoulos, B., and Barbas, H. (2013). Altered neural connectivity in excitatory and inhibitory cortical circuits in autism. Front. Hum. Neurosci. *7*, 609.